ABSOLUTE YIELDS AND GROUP CONSTANTS OF THE DELAYED NEUTRONS ~~FOR U^{235}, U^{238} AND PU^{239}~~ IN FAST FISSION

BY

PETER TAVOULARIDIS

DIPL. MECH. ELEC. ENGIN., NAT. TECH. UNIV. OF ATHENS, GREECE

MASTER OF SCIENCE, LONDON UNIVERSITY

OCTOBER, 1976

A THESIS SUBMITTED FOR THE DEGREE OF DOCTOR OF PHILOSOPHY OF THE UNIVERSITY OF LONDON AND FOR THE DIPLOMA OF IMPERIAL COLLEGE

MECHANICAL ENGINEERING DEPARTMENT

IMPERIAL COLLEGE

LONDON SW7

ABSTRACT

Absolute yields and group constants of the delayed neutrons from the fast fission of U^{235}, U^{238} and Pu^{239} have been measured. The method was based on irradiating a sample in the fast pulsed reactor VIPER and transferring it pneumatically to the neutron detector, outside the biological shield of the reactor. The decay of the delayed neutron emission rate was measured using two scintillation detectors.

The neutron efficiency of the detectors was measured by a number of neutron sources and account was taken of its energy response function. The Am-Li neutron source was used to determine the efficiency of the detectors for the delayed neutron yield measurement.

The fissions in the sample were measured by an activation technique. The 1596 Kev gamma activity of the sample, accompanying the β-decay of the La^{140} fission product, was measured using a high resolution detector. The necessary conversion factor of activity into the number of fissions was determined by a calibration experiment where a thin deposit of known mass was irradiated within a fission chamber, along with a thick foil which was subsequently gamma counted.

The absolute delayed neutron yields, determined by instantaneous irradiations, were found to be:

U^{235}	$0.0164 \pm .0006$	(n/F)
U^{238}	$0.0439 \pm .0017$	(n/F)
Pu^{239}	$0.00599 \pm .00022$	(n/F)

The delayed neutron emission decay curve was approximated by six groups, using the least squares method. The fictitious group constants preserved the period-reactivity ($) relationship calculated numerically using the prompt burst delayed neutron decay data technique. The period-

reactivity ($) relationship, using the present group structure, is in agreement with the currently used values to within 3% for any isotope and practically used period for the control rod reactivity worth calibration.

ACKNOWLEDGEMENTS

The author wishes to express his gratitude to his supervisor Dr. C.B. Besant for his help and advice during this work and to Prof. P.J. Grant, Dr. J.G. Williams, Mr. M.H. McTaggart and Mr. P.J. Challen for their advice and discussions.

The help of the Imperial College computer advisory, Consort reactor and VIPER reactor personnel is greatly appreciated.

CONTENTS

			PAGE
CHAPTER 1		INTRODUCTION	
	1.1	Delayed neutrons. Their importance in reactor kinetics	1
	1.2	Review of the previous measurements	3
	1.3	Period-reactivity relationships	9
	1.4	Reactivity worth calculations	12
	1.5	The object and a brief description of the present measurements	12
CHAPTER 2		MASS CALIBRATION OF THE DEPOSITS	15
	2.1	The double fission chamber	15
	2.2	Irradiation environment, NISUS-1B	18
	2.3	Electronics	19
	2.4	Setting of the electronics	19
	2.5	Experiment and corrections	28
	2.6	Results and discussion	29
CHAPTER 3		THE DELAYED NEUTRON MEASUREMENTS	33
	3.1	The irradiation facility	33
	3.2	The neutron detection system	36
	3.3	The efficiency of the detectors	42
		3.3.1 Short and long term variation of the efficiency	42
		3.3.2 Axial variation of the efficiency	43
		3.3.3 The efficiency calibration using the Am-Li neutron source	44
		3.3.4 Efficiency of the detectors for an irradiation	46
		3.3.5 Radial variation of the efficiency	47
		3.3.6 Energy response of the counters	50
	3.4	Experiments	55

CHAPTER 4		FISSION MEASUREMENTS	75
	4.1.1	Description of the sample	75
	4.1.2	The calibration experiment	76
	4.2.1	The Ba-140 technique	81
	4.2.2	The lithium drifted Germanium detector	82
	4.2.3	The 1596 Kev photopeak	85
	4.2.4	The photopeak analysis	89
	4.2.5	The stability of the efficiency of the Ge(Li) detectors	91
4.3		Measurements-Results-Errors-Discussion	94
CHAPTER 5		ANALYSIS OF THE DATA	103
5.1		The codes DATA, JOIN, FINAL	103
5.2		Linear regression analysis	106
5.3		The regression model. The least squares solution.	108
5.4		The code FITEXP	111
5.5		The code YIELD	112
5.6		Gardner's method	113
5.7		Peeling off method	119
CHAPTER 6		RESULTS	
6.1		The U^{235} isotope results	120
6.2		The U^{238} isotope results	135
6.3		The Pu^{239} isotope results	143
6.4		The effect of the radial efficiency variation on the yield measurement	148
CHAPTER 7		SUMMARY AND DISCUSSION	150
7.1		Group structure of the delayed neutrons	150
7.2		Absolute yield of the delayed neutrons	158
7.3		Conclusions and recommendations	162
CHAPTER 8		PROGRESS REPORT ON THE DELAYED NEUTRON SPECTRA MEASUREMENTS	164
8.1		Introduction	164

8.2 The proton-recoil proportional counter spectrometry technique 165

8.3 The response functions of spherical proton recoil counters in the case of beam neutron source 171

8.3.1 Calculation of the probability function F(B,L)

8.3.2 Wall correction-Probability F(L) 173

8.4 Recommendations 175

REFERENCES 180

APPENDIX A 184

APPENDIX B 189

APPENDIX C 193

LIST OF TABLES

PAGE

Chapter 1

Chapter 2

Table 2.1 Deposit characteristics 16

Table 2.2 Calibration experiment of Pu^{239} deposit 30

Table 2.3 Corrections applied for the Pu^{239} mass calibration experiment 31

Chapter 3

Table 3.1 Energy dependence of axial scanning of efficiency 71

Table 3.2 Axial variation of the efficiency 71

Table 3.3 Radial scanning of the efficiency 72

Table 3.4 The efficiency of the counters for the Am-Li source 73

Table 3.5 Systematic errors in efficiency (mean absolute yield) 73

Table 3.6 Response function of counters 73

Table 3.7 Characteristics of the experiments 74

Chapter 4

Table 4.1 Isotopic composition of samples 78

Table 4.2 Per atom fission ratio 79

Table 4.3 Analysis of the steady-state calibration experiment 1233 79

Table 4.4 Results of steady-state experiment 1233 80

Table 4.5 Summary of steady-state experiments 80

Table 4.6 Errors of the steady state results 80

Table 4.7 The back-bias of the analyser 86

Table 4.8 Energy of counted peak 87

Table 4.9 Decay of the 1596 Kev photopeak 92

Table 4.10 Stability of the detector efficiency 92

Table 4.11 U^{235} foil counting 98

Table 4.12 U^{238} foil counting 99

Table 4.13 Pu^{239} foil counting 99

Table 4.14 Total number of fissions of main isotope 100

Table 4.15 Systematic errors in foil counting 101

Table 4.16 Errors in number of fissions 101

Table 4.17 Flux gradient

Chapter 5

Table 5.1 Test of the fitting routines 112

Chapter 6

Table 6.1.1 Comparison of the absolute decay curves of the delayed neutrons predicted by the three U^{235} pulses 127

Table 6.1.2 Pulse joining. Normalisation factors. U^{235} isotope 128

Table 6.1.3 Comparison of the absolute decay curves of the delayed neutrons predicted by two U^{235} pulses 128

Table 6.1.4 Peeling-off method group constants U^{235} isotope 129

Table 6.1.5 Least squares method group constants U^{235} isotope. Six group structure 129

Table 6.1.6 U^{235} reactivity comparison. Six group structure 130

Table 6.1.7 U^{235} delayed neutron yield. Corrections. Uncertainties. 131

Table 6.1.8 Comparison of the delayed neutron yield measured by the two counters 132

Table 6.1.9 Effect of count rate on the measurements of counter-1 133

Table 6.1.10 Least squares method group constants. U^{235} isotope. Five group structure. 133

Table 6.1.11 U^{235} reactivity comparison. Five group structure 134

Table 6.2.1 Comparison of the decay curves in overlapping time intervals. U^{238} isotope 137

Table 6.2.2 Pulse joining. Normalisation factors. U^{238} isotope 138

Table 6.2.3 U^{238} delayed neutron yield. Corrections. Uncertainties. 139

Table 6.2.4 U^{238} group structure 140

Table 6.2.5	U^{238} reactivity comparison	141
Table 6.3.1	Comparison of the decay curves in overlapping time interval. Pu^{239} isotope	144
Table 6.3.2	Pulse joining. Normalisation factors. Pu^{239} isotope	145
Table 6.3.3	Pu^{239} delayed neutron yield. Corrections. Uncertainties.	146
Table 6.3.4	Pu^{239} least squares six group structure	147
	Chapter 7	
Table 7.1	Half-lives of the groups (present work) and identified precursors of delayed neutrons	154
Table 7.2	Errors in period-reactivity ($) calculations	154
Table 7.3	Comparison of the present absolute delayed neutron yields with published values	161
	Chapter 8	
Table 8.3.1	Integration results	176
Table 8.3.2	Comparison of probability functions	179
	Appendix A	
Table A1	Self multiplication corrections	
	Appendix B	
Table B1	Estimate of Pu^{239} group constants	
Table B2	Pu^{239} five group constants	
Table B3	Pu^{239} reactivity comparison	

LIST OF FIGURES

		PAGE
	Chapter 1	
Figure 1.1	Schematic representation of delayed neutron emission	2
	Chapter 2	
Figure 2.1	Demountable double fission chamber	17
Figure 2.2	Irradiation environment	20
Figure 2.3	Electronics for one side of the double fission chamber and for a monitor	22
Figure 2.4	Electronics for gated spectrum of monitors	23
Figure 2.5	Monitor 1 gated spectrum	25
Figure 2.6	Monitor 1 discriminator setting	26
Figure 2.7	Spectrum of fission fragments and settings of discriminators	27
	Chapter 3	
Figure 3.1	View of double fission chamber in the VIPER cavity in position for a steady-state irradiation	60
Figure 3.2	Neutron spectrum of VIPER reactor	61
Figure 3.3	Detectors installed around flight tube	62
Figure 3.4	View of dismantled rabbit, showing samples and aluminium spacers	63
Figure 3.5	Rabbit in the firing position of the flight tube	64
Figure 3.6	Detector arrangement	65
Figure 3.7	Electronics of the neutron detectors	66
Figure 3.8	Estimated axial efficiency variation	67
Figure 3.9	Spectral uncertainty of the calibration	68
Figure 3.10	Schematic representation of (γ,n) neutron sources	69
Figure 3.11	Detector count rate due to reactor background	70

Chapter 4

Figure 4.1 Electronics of the Ge(Li) detectors 87

Figure 4.2 Typical counted photopeak 88

Figure 4.3 Study of the flux gradient for the calibration experiment 102

Chapter 5

Figure 5.1 Test example of the Gardner method 117

Chapter 6

Figure 6.1.1 Peeling-off method results 124

Figure 6.1.2 U^{235} group structure. The Gardner method 126

Figure 6.2.1 U^{238} longest lived group 142

Chapter 7

Chapter 8

Figure 8.3.1 Geometry of the calculations 171

Appendix A

Figure A1 Monte Carlo calculation

Appendix B

Appendix C

Figure C1 Effect of the spectral response of detector on period-reactivity relationship.

CHAPTER 1

INTRODUCTION

1.1 Delayed Neutrons. Their importance in Reactor Kinetics

In addition to the prompt neutrons emitted from each fission event, a small number of delayed neutrons are emitted. Figure 1.1 gives the schematic representation of delayed neutron emission, according to the Bohr-Wheeler model. Neutron rich isotopes formed in fission (precursors) have large β-decay energies (Q_β), so that they can populate excited states in the emitter, above the neutron binding energy of the emitter (B_n), thus making possible the neutron emission. Because of the long half-life associated with the β-decay of the precursor, the neutron appears effectively with the half-life of its precursor.

It is now known that there are at least thirty eight isotopes formed in fission, which are delayed neutron precursors. The most important precursors are different Br and I isotopes which are responsible for most of the total delayed neutron activity, and especially for the long-lived one. Tomlinson[1] has reviewed the systematics of the known delayed neutron precursors in an attempt to explain the gross experimental results (group constants and spectra of delayed neutrons).

Lamarsh[2] shows that the time elapsed between two successive neutron generations in a reactor is determined by the delayed neutrons. So, the kinetic behaviour of a reactor will be determined by the delayed neutrons. Furthermore, since this generation time has reasonable values (compared with the small prompt neutron lifetime), the

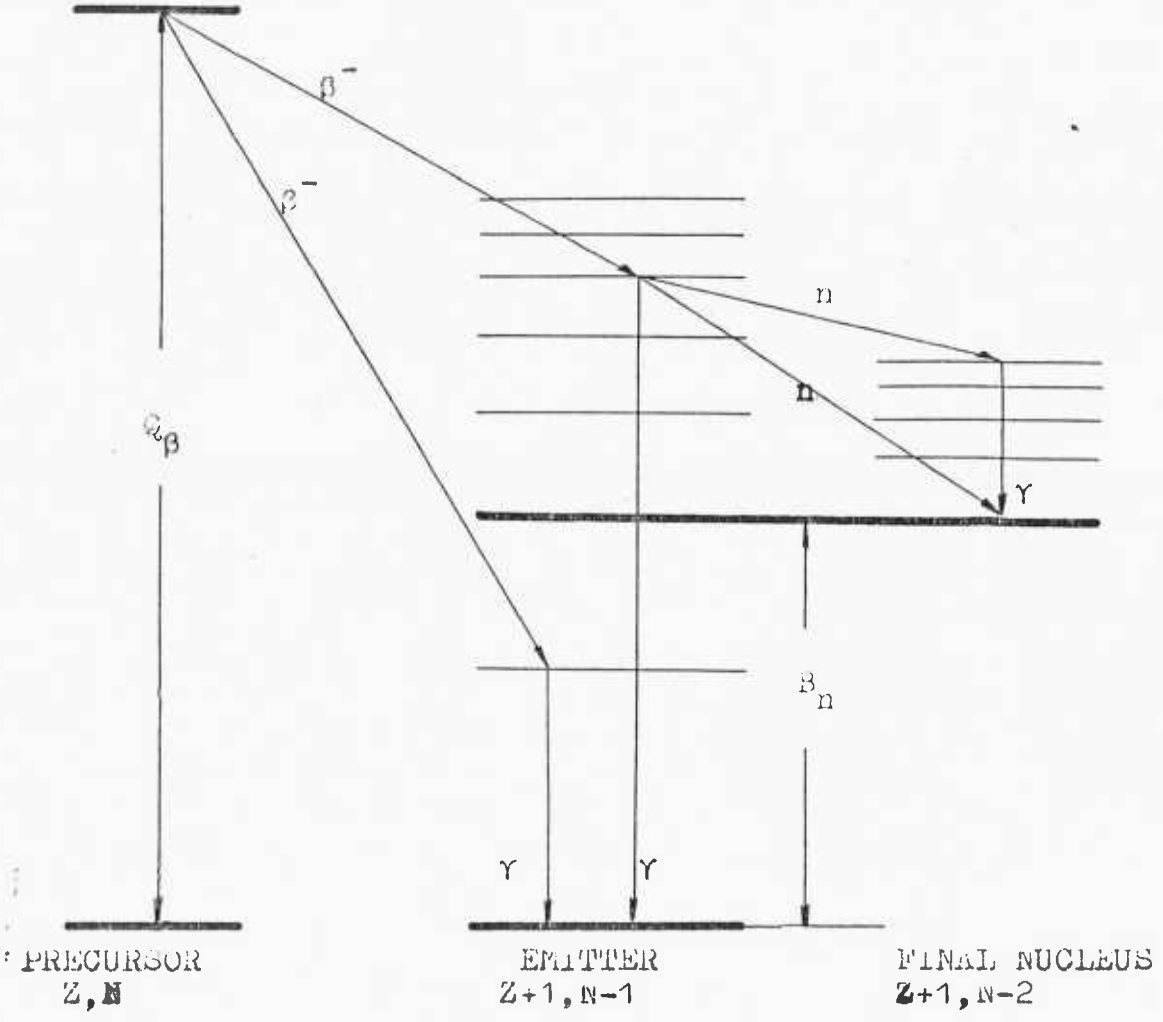

FIGURE 1.1 SCHEMATIC REPRESENTATION OF DELAYED NEUTRON EMISSION

existence of the delayed neutrons makes possible the electromechanical control of the reactors.

It is apparent that a detailed knowledge of the characteristics of all the precursors (decay constants, fission yields, neutron emission probabilities and neutron emission energy spectra) is required for the kinetic study of a reactor. Not only is such information difficult to acquire but, the resulting calculations will be very cumbersome.

1.2 Review of the previous measurements

The absolute yield of the delayed neutrons is the number of delayed neutrons emitted per fission. It has been customary - from the reactor kinetics point of view - to represent the delayed neutron precursors by a small number of fictitious precursors (groups). The delayed neutron group relative abundances and decay constants are chosen so that, it is possible to represent the measured gross time behaviour of the delayed neutron emission.

If we assume that a sample is irradiated over a time interval t_1, then the detected delayed neutron count rate at time t after the irradiation is

$$EF\ \sigma_f N\ \Phi \sum_{i=1}^{M} \alpha_i (1-e^{-\lambda_i t_1}) e^{-\lambda_i t}$$

where, N = number of fissionable atoms in the sample

σ_f = microscopic fission cross-section of fissionable material

Φ = neutron flux at the irradiation position

EF = neutron efficiency of the detector

α_i, λ_i = absolute delayed neutron yield and decay constant of group i

M = number of groups of delayed neutrons

If we assume that the irradiation time t_1 is much longer than $1/\lambda_i$ (i=1, ..., M) (ie saturation irradiation) then, the detected neutron count rate at time t after the irradiation is

$$EF\ \sigma_f N \Phi \sum_{i=1}^{M} \alpha_i e^{-\lambda_i t}$$

If we assume that the irradiation time t_1 is much shorter than $1/\lambda_i$ (i = 1, ..., M) (i.e. instantaneous irradiation) then, the detected neutron count rate at time t after the irradiation is

$$EF.F. \sum_{i=1}^{M} \alpha_i \lambda_i e^{-\lambda_i t}$$

where, $F = \sigma_f N \Phi t_1$ is the total number of fissions in the sample.

All the previously described types of irradiation have been used in practice. The instantaneous and saturation irradiations are of special importance because, the absolute delayed neutron yield can be measured without any knowledge of the group structure.

It is apparent that, the total number of detected delayed neutrons following an instantaneous irradiation (i.e. $t \varepsilon (0, \infty)$) is

$$EF.F. \sum_{i=1}^{M} \alpha_i$$

and the detected delayed neutron count rate immediately after a saturation irradiation is

$$EF\ \sigma_f N \Phi \sum_{i=1}^{M} \alpha_i$$

where $\sum_{i=1}^{M} \alpha_i$ is the absolute yield of the delayed neutrons.

Generally, in order to measure the absolute delayed neutron yield we have to use a neutron detector of known efficiency. Since the delayed neutron spectra are poorly known, neutron detectors with energy independent efficiency, from a few tens of Kev up to a few Mev (flat response detectors), have been used, so that, any neutron source with

a spectrum in this energy range can be used for the detector calibration. Fissions have been measured by activation techniques, and directly with absolutely calibrated fission chambers.

In order to measure the group constants of the delayed neutrons (relative abundance $\alpha_i / \sum_{i=1}^{M} \alpha_i$, and decay constant $\lambda_i, i = 1, \ldots, M$) we have to measure only the shape of a decay curve. The decay curves of the instantaneous and saturation irradiations are of particular importance because of the simplicity of the mathematical expressions. A neutron detector with a flat response is particularly required otherwise, the detection efficiency will be a function of the time t.

Below, we review the main features and the results of the measurements for the absolute delayed neutron yield and group structure from the U^{235}, U^{238} and Pu^{239} in fast fission, appropriate for a fast reactor. Tuttle[9] has reviewed the existing measurements for thermal and 14 Mev fission along with a few measurements at neutron energies appropriate for fast reactors, which produced only relative values for the yield of the delayed neutrons from the isotopes under interest.

Rose and Smith[3] 1957

Samples of known masses were irradiated in the ZEPHYR reactor and they were pneumatically transfered to the delayed neutron detector, which was enclosed in a borated paraffin neutron shield. The detector consisted of six BF_3 counters, embedded in a paraffin cylindrical moderator and arranged circularly around the arrest position of the sample. The absolute efficiency of the detector was measured by a number of (γ, n) and (α, n) neutron sources. The energy response of the

detector was not flat, and the efficiency for each delayed neutron group was calculated using the delayed neutron group spectra.

The per atom fission rate (for a particular power level), at the irradiation position, was determined using fission chambers loaded with absolutely calibrated deposits. The irradiation time of the sample was variable and known.

The sample was irradiated for a predetermined time and the detected delayed neutron count rate was analysed by the peeling-off method, to determine the absolute yields of the delayed neutron groups. Since the statistical accuracy of the delayed neutron emission decay curve was unfavourable, known decay constants for the delayed neutron groups have been used in the peeling-off technique. The irradiation time was variable so that it would be possible to enhance the contribution of particular group(s) in the delayed neutron emission decay curve.

The absolute delayed neutron group yield of five groups was determined in this work. The U^{235}, U^{238} and Pu^{239} absolute delayed neutron yield (based on five groups) was found equal to $.0174 \pm .0014$, $.037 \pm .004$ and $.0070 \pm .0006$, respectively.

Keepin et al[4] 1957

The samples were irradiated in the pulsed reactor Godiva and they were transferred pneumatically to the delayed neutron detector. The neutron detector was a long-counter, its efficiency determined by a number of (α,n) and (γ,n) neutron sources. The detector response was flat to within 5%. The sample-detector arrangement was enclosed in a neutron shield (saturated boric acid).

The number of fissions in a sample was determined by activation analysis. The Mo^{99} fission product was chemically separated from the sample and the 67 hr β-activity of a known aliquot was measured. A primary calibration of the number of fissions in a thin fissile foil of known mass against Mo^{99} β-activity from a thick foil of known mass, both foils having been irradiated in the same flux, determined the conversion factor of β-activity of Mo^{99} into fissions.

The absolute yield of the delayed neutrons was determined by instantaneous irradiation. The U^{235}, U^{238} and Pu^{239} absolute yield of the delayed neutrons was found equal to $.0167 \pm .0016$, $.0421 \pm .0043$, $.0064 \pm .0007$, respectively (fast effect correction of Godiva spectrum applied, Tuttle [9]).

Six groups of delayed neutrons were found necessary and sufficient to represent the delayed neutron emission decay curve, using the least squares technique. Since the delayed neutron count rate following an instantaneous irradiation is weighted by the decay constant, it is advantageous to use an instantaneous irradiation to determine the group constants of the short-lived groups and a saturation irradiation to determine the group constants of long-lived groups.

The group constants of the two longest-lived groups were determined by saturation irradiations. The delayed neutron emission decay curve after a saturation irradiation was approximated by four exponentials, for times higher than an appropriate value.

The detection count rate due to these two groups was subtracted from the delayed neutron emission decay curve following the instantaneous irradiation and four groups were fitted to the residuals.

Masters et al[5] 1969

Krick and Evans[6] 1972

Evans et al[7] 1973

The irradiation facility used in this work was an accelerator. The sample was irradiated for a short time, then, the neutron source was switched-off (deflection of charged beam) and the neutron counter detected delayed neutrons. This cycle is repeated with a period much shorter than the shortest delayed neutron group half-life. The sample is irradiated, initially, for a long time, without any delayed neutron counting. When saturation irradiation is achieved, the previously described periodic irradiation-counting process starts. Effectively, this technique is equivalent to the delayed neutron count rate measurement immediately after a saturation irradiation.

The sample was sandwiched between two fission chambers, loaded with deposits of known masses which were used to determine the number of fissions in the sample.

The neutron detector was a modified long-counter and its efficiency was measured using a number of sources. The response of the detector was flat to within 2%. The delayed neutron efficiency of the detector was determined by the ^{238}Pu-Li neutron source (E_{av}=.65 Mev).

We should recall that Masters et al[5] state that the detector efficiency was sensitive to the source position at a detector-sample distance of 11 inches.

Krick and Evans[6] used the previously described design to study the variation of the absolute yield of delayed neutrons with fissioning neutron energy. The yield of the delayed neutrons of U^{235} and U^{238} was independent of the neutron energy up to 5 Mev, where it decreased steeply with energy. The delayed neutron yield of Pu^{239} was independent

of the neutron energy up to 2 Mev(maximum studied).

Masters et al[5] and Krick and Evans[6] measured the absolute delayed neutron yields. These values have been revised by Evans et al[7] following a recalibration of the ^{238}Pu-Li neutron source and a recalibration of the masses of the deposits of the fission chambers. These revised values are summarised below.

Reference	Absolute delayed neutron yield		
	U^{235}	U^{238}	Pu^{239}
Masters et al[5] (3.1 Mev fission)	.0172 ± .0013	.0484 ± .0036	.0066 ± .0005
Krick and Evans[6] (.1 ÷ 1.8 Mev fission)	.0163 ± .0013	—	.0062 ± .0005

Cox[8] 1974

An accelerator, in the pulsed mode, was used for the irradiation of the samples and the delayed neutrons were counted by 21 BF_3 counters in a slab geometry. The detector efficiency was determined by a Ra-Be source and fissions were determined by fission chambers loaded with calibrated deposits.

Four energies of neutrons (up to 4 Mev) have been used and the mean absolute yield of the delayed neutrons (values published by Tuttle[9]) of U^{235}, U^{238} and Pu^{239} was found equal to .0167 ± .0010, .0434 ± .0026 and .00661 ± .00043, respectively.

1.3 Period-Reactivity relationships

Keepin[10] shows that the neutron population n(t), following a a step change in reactivity of a critical reactor at t=0, is

$$n(t) = \sum_{j=1}^{7} N_j e^{t/T_j} \qquad (1.1)$$

where $T_j (j=1, \ldots, 7)$ the solutions of the inhour equation

$$\frac{\Delta K}{k\gamma\beta} = \frac{1}{k\gamma\beta T_j} + \sum_{i=1}^{6} \frac{(\gamma_i \beta_i / \gamma\beta)}{1+\lambda_i T_j} \qquad (1.2)$$

assuming a six group structure for the delayed neutrons of the single isotope fueled reactor.

The quantities of equation (1.2) are,

K = multiplication factor of perturbed reactor

$\frac{\Delta K}{k\gamma\beta}$ = inserted reactivity in dollars

l = prompt neutron lifetime

β_i = delayed neutron fraction of group i

$\beta = \sum_{i=1}^{6} \beta_i$ = total delayed neutron fraction

γ_i = effectiveness of group i

$\gamma = \frac{1}{\beta} \sum_{i=1}^{6} \gamma_i \beta_i$

λ_i = decay constant of group i

The effectiveness factors γ_i (equation 6-9, reference 10) are characteristics of a particular reactor (flux and adjoint flux of unperturbed system) and are calculated using the delayed neutron group spectra and the prompt neutron spectra. Keepin[10] has shown that for bare metal assemblies it is reasonable to assume that $\gamma_i = \gamma$ (except for the first group which has a much softer spectrum than the other groups) and he has argued that the $1/k\gamma\beta T_j$ term of the equation (1.2) is negligible for most operating conditions of fast reactors.

So, equation (1.2) is written as,

$$\rho = \sum_{i=1}^{6} \frac{\alpha_i}{1+\lambda_i T_j} \qquad (1.3)$$

where ρ is the inserted reactivity and α_i is the relative abundance of group i.

The reactor period T is the unique positive T_j when the reactivity is positive or the minimum T_j (j=1,..,7) when the reactivity is negative.So, the neutron population of a reactor following a step change in reactivity is given by

$$n(t) \approx Ne^{t/T} \qquad (1.4)$$

for times t large enough so that the transients will die out.

The equations (1.3) and (1.4) are being extensively used for control rod reactivity calibration. Keepin[10] has examined the useful range of periods for the experimental calibration of control rods. Negative periods are not being used because of the long waiting times and the large propagation of error from period to the reactivity (especially for $T \to -1/\lambda_i$). Positive periods are being used from a few cents (power drift limit) to half a dollar reactivity (safety limit).

Keepin[10] has described two techniques for the period-reactivity calculation which do not make use of the fictitious group constants, namely, the rod-drop method and the prompt-burst delayed neutron decay data method (Laplace method).

If f(t) is the delayed neutron count rate following an instantaneous irradiation then,

$$\rho(T) = 1 - \int_0^\infty f(t) e^{-t/T} dt \qquad (1.5)$$

assuming that

$$\int_0^\infty f(t)dt = 1 \qquad (1.6)$$

The equations (1.5), (1.6) describe the Laplace method of calculating the reactivity-period relationship.

1.4 Reactivity worth calculations

The absolute reactivity worth ($\Delta k/k$) of small samples, introduced into a reactor, is calculated by perturbation theory (Lamarsh[2]) while it is experimentally determined through the control rod calibration (section 1.3).

The calculated central reactivity worths of small samples, introduced into existing fast assemblies, are higher than the experimentally determined ones using the data of Keepin et al[4]. The criticality of these assemblies is verified theoretically, and the per atom fission ratio calculations are in good agreement with experiments.

Little and Hardie[11] have reported and examined these discrepancies and they have suggested that the delayed neutron data are a likely source of error.

Tuttle[9] has evaluated the existing measurements on delayed neutrons and the values suggested for the absolute yield of the delayed neutrons (higher than those of Keepin[10]) should reduce the discrepancies.

1.5 The object and a brief description of the present measurements

Since the delayed neutron data in fast fission are a likely source of error, a programme was initiated at the A.W.R.E., Aldermaston, to determine the absolute delayed neutron yield and group constants from the fast fission of U^{235}, U^{238} and Pu^{239}.

The sample was irradiated in the pulsed fast reactor VIPER (instantaneous irradiation) and it was transferred pneumatically to the neutron detection system. This detection system was placed in a low background area.

The neutron detection system consisted of a polythene cylindrical moderator, the thickness of which was optimised so that a flat response could be achieved, and of two slow neutron scintillation counters which were displaced 180 degrees apart. The sample was arrested at the axis of the cylindrical moderator by a polyurethane cylindrical stopper.

The efficiency of a single neutron counter was very sensitive with the radial position of a Cf source, within the flight tube at the arrest position of the sample. This is consistent with the argument of Masters et al[5] (section 1.2) because, the sample-counter distance was very short. However, it was found that the efficiency of the detection system, consisting of two counters and displaced by 180 degrees, was insensitive to the radial position of the source to within an acceptable error.

The detection efficiency was studied by a number of (γ,n) and (α,n) neutron sources. The detection efficiency for the delayed neutrons was determined by the Am-Li source because, the spectrum of this source is similar to that of the delayed neutrons.

The fissions in the sample were measured by an activation technique. The 1596 kev La^{140} gamma activity of the sample was measured by a Ge(Li) detector. A thick foil and a known mass thin deposit were irradiated in a demountable fission chamber, at the same position as the sample. The counting of the fissions in the deposit and the counting of the 1596 kev activity of the foil provided the calibration factor for converting the 1596 kev gamma activity into fissions. The

deposit masses were also determined in this work.

The delayed neutron emission decay curve, because of the instantaneous irradiations, was measured. An ARGUS-500 on-line computer was used to multiscale the time intervals over which the delayed neutron counts were accumulated. Then, this delayed neutron emission decay curve was approximated by six groups, using the least squares technique to determine the delayed neutron group constants. A number of other techniques were used to support the least squares method. The reactivity (dollars) - period relationship was directly (numerically) calculated from the prompt burst irradiation data (Laplace method) and the fictitious group constants were checked to see if they were capable of adequately preserving this information.

The programme was initiated by Clifford[12] who designed and used one of the present counters to measure the absolute yield of the delayed neutrons of U^{235} and U^{238} in fast fission.

CHAPTER 2

MASS CALIBRATION OF THE DEPOSITS

In order to measure the number of fissions of a sample irradiated in the VIPER reactor, we have to use deposits of known masses. The mass of the U^{235} and Pu^{239} deposits has to be a few hundred micrograms, otherwise large dead time corrections will be necessary for the calibration experiment (Chapter 4).

Standard AWRE deposits have been used. The masses and isotopic composition of these deposits are given in table (2.1).

In this chapter, we describe the method used to determine the mass of the Pu^{239} deposit; this mass determination was particularly necessary because, the backing of the deposit was slightly bent.

The ULRC double fission chamber was used to irradiate the U^{235} and Pu^{239} deposits in the NISUS-1B assembly, simultaneously. Azimi[13] has measured the NISUS-1B per atom fission ratio of these isotopes, using standard deposits of the National Bureau of Standards. Furthermore, the per atom fission rate of each isotope has been calibrated against the count rate of two permanently installed monitors, using the N.B.S. deposits.

2.1 The Double Fission Chamber

The demountable double fission chamber used in this experiment is given in figure (2.1). The deposits are mounted back-to-back, between two square aluminium plates, with holes larger than the area of the deposits. The aluminium plates are fitted into a groove, so that both deposits will face the anodes. The backings of the deposits

TABLE 2.1 DEPOSIT CHARACTERISTICS

ISOTOPIC COMPOSITION OF DEPOSITS* (atomic)

CONSTITUENT ISOTOPE	ISOTOPIC COMPOSITION		
	U^{235} (71/4)	U^{238} (71/7)	Pu^{239} (71/1)
U^{234}	.0114	.00000347	
U^{235}	.9271	.000354	
U^{236}	.00229	.00000032	
U^{238}	.0592	.99964	
Pu^{239}			.9990
Pu^{240}			.0010
Pu^{241}			traces

*Uncertainty ±7%

MASS OF THE MAIN ISOTOPE IN DEPOSIT

DEPOSIT	MASS (μgm)
U^{235} (71/4)	129.1 ± 1.3%
U^{238} (71/7)	1270 ± 1.5%
Pu^{239} (71/1)	112.8 ± 1.3%

TABLE 2.1(a) BASIS OF CLAIMED DEPOSIT MASSES

Deposit No.	Mass of principal isotope (μg)	Method
U235 No. 71/4	128.3	Low geometry alpha assay[c] (Smith)[1]
	126.4	14MeV fission counting (σ_F=2.17b) (Smith)[1]
	127.6	Intercomparison with T4[a] [c] (Smith)[1]
	127.9	Intercomparison with NBS 25S-2-3
	127.6 ± 1.7	Mean
U238 No. 71/7	1280	14MeV fission counting (σ_F=1.13b) (Smith)[1]
	1285	Intercomparison with Winfrith foils[b] [c] (Smith)[1]
	1276	Intercomparison with NBS 28HD-5-1
	1280 ± 20	Mean
Pu239 No. 71/1	112.3	Low geometry alpha assay[c] (Glover)[2]
	112.9	Low geometry alpha assay[c] (Smith)[1]
	113.2	Low geometry alpha assay[c] (Sweet)[3]
	112.8	Intercomparison with Winfrith foils[b] [c] (Smith)[1]
	113.2	Intercomparison with NBS 49I-1-1
	112.9 ± 1.5	Mean

NOTES: (a) T4 deposit standardised by White[4]

(b) Winfrith foils standardised by Sweet[3]

(c) Data adjusted to be consistent with Vaninbroukx[5]

REFERENCES

(1) Smith, D.L.E. A.W.R.E., Aldermaston. Private Communication (1974)

(2) Glover, K.M. Preparation and Calibration of alpha active sources of the actinide elements. Conf. on Standardisation of Radionuclides, I.A.E.A., Vienna (1967)

(3) Sweet, D., A.E.E.W., Winfrith. Private Communication, (1974)

(4) White, P.H., A.W.R.E., Aldermaston. Private Communication, (1969).

(5) Vaninbroukx, R. Half life of some Long Lived Actinides, a compilation. EUR 5194e. (1974)

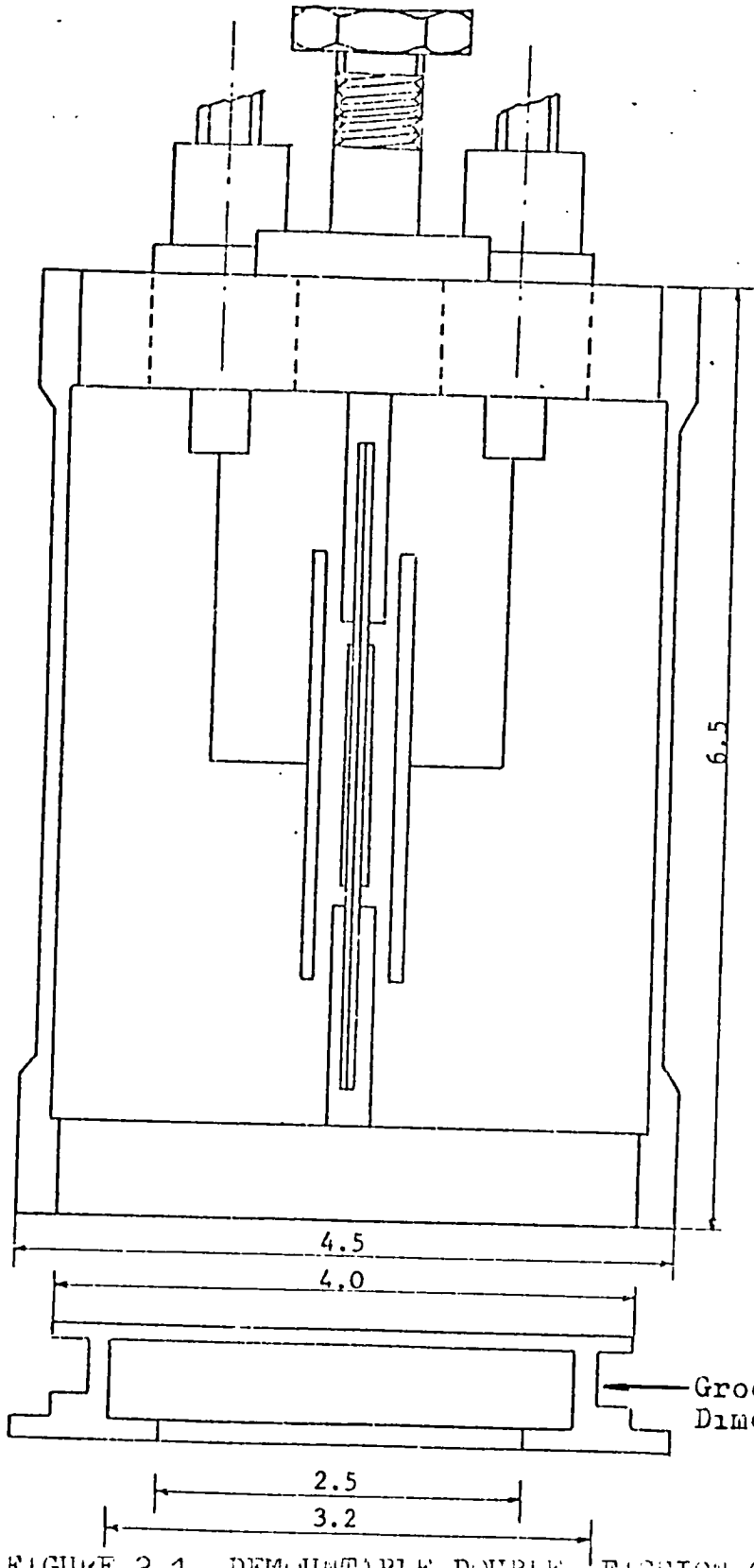

FIGURE 2.1 DEMOUNTABLE DOUBLE FISSION CHAMBER

are the common cathode of both chambers. The anodes are disks with diameter larger than the diameter of the deposits so that, edge effects will be minimised.

The counters are filled with 90% argon and 10% methane at a pressure of 1 atmosphere above atmospheric pressure. The counter was outgassed (pressure .01 Torr) and filled three times, so that the air content will be minimised. The filling and outgassing are performed through a nitrogen trap, so that no oil vapour will reach the deposits.

The deposits have a diameter of 28mm and they are deposited on a platinum backing of 39 mm diameter. They are oxides of the type X_3O_8.

2.2 Irradiation environment, NISUS-1B

The NISUS-1B assembly has been used for the irradiation of the double fission chamber. Besant et al[14] have described the NISUS facility, and a brief description is given below.

A spherical cavity (diameter 50cm) has been hollowed out of a graphite cube (60x60x60 cm^3). Within this spherical cavity, two concentric shells have been placed. The outer shell is made of natural uranium (I.D. = 157.48 mm, O.D. = 254.0 mm) and the inner shell is made of Boron Carbide (I.D. = 123.4 mm, O.D. = 157.4 mm). The internal spherical cavity is the irradiation facility. The NISUS subcritical assembly is placed within a thermal collumn of the reactor CONSORT. Two independent fission chambers have been permanently placed in the graphite stack for monitoring purposes.

Access into the irradiation cavity is achieved through a hole in the graphite stack and the uranium-boron shells. When the detector has been fully inserted into the cavity, a graphite plug and a

uranium plug fill up the hole in the graphite and complete the uranium shell, respectively. An aluminium tube supports the detector and uranium plug onto the graphite plug. The EHT-signal cables go through the graphite plug's hole and through the aluminium tube.

Thermal neutrons can reach the internal cavity streaming through the Boron-carbide shell's cladding, as well as, through the aluminium tube. This effect can cause errors in calculating the per atom fission ratio of a threshold and non-threshold reaction . For this reason Azimi[13] has used a Cd-shield to cut off the streaming. Since this experiment will use the results of Azimi's measurements, we have used the same shield so that, we will reproduce the irradiation environment. Figure (2.2) gives the basic features of the irradiation environment for this experiment.

2.3 Electronics

Figure (2.3) gives the electronics which have been used for one side of the double fission chamber and for one of the fission chamber monitors. For each side of the double fission chamber, there are three differential (in time) scalers. Each monitor has a differential scaler and an integral scaler. The eight differential scalers are controlled by the same timer unit, so, the eight measurements are obtained under identical conditions. Grundl et al[15] have suggested the use of three differential scalers, for each side of the double fission chamber, and the reason will be given later.

2.4 Setting of the electronics

The efficiency of this fission chamber is less than one because of the discrimination bias and self absorption of the deposit. So, a

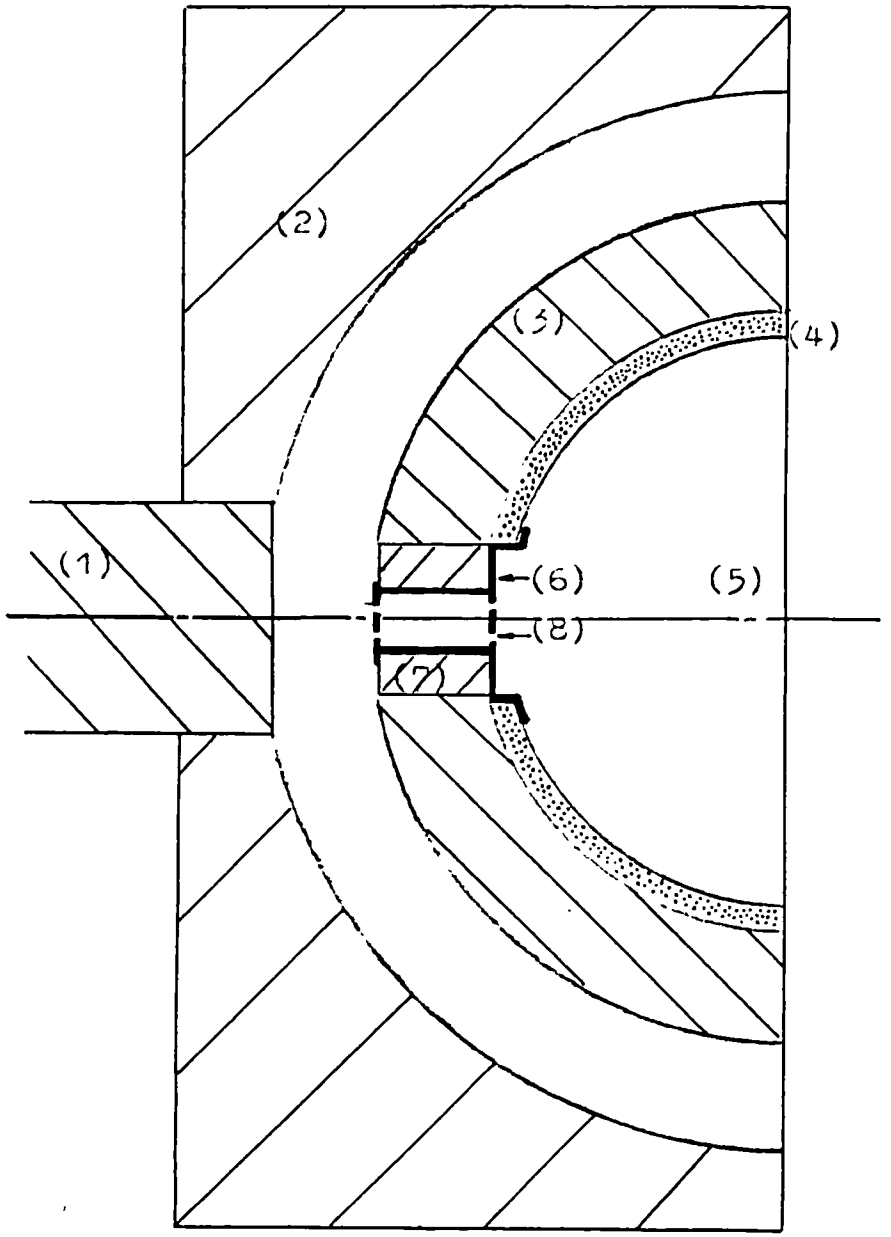

FIGURE 2.2 IRRADIATION ENVIRONMENT

(1) Graphite plug
(2) Graphite cube
(3) Uranium shell
(4) Boron carbide shell
(5) Irradiation cavity
(6) Cadmium shield
(7) Uranium plug
(8) Holes in cadmium for cables

correction has to be made for these effects.

The energy spectrum of the fission fragments, obtained by a fission chamber, has the following features.

1. At very low energies pulses are due to α-particles, gamma rays and electronic noise. So, there is a sharp decrease of the spectrum with increasing energy.

2. At higher energies, there is a plateau followed by a double-peak (assuming large distances between the cathode-deposit and the anode) which are due to the fission fragments.

Figure 2.7 shows a typical spectrum, where the previous features are obvious.

It is apparent that the discriminator has to be set on the plateau, so that, we will discriminate against the noisy pulses and so that the recorded counts will be insensitive to gain and discriminator level instabilities. A correction is made for the unrecorded fission fragments (Extrapolation to Zero bias).

For each side of the double fission chamber two discriminators are set on the plateau of the energy spectrum so that, the previously mentioned correction can be calculated. The third discriminator is used as a gain sensitive indicator . The technique used to set the discriminators, for each side of the double fission chamber, is described below.

The energy spectrum of the fission fragments was obtained, connecting the output of the main amplifier to the multichannel analyser (through a wide band amplifier). The output pulses of the main amplifier were observed with the oscilloscope (figure 2.3). The shape of the pulses, due to fission fragments, was obtained. Then, a BNC pulser was connected

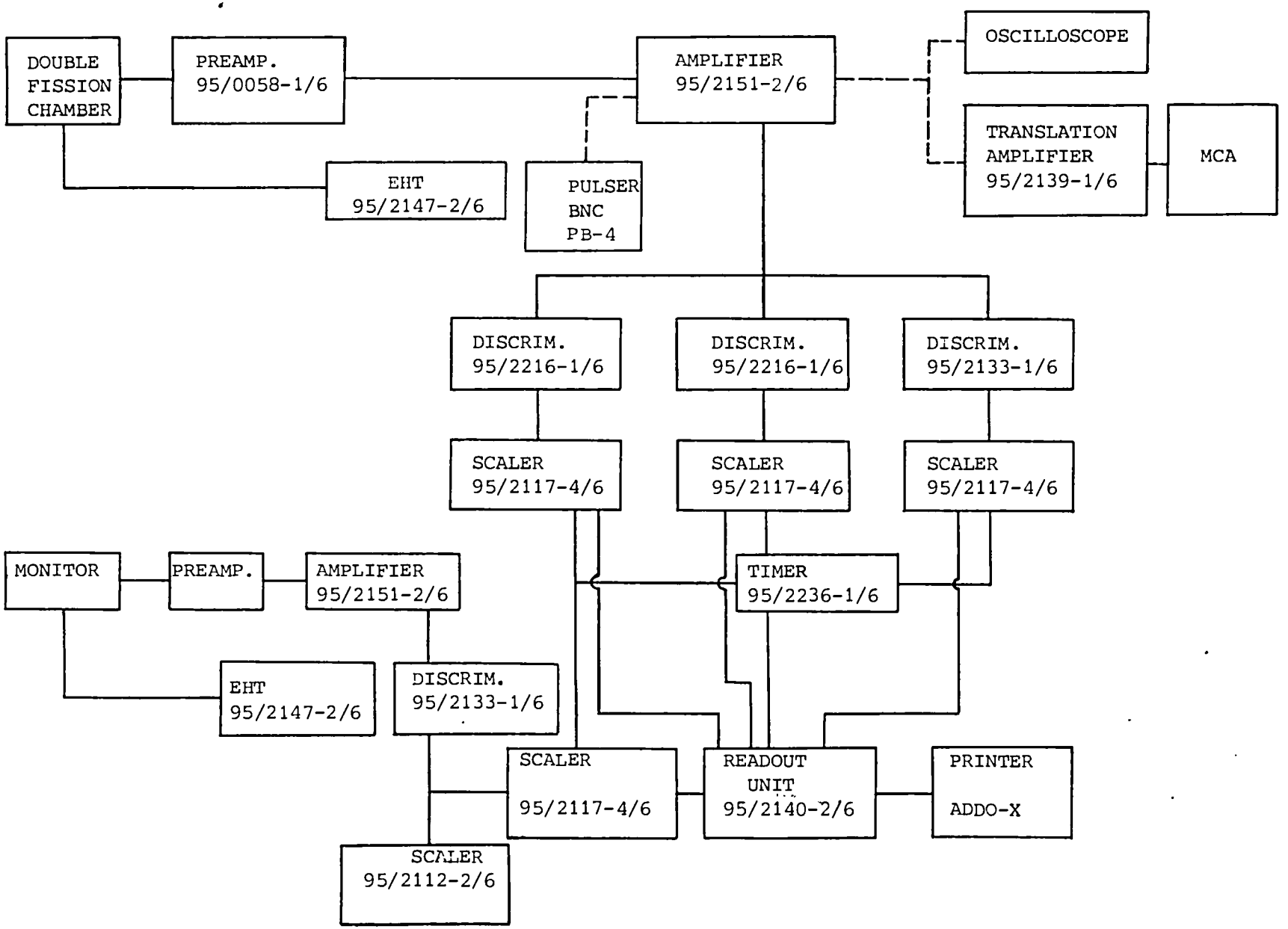

FIGURE 2.3 ELECTRONICS FOR ONE SIDE OF THE DOUBLE FISSION CHAMBER AND FOR A MONITOR

FIGURE 2.4 ELECTRONICS FOR GATED SPECTRUM OF MONITORS

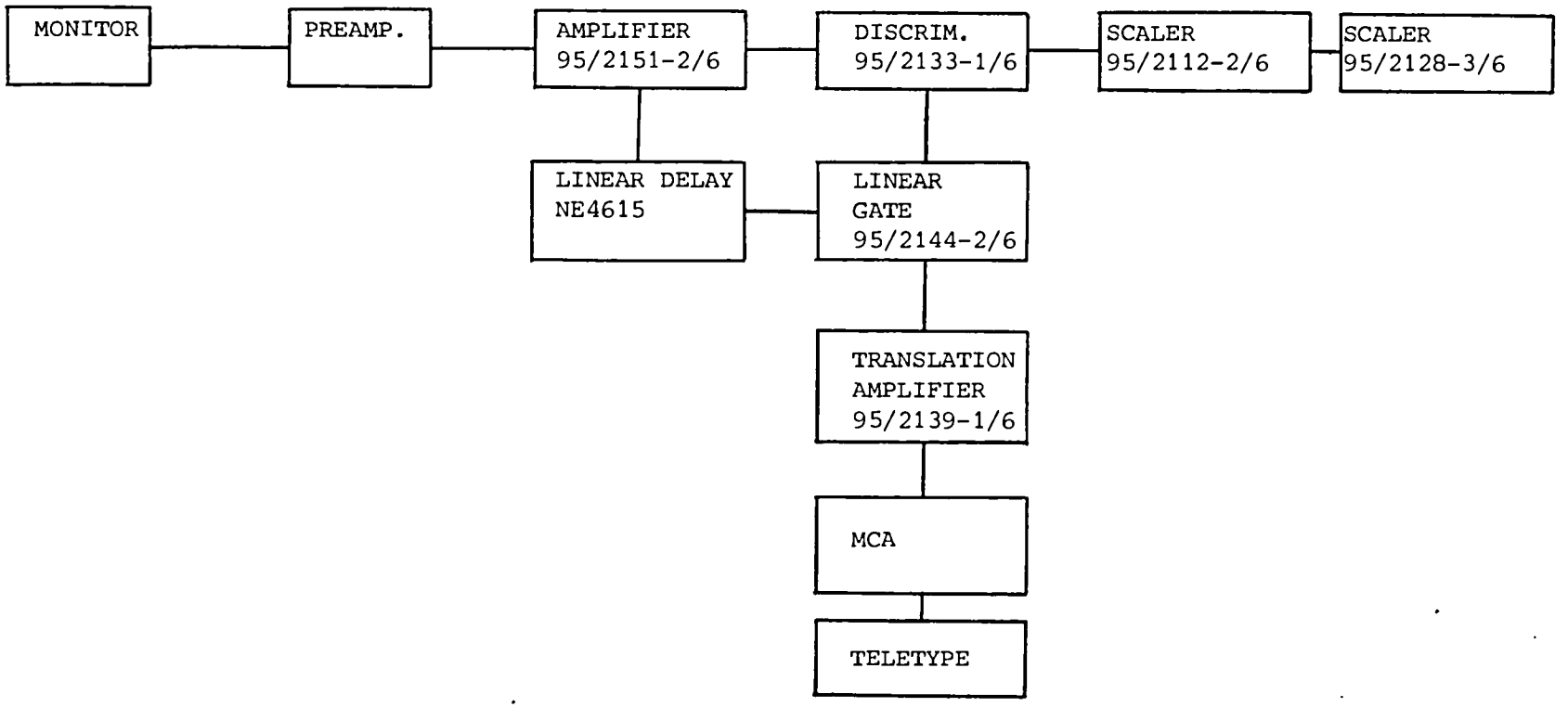

to the input of the amplifier (the preamplifier can not be reached) and the shaping of the output pulses of the pulser was adjusted so that, the pulses observed on the oscilloscope had a similar shape with those due to the fission fragments. The necessary pulser shaping was t_r (rising time) = .1μs and t_f (falling time) = 200μs, the latter being consistent with the long differentiation time constant of the preamplifier (100μs). The following work was done using this shaping.

The voltage output of the pulser was adjusted (V_{PEAK}) so that the pulses, observed on the multichannel analyser, coincided with the peak channel of the fission fragment energy spectrum. Then, three voltages were selected on the pulser $V_L = .36V_{PEAK}$, $V_v = .54V_{PEAK}$ and $V_{GC} = 1.40V_{PEAK}$. Each discriminator was set very carefully at such a level so that, only pulses higher or equal to the previous levels (at the input of the amplifier) will be recorded by the corresponding scalers.

Let S_L, S_V, S_{GC} be the number of pulses which exceed V_L, V_V and V_{GC} at the input of the amplifier, respectively. The S_L counts is the number of counts used to determine the number of fissions while, the S_V counts are used to take into account the unrecorded number of fissions (extrapolation to zero bias). So, both discriminator levels should be on the plateau of the fission fragment spectrum. The channels of the multichannel analyser, corresponding to V_L and V_V voltages of the pulser were recorded. They are shown in figure (2.7) and it is apparent that they are on the plateau.

The monitor will detect fission fragments with energies higher than the discriminator level. The fraction of unrecorded fission fragments depends on the gain of the amplifier and the discriminator level.

FIGURE 2.5 MONITOR 1 GATED SPECTRUM

1. C,D are the peak channels.
2. Counts at E channel are half the counts at D channel.
3. Counts at A channel are half the counts at the plateau.
4. Counts at B channel are equal to the mean counts of channel C and plateau.

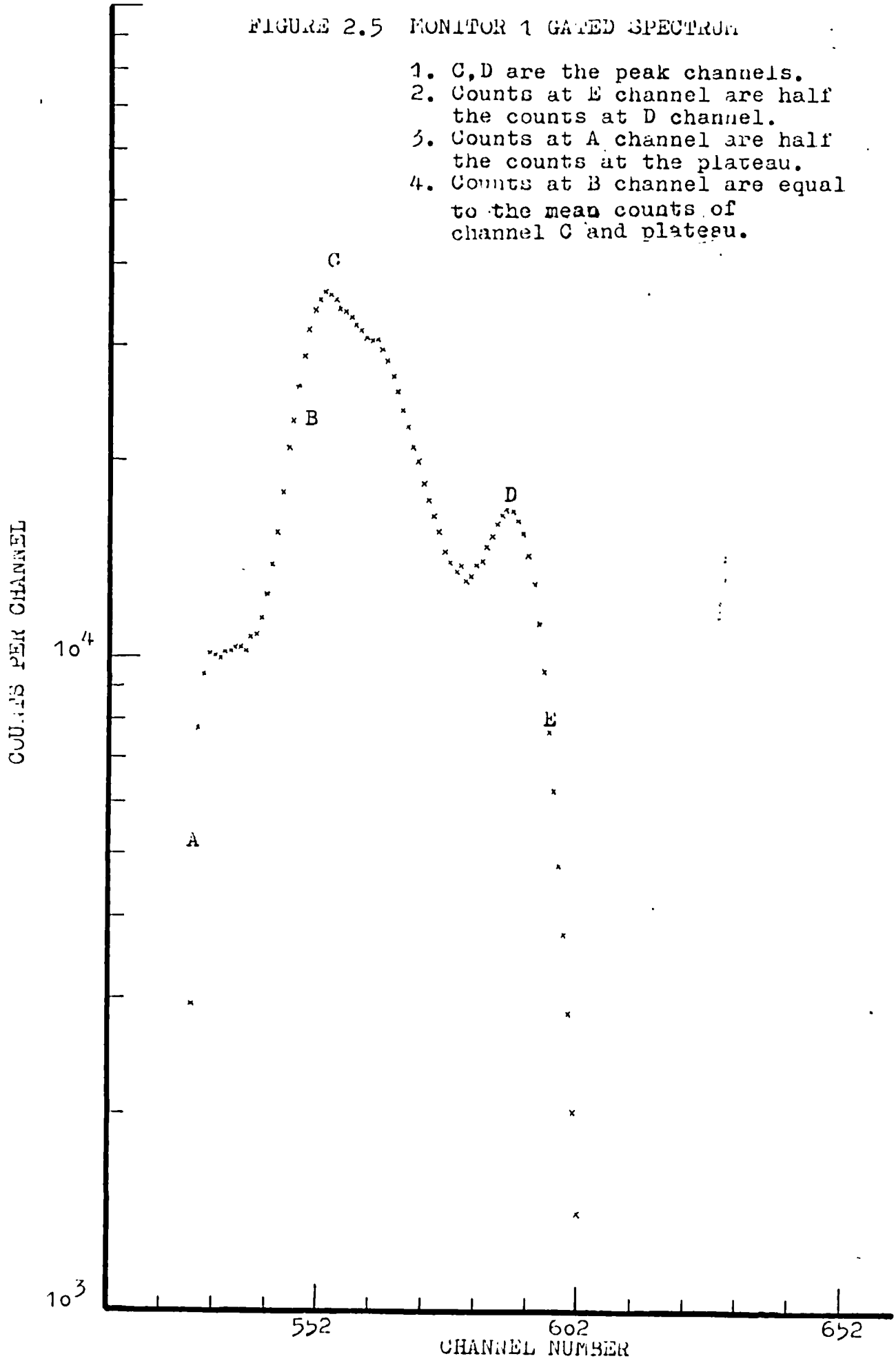

FIGURE 2.6 MONITOR 1 DISCRIMINATOR SETTING

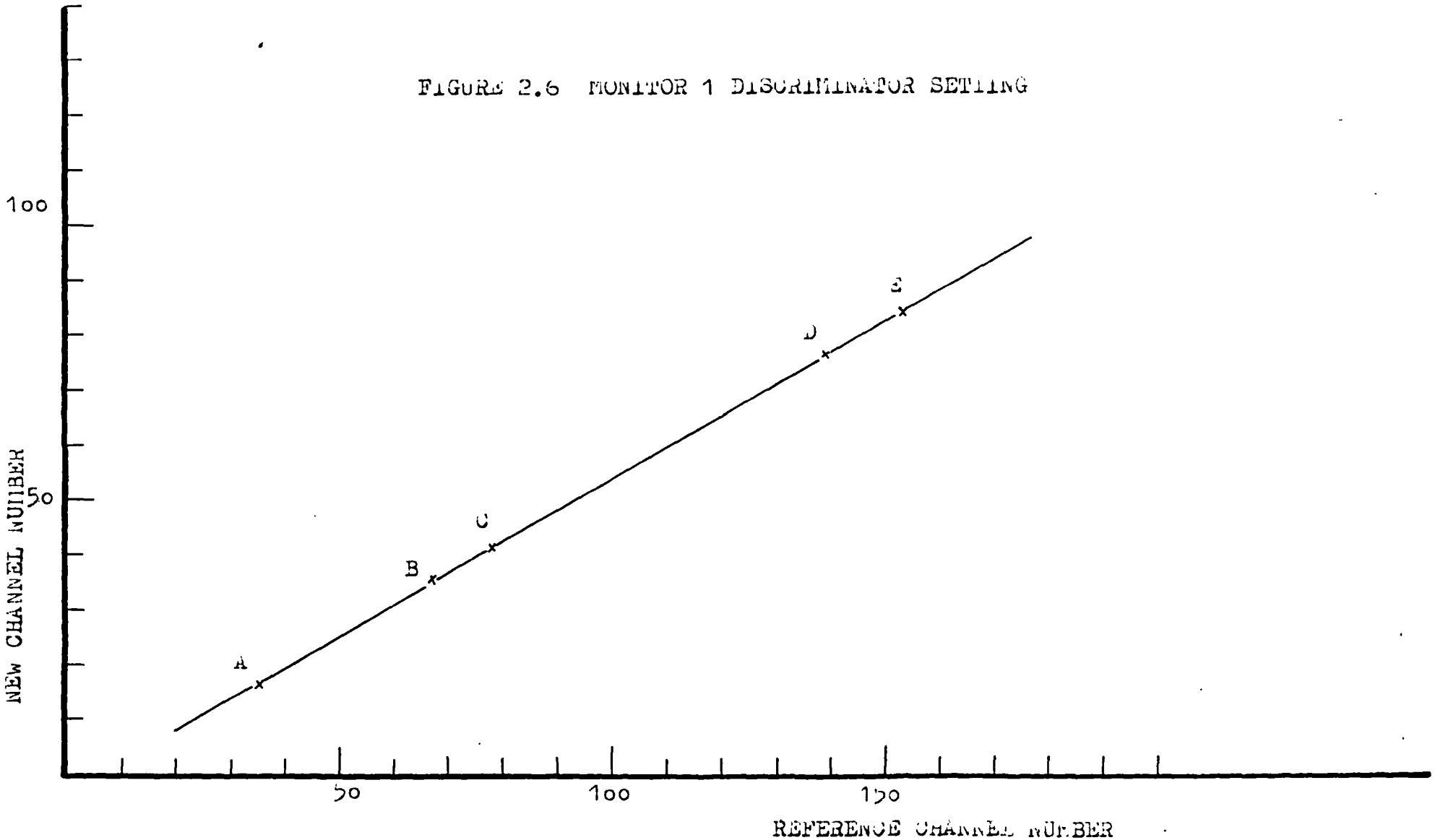

FIGURE 2.7 SPECTRUM OF FISSION FRAGMENTS AND SETTINGS OF DISCRIMINATORS (U-235 chamber)

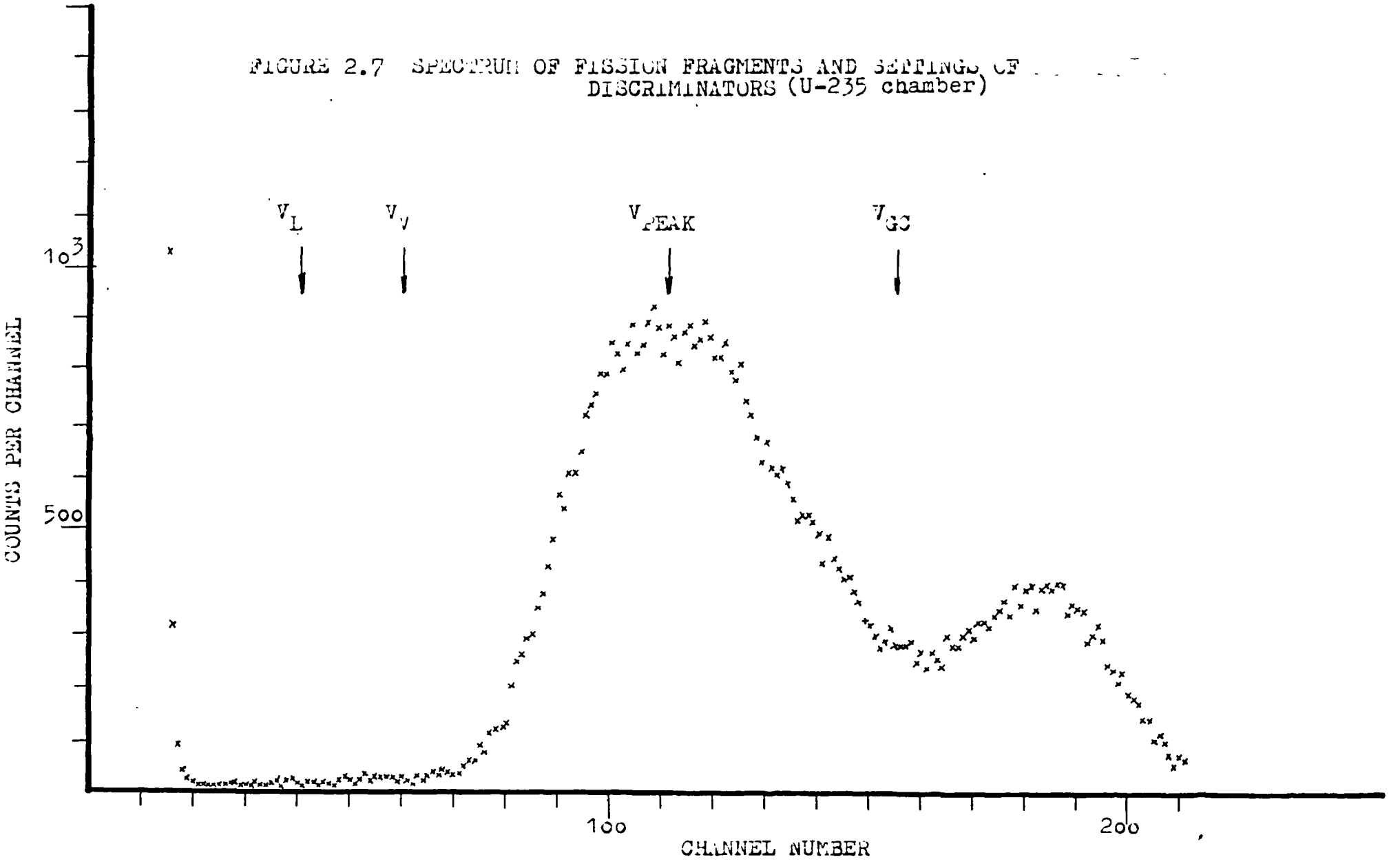

Standard settings were used [16] and a technique developed by Williams[16] was employed to adjust for any drifting of the electronics.

The electronics used for this adjustment are given in figure (2.4). The obtained gated spectrum (figure 2.5) does not show the noisy pulses because the discriminator level has been set at the previously mentioned plateau. The gate opens by the output signal of the discriminator. Five standard points are selected on the spectrum and the corresponding channel numbers are read off (figure 2.5). This new set of channel numbers was plotted against the reference set and the discriminator level has been adjusted so that the point A will be on the straight line determined by the points B, C, D, E. The result of this work is shown in figure (2.6).

2.5 Experiment and corrections

The timer was set at 600 sec and the S_L, S_V, S_{GC} quantities were obtained at the end of the counting time, for each side of the double fission chamber. Also, the measurements of the two monitors were obtained at the end of each counting period. Twenty-two measurements were obtained and they are given in table (2.2). We can see that the measurements are consistent within the statistical errors, except of S_{GC} for the Pu^{239} chamber. Since the ratio S_L/MONITOR 1 is constant (to within the errors) we conclude that there is a continuous increase of the discriminator level of S_{GC}, for this particular experiment, for the Pu^{239} chamber.

The corrections necessary for this experiment are listed below;

1. Extrapolation to zero bias

The counts S_L have to be corrected because of the discriminator level. Assuming a flat plateau, the necessary correction is $2(1- {}^{S}V/S_L)$ because of the relationship between V_L and V_V.

2. Fission fragment absorption

Fission fragments, stopped within the deposit, do not cause ionisation in the filling gas, thus they are not being detected. Assuming a thin deposit of infinite area, the correction is t/2R where t is the thickness of the deposit and R is a yield weighted mean range of the fission fragments. Grundl et al[15] have suggested the value of 7.74mgm/cm² for R. An uncertainty of .35% or .25 of the correction (whichever is higher) has been suggested for this correction, too.

3. Dead time losses

The count rate is 65 c/sec so that no correction has been applied.

4. Impurity fissions

These are fissions caused in isotopes other than the main isotope of the deposit.

A summary of the corrections is given in table (2.3).

2.6 Results and discussion

Williams[16] compared the mass of the U^{235} and U^{238} deposits, with the reference deposits of NBS. The masses of these deposits were measured and are as follows:-

AWRE U^{235} deposit mass = 127.9 ± 2 μgm

AWRE U^{238} deposit mass = 1276 ± 22 μgm

The Pu^{239}/U^{235} per atom fission ratio in NISUS-1B was found[13] to be 1.177 ± 2.06%, using the NBS deposits. So,

AWRE Pu^{239} deposit mass = 113.2 ± 3 μgm

There is a good agreement between these values, for the masses of the deposits, and the values provided by the AWRE (table 2.1). So, the AWRE values have been used.

TABLE 2.2 CALIBRATION EXPERIMENT OF Pu^{239} DEPOSIT

MONITOR 1	MONITOR 2		U^{235} CHAMBER					Pu^{239} CHAMBER				
COUNTS / 600 SEC	COUNTS / 600 SEC	MONITOR 1 / MONITOR 2	S_L	S_V	S_{GC}	S_L/S_V	S_L/MONITOR 1	S_L	S_V	S_{GC}	S_L/S_V	S_L/MONITOR 1
			COUNTS/600 SEC					COUNTS/600 SEC				
809164	336389	2.4054	38999	38645	6614	1.0092	.04820	39825	39570	4770	1.0064	.04922
806575	334647	2.4102	38703	38400	6575	1.0079	.04798	39559	39334	4648	1.0057	.04905
807524	335776	2.4049	38840	38524	6655	1.0082	.04810	39421	39203	4605	1.0056	.04882
808214	336281	2.4034	38591	38306	6448	1.0074	.04775	39707	39484	4410	1.0056	.04913
809164	335891	2.4090	38564	38256	6520	1.0081	.04766	39748	39501	4348	1.0063	.04912
808569	336988	2.3994	38648	38336	6307	1.0081	.04780	39671	39421	4332	1.0063	.04906
811079	336739	2.4086	38884	38579	6400	1.0079	.04794	39768	39546	4230	1.0056	.04903
808758	337664	2.3952	39082	38746	6512	1.0087	.04832	39330	39085	4201	1.0063	.04863
807321	337324	2.3933	38836	38523	6606	1.0081	.04810	39142	38899	4050	1.0062	.04848
809865	335475	2.4141	38835	38552	6442	1.0073	.04795	39867	39624	4226	1.0061	.04923
807302	336775	2.3972	38762	38472	6511	1.0075	.04801	39979	39738	4172	1.0061	.04952
810569	336326	2.4101	38972	38692	6400	1.0072	.04808	39543	39298	4110	1.0062	.04878
809065	336073	2.4074	38771	38448	6532	1.0084	.04792	39846	39591	4000	1.0064	.04925
808825	334640	2.4170	38620	38305	6456	1.0082	.04775	39704	39437	3898	1.0068	.04909
810217	336126	2.4105	38899	38587	6520	1.0081	.04801	39679	39448	4076	1.0059	.04897
808817	334439	2.4184	38736	38398	6442	1.0088	.04789	39718	39502	3970	1.0055	.04911
811153	335633	2.4168	38908	38589	6523	1.0083	.04797	39826	39612	3788	1.0054	.04910
811502	336408	2.4123	39054	38774	6415	1.0072	.04813	40007	39765	3792	1.0061	.04930
809870	335658	2.4128	38866	38550	6478	1.0082	.04799	39650	39394	3837	1.0065	.04896
809131	335248	2.4135	38880	38570	6603	1.0080	.04805	39689	39447	3783	1.0061	.04905
810560	336667	2.4076	38805	38497	6406	1.0080	.04787	39626	39402	3777	1.0057	.04889
809682	335857	2.4108	38724	38418	6273	1.0080	.04783	39480	39232	3853	1.0063	.04876
±899	±579	±.0049				±.0072	±.00025				±.0071	±.00025
		AVERAGE 2.4081 ±.0010				AVERAGE 1.0080 ±.0015	AVERAGE .04797 ±.00005				AVERAGE 1.0061 ±.0015	AVERAGE .04903 ±.00005

TABLE 2.3 CORRECTIONS APPLIED FOR THE Pu^{239} MASS CALIBRATION EXPERIMENT

Correction	U^{235} CHANNEL	Pu^{239} CHANNEL
Extrapolation to zero bias	1.016 ± .30%	1.012 ± .30%
Fission fragment absorption	1.001 ± .35%	1.001 ± .35%
Impurity fissions	.994 ± .20%	1.000

The U^{235} per atom fission rate per count rate of monitor-1 is $1.479\ 10^{-19} \pm .50\%$ and Azimi[13] gives this value equal to $1.493\ 10^{-19} \pm .22\%$, the errors being only statistics since the same deposit has been used. We conclude that the present irradiation environment is identical to that of the reference measurements.

CHAPTER 3

THE DELAYED NEUTRON MEASUREMENTS

In this chapter, we will describe the characteristics of the irradiation facility and delayed neutron detection system used for the delayed neutron measurements.

3.1 The irradiation facility

The instantaneous irradiation, which was used in this work, was simulated by the pulsed reactor VIPER[17]. The core of this reactor consists of a central fixed section and two movable sections, so that, the overall geometry is approximately cylindrical. The core is completely surrounded by copper. The reactor has a central pulsed fuel rod which is inserted completely into the reactor core within 220 msec, its reactivity worth being 1.27 dollars.

The fuel elements of the reactor are made of enriched uranium (37.5%) alloyed with molybdenum (1.25%). The space between the fuel elements is filled up with alternate layers of copper and epoxy resin moderator thus, the neutron spectrum being similar to the neutron spectrum of a fast reactor. The reactor does not have any cooling system and for this reason it is operated normally once (maximum twice) per day.

The irradiation position is the large irradiation cavity in the south side of the reactor. The sample irradiation position and the irradiation position of the double fission chamber (chapter 4) are shown in figure 3.1. Figure 3.2 gives the neutron energy spectrum appropriate for the present irradiations.

The reactor operates in the steady-state mode (calibration experiment, chapter 4) and as a pulsed neutron source (sample irradiation for delayed neutron measurements). The maximum allowed neutron fluence is determined by the maximum allowed heat production. The basic features of the pulsed mode operation are described below.

A movable section of the core is lowered, so that, the reactor becomes subcritical. The reactor remains in this state for fifteen minutes, so that, the existing neutron population will diminish. Then, the movable section is restored to its normal position thus the core being completed. Then, the pulsed fuel rod is shot into the reactor core, the reactor being supercritical. The pulse size of the reactor is determined by the excess reactivity, the 1.27 dollars worth of the pulsed rod corresponding to a full size pulse. Four boron loaded control rods are used to adjust the excess reactivity of the reactor (before the fuel rod shooting) for lower size pulses. When the rod is fully inserted into the core, a neutron source of very short duration is fired into the reactor (accelerator) and the neutron population is self-multiplied in the supercritical assembly.

The neutron population increases with increasing period because of negative temperature feedback (fuel expansion, U^{238} Doppler effect) and a peak power of 20 GW is achieved. When the power has been reduced significantly, the delayed neutron emission from the core becomes important. In order to reduce their contriburion to less than 10% of the total neutron output, both movable sections of the core start moving 10 m sec after the source firing. So, the resulting pulse is a spike (400 μsec FWHM) followed by a plateau because of the delayed neutron emission. The reactor operation is inherently safe because, the excess reactivity is removed by negative temperature feedback.

A scintillation counter, installed on the north side of the reactor, provides an electric signal when the reactor power is 10Kw. This signal is the basis of the timing of the delayed neutron measurements. The time elapsed between the 10 Kw power signal and the reactor peak power is 1.4 msec[18].

The total number of fissions per gm of U^{235} in the large cavity is 10^{12} (full size pulse) thus, small samples can be irradiated so that, the self-multiplication of the delayed neutrons will be small.

The delayed neutron counters have been placed in a low background area (section 3.4, transient background). Figure 3.3 shows the delayed neutron counters placed outside the irradiation cavity, behind a six ft thick concrete shield.

The irradiated sample is transferred from the irradiation cavity to the neutron counters, pneumatically. The sample is mounted inside a rabbit (Figure 3.4). The rabbit is made of titanium, its internal diameter and thickness being .75cm and .24cm, respectively. Figure 3.4 gives the characteristics of a sample irradiated in a VIPER pulse. We describe the sample in chapter 4 because, its arrangement is determined by the fission measurements.

The pneumatic transfer system[19] is capable of transferring samples of up to 20 gm from the irradiation to the counting position, within 35 msec. This transfer time is much shorter than the shortest delayed neutron group half-life. Figure 3.5 shows the basic features of the operation of the transfer system. Argon gas is admitted between the two "O" rings of the rabbit and the rabbit remains at this position because there is no net force. This equilibrium is disturbed by the firing of a squib which is located behind the rabbit. The squib firing disturbs the equilibrium and the rabbit is shot down the flight tube by the gas.

Three polyurethane cylinders were inserted into the flight tube at the counting position (Figure 3.5). The cylindrical holes of the first two cylinders were used to guide the rabbit in the enlarged diameter flight tube, the rabbit being arrested in the last polyurethane cylinder. For a loaded rabbit of specific mass and for a specific argon pressure, the arrest position of the rabbit was not reproducible. The trace of the rabbit in the polyurethane foam cylinders was used to determine the actual stopping position of the sample (axial efficiency correction). Before each experiment, a test firing of the loaded rabbit was done to determine the expected position of sample arrest, for the particular experiment.

The squib firing was determined by the 10 Kw power signal of the reactor. A variable (up to 50 sec) and predetermined firing delay, between the 10 Kw power signal and the squib firing, was used (section 3.4) to avoid the detector saturation at the early times of counting of a large sample irradiation.

3.2 The neutron detection system

The neutron detector has to satisfy a number of requirements which are either common to all the delayed neutron yield and group constant measurements or which arise because of the particular experimental arrangement.

a) The neutron efficiency of the detector must be independent of the neutron energy, in the energy interval where most of the delayed meutrons are emitted (at least). The main feature of the flat response detectors, which have been designed (Allen[20]), is the thermalisation of the fast neutrons and subsequent detection by a thermal neutron detector. This principle has been used in the design of the present detector.

We have to use a flat response detector for the delayed neutron yield measurement, so that, the uncertainty of the absolute calibration of the efficiency of the detector (because of different energy spectra of the calibration source and delayed neutrons) will be minimised.

b) The absolute neutron efficiency of the detectors must be compatible with the maximum expected delayed neutron count rate (pulse size, maximum allowable sample mass), so that, adequate statistical accuracy can be achieved in a reasonable number of experiments.

c) It is necessary to obtain measurements at times higher than 300 sec after the irradiation, of reasonable statistical accuracy, so that, a successful group analysis can be achieved (section 3.4). Since the delayed neutron count rate decreases by a factor of $2.6\ 10^{-5}$ in the time interval (0, 300 sec), the resolving time of the detection system must be very short so that, a single (ideally) irradiation can be used to cover the whole time interval of interest. This requirement favours the use of scintillation counters.

d) The irradiated sample is highly gamma (delayed) active. So, the detector must be capable of adequately discriminating against gamma radiation.

e) Since there is an obvious uncertainty in the arrest position of the sample in the polyurethane foam, the detector efficiency must be insensitive to the arrest position of the sample.

Generally, the accuracy and feasibility of the measurements will depend on the previously described factors.

The detection system used in this work is shown in Figure (3.6).The electronics associated with the counters are shown in Figure (3.7).

The detection system consists of two independent thermal neutron scintillationcounters. Counter-1 contains a Lithium compound (enriched in Lithium-6, 95%) dispersed in a ZnS(Ag) phosphor matrix (Nuclear Enterprises, NE422). Counter-2 employs a boron glass, enriched in Boron-10 to 90%, with a ZnS(Ag) phosphor (NE 402). The counters are grooved disks (d = 4 inch) coupled to 5 inch photocathodes, through a 5 inch diameter light pipe. The counters and their photomultiplier tubes are enclosed in tinplate cylindrical housings.

Price[21] has described the general features of the scintillion counting and Kroontz et al[22] have described different methods for fast neutron counting using the ZnS(Ag) phosphor.

Thermal neutrons (mainly) produce charged particles, reacting with B^{10} and Li^{6} according to

$$B^{10} + n \rightarrow Li^{7} + \alpha + Q$$

$$Li^{6} + n \rightarrow H^{3} + \alpha + Q'$$

The ionisation and excitation produced by the charged particles in the ZnS(Ag) phosphor is converted into light, which emitts photoelectrons from the photocathode of the photomultiplier. The photoelectrons are multiplied in the photomultiplier and the electrical signal is shaped and registered in the associated electronics.

Fast neutrons (delayed neutrons) are thermalised by the cylindrical polythene moderator (figure 3.6). The length of this cylinder is 25 cm and its thickness was optimised by Clifford[12], using Counter-1, so that the response of the detector would be flat. The optimum thickness of polythene was 5 cm and a 5 cm thick lead gamma shield has been used to improve the gamma discrimination of the detection arrangement.

Generally, the integral bias curve (counts above a discriminator bias versus the bias, for constant gain) of a counter employing the ZnS(Ag) phosphor bombarded with monoenergetic charged particles, should have a plateau. Since the charged particles, which will reach the ZnS(Ag) phosphor, will have any energy in the interval (O,Q) depending on the ionisation produced in the other contents of the counter (where they have been produced) before reaching the phosphor, the integral bias curve of the present detector should not have a plateau. It is shown experimentally[22] that they indeed do not have such a plateau.

The lack of a plateau means that the efficiency will be sensitive to the overall gain and discriminator threshold instabilities. For this reason, the detectors and their photomultipliers have been placed in a constant temperature box to assure short term stability of the efficiency. The short term stability of the efficiency is checked by an efficiency calibration (section 3.3, Pu^{240} source) before and after each experiment.

Kroontz et al[22] have shown that, although the neutron and gamma detection efficiency decreases simultaneously by increasing the discrimination bias, the gamma efficiency decreases much faster. So, the discriminator setting can be used to achieve a required gamma/neutron efficiency ratio.

Clifford[12] studied the gamma/neutron emission rate ratio following the irradiation of 1 gm of U^{235} in a full size VIPER pulse, and it was found that the gamma/neutron (delayed) emission rate ratio increases monotonically from 30 up to 1000 in the time interval (.2, 500 secs) after the irradiation.

For the discriminator setting (and overall gain) used, we found that the neutron and gamma efficiencies of the detectors are;

SOURCE	ABSOLUTE EFFICIENCY	
	COUNTER 1	COUNTER 2
Pu^{240} neutron source	$4.7\ 10^{-4}$	$2.6\ 10^{-4}$
La-140 (1.6 Mev) gamma source	$5.4\ 10^{-10}$	$1.2\ 10^{-10}$

So, we conclude that the delayed gamma contribution to the measurements will be less than .1%, at any moment after the irradiation.

Since we want to study the group structure of the delayed neutrons, measurements at times higher than 300 sec after the irradiation (section 3.4) are required. Typically, a 20 gm (maximum) U^{238} sample irradiated in a full size VIPER pulse will emit less than 60000 delayed neutrons per sec, at times higher than 300 sec after the irradiation. We conclude that, the efficiency of the detectors is not probably adequate for resolving the longest lived group of the U^{238} delayed neutrons, unless we perform a large number of irradiations to improve the statistical accuracy of the measurements.

The detector arrangement (Figure 3.6, Figure 3.3) is rigidly mounted on two aluminium disks, sliding along the flight tube. This mounting allows the whole detector arrangement to move relative to the tube, as a solid body, thus, preserving the counting geometry. Two rulers (figure 3.3), permanently installed at the base of the box, allow the exact axial repositioning of the detector arrangement. The axial distance X (section 3.3) is measured from the left end (figure 3.3) of the flight tube.

Kroontz et al[22] have found that the initial time-decay constant τ of the ZnS(Ag) phosphor is .04 μsec. This short decay constant allows the use of a short clipping time, without significant loss in pulse height, so that short resolving times can be achieved. Double delay line shaping has been used with a clipping time equal to .1 μsec.

The amplified and shaped signal (Figure 3.7) is registered by the scalers. The time dependence of the delayed neutron emission rate is obtained by the on-line ARGUS-500 computer. The computer allows the scalers to collect data over a predetermined time interval (channel); At the end of this counting interval the computer stops the scalers (inhibit input), reads the number of counts collected and stores them and then clears the scalers, the operation being repeated. Time channels of 10,100 and 1000 msec can be used in any predetermined combination,thus allowing the multiscaling of the delayed neutron counting.

The 10 Kw power signal (section 3.1) initiates the previously described operation. The timing of the measurements is provided by the 10Kw power signal and the preselected number and type of the time channels. Thus, the time elapsed between the onset of the N^{th} time channel and the 10 Kw power signal is equal to the sum of the durations of the previous (N-1) selected time channels.

The previously described read-store-clear operation corresponds to a dead time per channel, during which pulses are not registered by the scaler. This time was measured[12] equal to 70 μs. It is apparent that if the duration of a time channel is T, pulses are registered over the time interval (T-70 μs). This dead time corresponds to a correction of .7%, at the worst. So, the dead time is not important and it has not been verified in this work.

The dead time of the detection system (excluding the Argus computer) was measured by Clifford[12] equal to 2.12 ± 10% μsec. Although we did not measure this value directly, it was found that this is an acceptable value provided that we restrict the detected neutron count rate below 30000 c/sec (chapter 6). This check was possible because we have used samples of different masses and counting has been done in overlapping time intervals.

3.3 The efficiency of the detectors

In this section, we will describe the study of the efficiency of the detectors. While the efficiency determination is straight forward we have studied the different factors which affect the efficiency so that, we could estimate a realistic error.

The detector efficiency was studied using different neutron sources. The flat surfaces of two long polyurethane cylinders were hollowed out, so that, they could accommodate the neutron source. The shape and dimensions of the mounting cavity have been chosen so that, repositioning of the source in the cavity is ensured and the axis of the source coincides with the axis of the flight tube at the counting position of the source (except in the case of the radial efficiency variation, section 3.3.5). The two polyurethane cylinders containing the neutron source, were inserted in the flight tube, from the opening side of the tube (figure 3.3, left hand side), and the diameter of the polyurethane cylinders matched the diameter of the flight tube at the counting position.

3.3.1 Short and long term variation of the efficiency

The spherical (d=2.1 cm) Pu^{240} spontaneous fission neutron source (Fieldhouse et al[26]) was used to take into account the short and long term stability of the efficiency of the two counters. The source strength was 1.85 10^4 n/sec and no error was assigned, because the measurements are relative ones (except in table 3.6, study of the energy dependence of the efficiency). The Pu^{240} source is mounted between two

long polyurethane cylinders, which are pushed into the flight tube (shortening of the diameter of the flight tube, figure 3.5, ensures repositioning). The length of the cylinders has been chosen, so that, the source is placed at the axial distance, X = 43 cm. The same cylinders have been used always, to ensure repositioning of the source.

The counters were moved at the axial distance X = 43 cm, so that the source will be in front of the counters.

The previously described counting configuration was constructed before and after each VIPER pulse or absolute efficiency calibration experiment (i.e. Am-Li and (γ,n) calibration experiments) of the detectors. The counting of the Pu^{240} source before and after each experiment was done, so that, we could check the efficiency stability of the detector during the experiment. This counting of the Pu^{240} source was used to calculate the variation of the efficiency of the detectors during the extended time interval of the measurements (years).

3.3.2 Axial variation of the efficiency

Since the arrest position of the sample is not known in advance, it is necessary to study the variation of the efficiency with the axial position of the sample.

This study was done using a small Po-Be neutron source. The detectors were placed at the axial distance X = 43 cm and the source was counted at different axial positions, X, along the axis of the flight tube.

The efficiency versus distance, X, curve was approximated by a polynomial and the least squares technique was used to estimate the polynomial coefficients, so that the axial efficiency variation could be predicted at any intermediate distance, X. Polynomials of first up to eighth degree were fitted to the experimental points and the poly-

nomial degree was chosen, so that, the quality of the fitting

$$\frac{\sum_{i=1}^{M} \frac{e_i^2}{\sigma_i^2}}{M-K-1}$$

evaluated at the optimum, will be minimum. The quantities e_i, σ_i^2, M, K are the difference between the experimental and fitted value at the point i, the variance at the point i, the number of points and polynomial degree, respectively.

Table (3.2) and figure (3.8) give the theoretically and experimentally predicted axial variation of the efficiency.

The neutron spectrum of a Po-Be neutron source is much harder than the spectra of the delayed neutrons. In order to check the effect of the neutron spectrum on the axial variation of the efficiency, the work was repeated using a small cylindrical Cf^{252} (d = .8 cm, L = 1.5 cm) spontaneous fission neutron source. The spectrum of this source is much softer than the spectrum of a Po-Be neutron source.

Table (3.1) summarises the experimentally determined axial variation of the efficiency, predicted by the Cf and Po-Be neutron sources (the efficiency has been arbitrarily normalised at the detector position, X = 43 cm).

We argue that the effect of the neutron spectrum, in studying the spatial variation of the efficiency, is not significant.

3.3.3 The efficiency calibration using the Am-Li neutron source

In order to determine the absolute efficiency of the detectors, a neutron source with a neutron spectrum similar to the steady state delayed neutron spectrum must be used, unless the detector efficiency

is independent of the neutron energy.

The Am^{241} - Li^{7} source has a neutron spectrum similar to the steady state delayed neutron spectrum. The neutrons are produced because of the reaction

$$Li^{7} + \alpha \rightarrow B^{10} + n - 2.79 \text{ Mev}$$

The threshold of this reaction is 4.38 Mev and the α-particles emitted by the Am^{241} have an energy equal to 5.46 Mev. Another source which could be used is the Po^{210} - Li^{7} neutron source.

The Am-Li source, which was used in this work, was fabricated at the Radiochemical centre at Amersham. It was made of a homogeneous mixture of AmO_2 (3C) and 10g of LiH. The source material was placed in a cylindrical steel capsule (d = 22.4 mm, L = 48.5 mm, X14 capsule).

The source was calibrated at the National Physical Laboratory, using the manganese bath method and the source strength was $2.044\ 10^{5} \pm .3\%$ neutrons/sec. The spectrum of a similar source has been measured by Werle[23] using proton recoil proportional counters.

Table 3.4 summarises the results of the absolute efficiency calibration of the two counters. A small correction (.3% and .7% for Counter-1 and Counter-2, respectively) has been applied because of the non-zero length of the Am-Li source. The efficiency uncertainty, because of this correction, was assumed equal to .3%.

The counters were placed at the axial distance X = 43 cm, and the source was inserted in the flight tube at the axial position, X = 43cm. The Pu^{240} source was counted before and after the Am-Li source counting.

The efficiency of the detectors, determined by the Am-Li source, was used as the efficiecny of the detectors for the delayed neutron yield measurement.

3.3.4 Efficiency of the detectors for an irradiation

The counting of the irradiated samples is done at different detector positions.

The counters are placed at the axial distance X = 43 cm, before and after each pulse, and the Pu^{240} source is counted at the reproducible position described in section 3.3.1. These counting conditions are identical with the Pu^{240} counting conditions of the calibration experiment with the Am-Li neutron source (section 3.3.3). So, any change in the detection efficiency of the detectors will be due to the expected long-term variation of the efficiency.

The test pulse (section 3.1) determines the expected arrest position of the rabbit and the detectors are placed at this expected position. Then, the sample is irradiated and the counting of the sample is done at this detector position. Table 3.7 gives the actual detector position used for each experiment. It was necessary to use the previously described variable detector position, so that, we could reduce the axial efficiency correction within an acceptable size.

Let us assume that δ is the relative distance between the arrest position of the sample and the actual detector position for the irradiation (determined by the trace of the sample in the polyurethane cylinders).

The efficiency of the i^{th} (= 1,2) counter, EF_i, the date the irradiation was done, at the axial arrest position of the sample and for the delayed neutrons is

$$EF_i = E_{i1}(Pu^{240})\ f(43 + \delta)\ \frac{E_i(Am\text{-}Li)}{E_{i2}(Pu^{240})} \qquad (3.1)$$

where

$E_{i1}(Pu^{240})$ = efficiency of counter i, using the Pu^{240} source, the date the irradiation was done

$E_{i2}(Pu^{240})$ = efficiency of counter i, using the Pu^{240} source, the date the calibration experiment was done (Am-Li calibration experiment).

$E_i(Am\text{-}Li)$ = efficiency of counter i, using the Am-Li neutron source.

$f(X)$ = normalisation factor (≤ 1) of the efficiency because of the arrest position of the sample at the X axial position, when the detector was placed at 43 cm.

The use of equation (3.1), to determine the efficiency of the counters for the delayed neutrons, assumes that the efficiency of the counters for the Am-Li neutron source is independent of the axial distance where the calibration experiment (section 3.3.3, X = 43 cm) was done. This is justified because, the counters have never been displaced by more than 3 cm (table 3.7) from the position of the counters, where the Am-Li efficiency calibration experiment was done.

3.3.5 Radial variation of the efficiency.

The Am-Li neutron source, which was used for the absolute efficiency calibration of the counters, is geometrically different from the foils which effectively constitute the delayed neutron source. The small increase in the efficiency of the counters, because of the non-zero length of the Am-Li neutron source (section 3.3.3), took into account the source length, so that it was necessary to study the effect of the different diameters of the foils and calibration source.

The Cf^{252} neutron source was used to study the radial variation of the efficiency. The counters were placed at the axial distance X = 43 cm and the neutron source was mounted on the polyurethane cylinders eccentrically, the cylinders rotating around the axis of the flight tube, so

that, the neutron source was at the axial distance X = 43cm, always. The efficiency of the counters was measured placing the Cf^{252} source at the axis of the flight tube, too (we call this position the Cf reference position). Let $EF_i(r,\theta)$ be the efficiency of the i^{th} counter when the source is placed at the (r,θ) position (polar coordinates, r measured from the axis of the flight tube, θ measured around this axis from the counter -1) and let EF_{ic} be the efficiency of the i^{th} counter when the source is placed at the Cf reference position. The relative efficiency $EF_i(r,\theta)/EF_{ic}$ was studied for two radii and eight angular positions for both counters. The results are given in table 3.3.

We observe that there is an unacceptable large radial variation of the efficiency of a counter. This large radial variation of the efficiency will introduce errors in the efficiency determination because of the different radii of the Am-Li source and foils and because of uncertainties in the radial arrest position of the foil and positioning of the Am-Li source. Let us assume that the sample is arrested at the radial position S and that the efficiency of the i^{th} counter, when the Cf source is placed at this position, is EF_{is}. Let us assume that the cross section of the Am-Li source is divided into N small equal surfaces and that the efficiency of the i^{th} counter, when the Cf source is placed at the p(= 1, ...,N) position, is EF_{ip}.

Let us assume that Y is the number of delayed neutrons per fission which are emitted by the sample in $t\varepsilon(0,\infty)$ (i.e. delayed neutron yield). The average yield, Y_m, calculated by the two counters is

$$Y_m = \left[\frac{Y\ EF_{1s}}{\frac{1}{N}\sum_{p=1}^{N} EF_{1p}} + \frac{Y\ EF_{2s}}{\frac{1}{N}\sum_{p=1}^{N} EF_{2p}} \right] .5$$

Let us assume that

$$EF_{is} = EF_{ic}\ (1 + \varepsilon_{is})$$

$$EF_{ip} = EF_{ic}\ (1 + \varepsilon_{ip})$$

where the quantities ε_{is} and ε_{ip} are the errors because of the radial efficiency variation. Then the average yield is

$$Y_m = .5Y\left[\frac{1+\varepsilon_{1s}}{1+\frac{1}{N}\sum_{p=1}^{N}\varepsilon_{1p}} + \frac{1+\varepsilon_{2s}}{1+\frac{1}{N}\sum_{p=1}^{N}\varepsilon_{2p}}\right] \qquad (3.2)$$

Table 3.3 shows that for a source, with its axis coinciding with the axis of the flight tube (or any small accidental eccentricity), the quantity

$$\frac{1}{N}\sum_{p=1}^{N}\varepsilon_{ip} \qquad i = 1,2 \qquad (3.3)$$

will be of the order of .01, so that, neglecting second order effects (equation 3.2) we write,

$$\frac{Y_m - Y}{Y} = \frac{\varepsilon_{1s}+\varepsilon_{2s}}{2} - \frac{1}{N}\sum_{p=1}^{N}\frac{\varepsilon_{1p}+\varepsilon_{2p}}{2} \qquad (3.4)$$

Ideally, we wanted $(\varepsilon_{1p} + \varepsilon_{2p})/2$ to be zero for any point p. This quantity has been calculated (table 3.3) for the sixteen points (r,θ) studied and, we observe that it is almost zero for any of the points. So, the use of the two counters should reduce the error because of the large variation of the efficiency of a single counter. The sixteen values studied have a mean equal to -.003 and a standard deviation equal to .014.

So, we may write that

$$\frac{1}{N}\sum_{p=1}^{N}\frac{\varepsilon_{1p}+\varepsilon_{2p}}{2} = -.003$$

and that

$$\frac{\varepsilon_{1s}+\varepsilon_{2s}}{2} = 0 \pm .014$$

We conclude that the mean delayed neutron yield, calculated by the two counters, will be the actual delayed neutron yield and the errors because of the variation of the efficiency will be 1.4% because

of the sample, and .3% because of the calibration source.

The large radial variation of the efficiency of a single counter could be avoided by increasing the distance between the counter and the sample. This alternative solution was not practical because, even at this short counter-sample distance the absolute efficiency of the counters does not allow a complete study of the group structure of the delayed neutrons from U^{238}.

The large radial variation of the efficiency of a single counter will be certainly responsible for any large discrepancy between the delayed neutron yield values measured separately by each counter.

3.3.6 Energy response of the counters.

We have used the Am-Li neutron source for the absolute calibration of the efficiency of the detectors, appropriate for the delayed neutron yield measurement.

It is apparent that, the efficiency of the detectors for the delayed neutrons may be different because of the different spectra of the calibration source and the delayed neutrons. In order to estimate the uncertainty introduced, we must know the variation of the efficiency of the counters with neutron energy and the spectra of the calibration source and the delayed neutrons. In particular, the steady state delayed neutron spectrum (group spectra weighted by the relative abundances of the groups) must be used, in order, to estimate the delayed neutron yield measurement uncertainty.

Figure (3.9) gives the steady state delayed neutron spectrum obtained from the thermal U^{235} fission. The adopted five group (energy) structure and the corresponding numerical values have been obtained from Keepin[10]. This spectrum has been mainly based on the measurements of Batchelor and Hyder[24].

The thermal fission U^{235} steady state delayed neutron spectrum measured by Fieg[25] is in very good agreement with the previous measurement; The 14 Mev fission U^{235} delayed neutron group spectra, measured by Fieg[25], are in agreement with the thermal fission ones, to better than 50%. The mean energies of the group and steady state delayed neutron spectra from the U^{235} thermal fission (Batchelor and Hyder[24]) are in good agreement with the mean energies of the corresponding spectra from the 14 Mev fission of U^{235}, U^{238} and Pu^{239} (Fieg[25]). Thus, the steady state delayed neutron spectrum given in Figure (3.9) has been accepted as the steady state delayed neutron spectrum from all isotopes, to within 50%.

Figure (3.9) gives the five group representation of the Am-Li source, too (measurement of Werle[23]).

It is apparent that, we require the energy response of the detector in the energy interval (0,1 Mev) at least. The energy response of each counter was measured using the La(γ,n) D, La(γ,n)Be and the Pu^{240} sources. Figure (3.10) gives the schematic representation of the two (γ,n) sources.

Table (3.3) shows that the mean relative efficiency, calculated around a circle having its centre on the axis of the flight tube, is approximately equal to 1 (actually, .99, 1.00, .99 and 1.01 for the two counters and the studied radii). So, we argue that axially symmetric sources can be used to determine the efficiency of the two counters, corresponding to small sources placed at the Cf reference position, to within 1%. So, the absolute efficiencies of the counters measured in this work (Am-Li, La-Be, La-D_2O, Pu^{240}) correspond to the Cf reference position thus, they are compatible.

Theoretically, the two (γ,n) sources emit neutrons in a very limited energy band given by,

$$E_n = \frac{A-1}{A}\left[E-|Q|\right] \pm E\sqrt{\frac{2(A-1)(E-|Q|)}{931\ \text{Mev}\ A^3}}$$

where E_n, E, Q, A are the neutron energy, the photon energy, the reaction threshold and atomic number of target, respectively.

The two (γ,n) sources are based on the reactions

$$Be^9 + \gamma \rightarrow Be^8 + n - 1.666\ \text{Mev}$$

$$H^2 + \gamma \rightarrow H^1 + n - 2.225\ \text{Mev}$$

the γ being emitted by the La^{140} (2.52 Mev) isotope.

The sources were activated-manufactured at AERE and they were calibrated at the National Physical laboratory, using the manganese bath method.

The gamma activity of the two (γ,n) sources was high and for this reason, the gamma core was inserted in the flight tube and the gamma background was counted. Then, the gamma core was placed in the jacket and the previously measured gamma background was subtracted from the measurements.

The previous treatment of the gamma background assumes that the gamma efficiency will be the same, with and without the jacket. It is estimated that (Be thickness 1 cm, D_2O thickness 1 cm and total brass container thickness .5mm) 8% of the 1.6 Mev gammas emitted by La^{140} will undergo a Compton scattering in the jacket, the absorption processes being negligibly small. Thus, the same number of gammas will escape the source, with and without the jacket, but their energy and angular distribution will be different.

The gamma background correction done was 45% and 10% for counter 1

and counter 2, respectively. We have assumed that the efficiency uncertainty, because of the background correction, is 25% of the modified background correction.

The Pu^{240} source was counted, before and after each calibration experiment, and the efficiency of the counters has been normalised to the same Pu^{240} efficiency given in table 3.4. The results of these calibration experiments are given in table (3.6) and figure (3.9).

The neutrons emitted by the (γ,n) sources are not monoenergetic because of the different gamma energies of the La^{140} gamma source and moderation of neutron in the jackets. The most prominent gamma of energy higher than the threshold of the reactions, which is emitted by La^{140}, has an energy equal to 2521 kev. The calculated neutron energies are equal to 148 kev and 760 kev for the $La(\gamma,n)D$ and $La(\gamma,n)Be$ sources, respectively. The adopted energies for the $La(\gamma,n)D$ and $La(\gamma,n)Be$ sources are 150Kev and 750 Kev, respectively.

While the (γ,n) sources emit neutrons within a limited energy band the Pu^{240} source has a broad spectrum. The use of these sources only, to determine the response function of the counters will undoubtedly introduce some assumptions about the shape of the response function.

The response function of the counters was approximated by a straight line in the energy interval (0,900 kev). The two calibration points have been used to determine this straight line and the error assumed for the efficiency at any energy E is equal to the errors of the experimental points. The response of the counters was assumed to be flat above the 900 kev energy and the mean efficiency for the La-Be and Pu^{240} sources was accepted as the value for the efficiency, their difference being the error of the efficiency. Figure (3.9) shows this assumed response function of the counters.

The calculated efficiency of the counters for the delayed neutrons is equal to $(5.09 \pm 3.5\%)\ 10^{-4}$ and $(3.19 \pm 3\%)10^{-4}$ for counter 1 and counter 2,respectively. The calculated efficiency of the counters for the Am-Li source is equal to $(5.08 \pm 3.5\%)10^{-4}$ and $(3.19 \pm 3\%)10^{-4}$ for counter 1 and counter 2, respectively. The good agreement between these calculated values, for the efficiency of the counters, substantiates the use of the Am-Li source for the experimental determination of the efficiency of the counters for the delayed neutron measurements.

In order to estimate the sensitivity of the previous argument to the spectra of the delayed neutrons, let us assume that α_i, c_i $(i = 1, ..,4)$ are the number of delayed neutrons emitted in the energy group i and the efficiency of a counter for the energy group i, respectively. Then, the efficiency change δC because of $\delta\alpha_i$ $(i=1,..,4)$ changes is

$$\delta C = \sum_{i=1}^{4} c_i \delta\alpha_i \qquad \sum_{i=1}^{4} \delta\alpha_i = 0$$

which is rewritten as,

$$\delta C = \delta\alpha_1(c_1 - c_3) + \delta\alpha_2(c_2 - c_3) + \delta\alpha_4(c_4 - c_3)$$

Since the third energy group has the maximum efficiency (Figure 3.9), δC will be maximum (minimum) when all $\delta\alpha_i (i = 1,2,4)$ will have their minimum (maximum) value.

Assuming that the delayed neutron spectrum of Figure (3.9) is correct to within 50%, the spectral error of the efficiency will be less than 3.5% and 1.7% for counter 1 and counter 2 respectively. This uncertainty is probably an overestimate because of the discontinuous efficiency representation (Figure 3.9).

Table (3.5) summarises the systematic errors of the efficiency, applied to the average measured delayed neutron yield of the two counters.

The group spectra have the same approximately shape but the spectrum of the longest lived group is much softer than the spectra of the other groups. Since the relative contribution of each group varies with the time after the irradiation, the efficiency of the detectors will be a function of time. The steady-state delayed neutron spectra must be used for the efficiency determination of the yield measurement, using an instantaneous irradiation. The variation of the efficiency with time will introduce systematic errors in the group constants determination and this effect will be less important for the COUNTER-2 measurements. The measurements of COUNTER-2 have only been used for the determination of the group constants and the reactivity-period relationship.

3.4 Experiments

Since the group constants of Keepin et al[4] indicate that the delayed neutron count rate is mainly due to the longest lived group (U^{235}, >95%) for times higher than 300 sec after an instantaneous irradiation, measurements of adequate statistical accuracy are required over a long time interval. Since the delayed neutron count rate decreases by a factor of 2.610^{-5} in the time interval (0,300 sec), it is not possible to obtain statistically accurate data over the required time interval using a single irradiation, otherwise unacceptable high pulse pile-up will occur.

It has been decided to use more than one irradiations to cover the time interval of interest. Since the VIPER reactor is pulsed only once per day, three pulses have been used for each isotope only. A much larger number of irradiations would be uneconomic.

The delayed neutron count rate at time t after the irradiation is proportional to the sample mass (maximum 20gm) and reactor pulse size. These were the variables used to improve the statistical accuracy

of the overall measurements of an isotope, without exceeding an acceptable maximum count rate (30000 c/sec, chapter 6).

The sample mass and VIPER pulse size were chosen, for the small sample mass irradiation, so that the detected delayed neutron count rate, immediately after the irradiation, would be approximately the maximum acceptable (COUNTER-2 measurements). Then, we have progressively increased the pulse size and/or sample mass, so that, measurements of improved statistical accuracy were obtained. The measurements of the small sample irradiation were used in the time interval immediately after the irradiation while the measurements of the intermediate and large sample irradiations have been used at intermediate and large times after the pulse. This combination of the three pulses (small, medium, large) provided a composite decay curve of improved statistical accuracy, without exceeding the maximum allowable count rate.

The three independent measurements provide data in overlapping time intervals after the irradiation. The measurements in the overlapping time interval of two successive pulses allow a strict check on the reproducibility of the experiment or required adjustment. Since most of the delayed neutrons are emitted immediately after the irradiation, the yield of the delayed neutrons is determined by the small sample mass pulse. For this reason, this experiment has been repeated for all the isotopes to check the reproducibility of the yield measurement.

It is apparent that the measurements immediately after the irradiation of a large sample irradiation are useless, because they exceed the maximum allowable count rate. This excessively high count rate may saturate the detection system shortly after the irradiation with a consequent effect on the measurements at later times. For this reason,

the intermediate and large samples are kept in the irradiation cavity for a period of time (firing delay, section 3.1) shortly after the irradiation.

Although the flight time of a sample is only .35 msec (section3.1), the onset of the measurements is much higher because of the transient background. Figure (3.11) gives the detected counts per time channel (COUNTER-2) from a 37mgm U^{235} irradiated sample and an empty rabbit irradiated in the same size VIPER pulses. We observe that the reactor background (empty rabbit irradiation) contribution is significant at the early times after the irradiation and it decays much nore rapidly than the delayed neutron count rate.

We have decided that the onset of the measurements will be 110msec (11 channels) after the irradiation so that, the background contribution will be less than 1.5% at any moment after the irradiation. No correction has been done because of the transient background. The background contribution to the yield measurements is negligibly small, although it slightly affects the measurements shortly after the irradiation.

Table (3.7) summarises the characteristics of the VIPER pulses used.

The reactor temperature (RTR) is proportional to the pulse size, an RTR of 200°C corresponding to a full size pulse. The sample description affects the fission measurements. The sample mass of the small-sample-pulse has been reduced, increasing the pulse size to achieve the required count rate, so that the self-multiplication in the sample will be reduced. The number and type of time channels used for each irradiation is determined by the time interval where the data will effectively be used. The criterion, by which they have been chosen, is described in Chapter 5.

An experiment consists of the following steps. These steps have been described in detail previously.

The loaded rabbit is fired into the detector (test firing), without performing an irradiation, to determine the expected arrest position of the sample for the particular experiment.

The counters are moved at the reference, X = 43cm, axial position and the Pu^{240} source is counted at the reproducible position (i.e. in front of the counters). The laboratory background is measured, too.

Then, the counters are moved at the expected axial position, determined previously, and the sample irradiation is performed.

The firing delay (delay between the 10kw power signal and squib firing) has been chosen, so that, when the sample will arrive at the detectors the detected count rate will be less than twice the maximum allowable count rate (approximately)for the medium and large sample pulses.

The flight time is the time between the squib firing and the breaking of an electrical contact, at the detector position, by the rabbit.

It is apparent that, the firing delay and flight time should be less than 110 msec for the small sample irradiations. Both these timings do not contribute to the timing measurements of the delayed neutron emission rate.

The 10 kw power signal will initiate the ARGUS operation, which provides the absolute timing measurements. In analysing the data, we have shifted the time scale by 1.4 msec (section 3.1) so that, the zero time will correspond to the peak power of the pulse.

The stopping position of the sample in the polyurethane cylindrical catchers determines the relative distance δ between the sample arrest

position and counter position.

The detectors are moved at the reference position X = 43 cm, and the Pu^{240} calibration and background counting is repeated.

Table 3.7 gives the background of each measurement and the Pu^{240} source efficiency the date the experiment was done at the arrest position of the sample (i.e. $E_{i1}(Pu^{240}).f(43 + \delta)$ from equation (3.1)). These values are the mean values obtained from the before and after the pulse measurements. The background contribution in the yield is less than .1% and the statistical accuracy of the efficiency calibration is typically .7% and .5% for COUNTER 2 and COUNTER 1, respectively.

Since the yield is effectively determined by the small sample mass pulse, we have not used any axial efficiency correction for U^{235} and U^{238} and the axial correction for Pu^{239} is 3% (Pulse 634), approximately.

The missing data in Table 3.7 have not been used and for this reason they are not being reported.

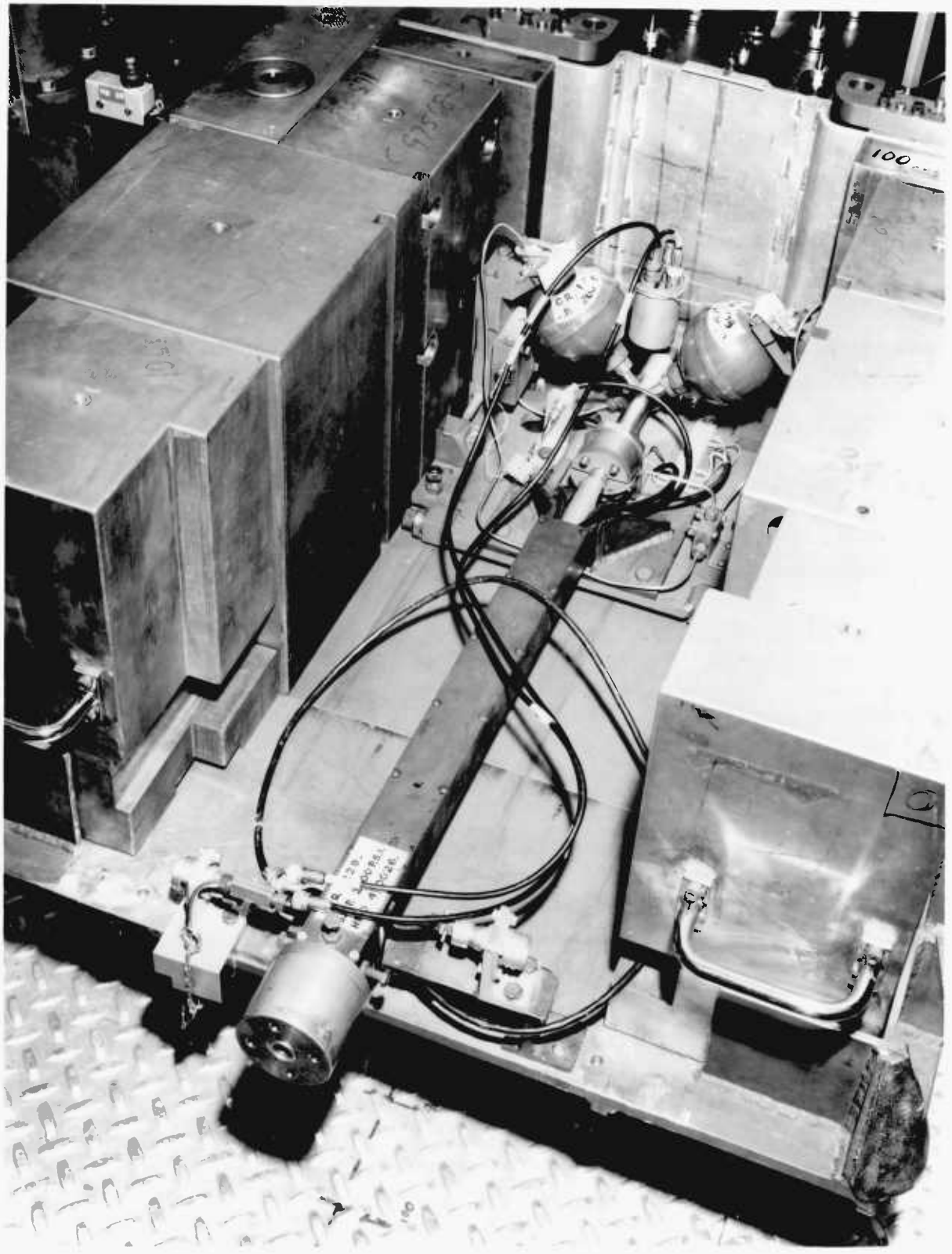

FIGURE 3.1

View of double fission chamber in the VIPER cavity in position for a steady-state irradiation

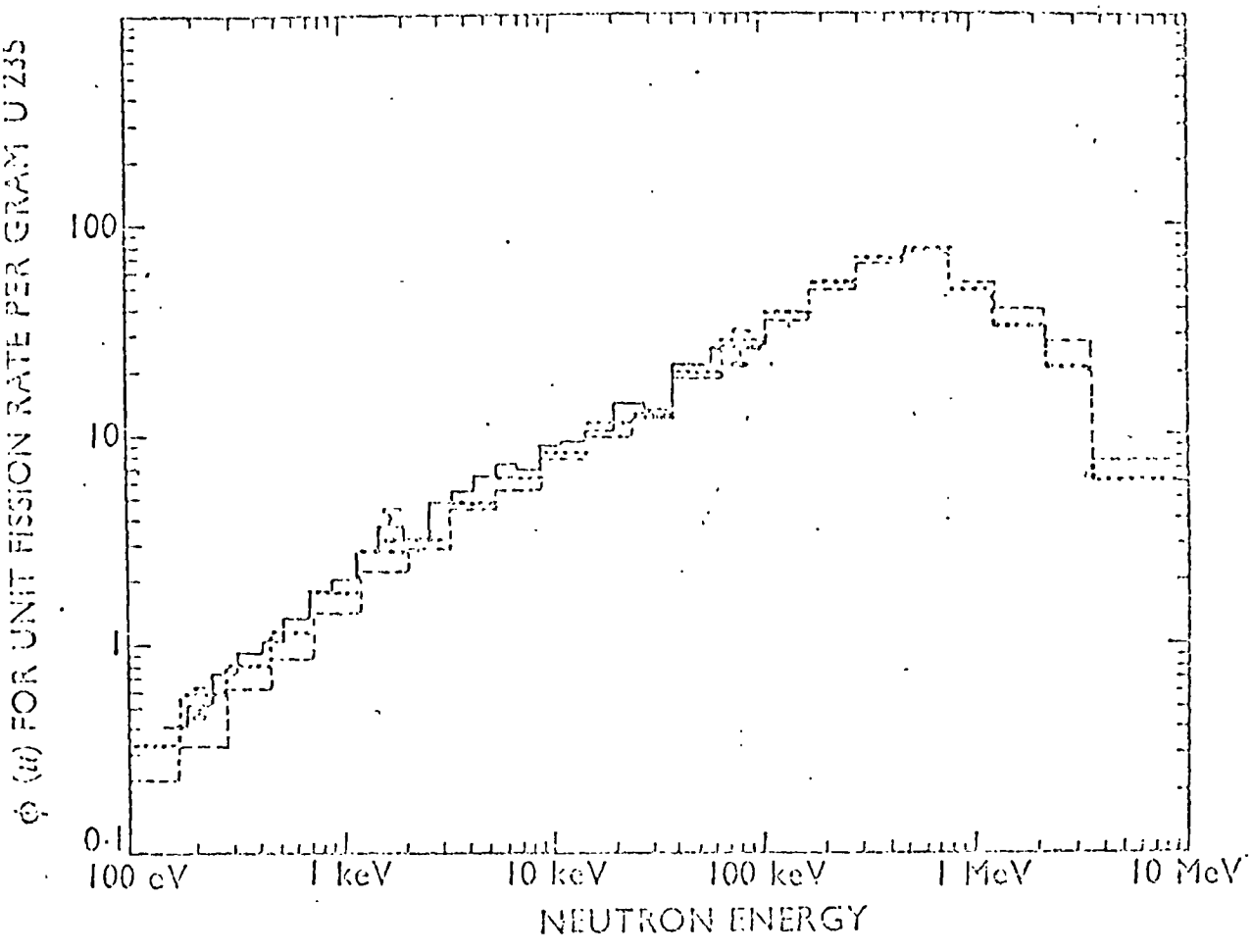

—— Time of flight results normalized at 337 eV using Mn foils, calibrated in VERA 5A, showing 1 standard deviation errors
- - Two dimensional S_8 TURTLE calculation using FD2 data (critical)
. . . SWAN calculation using effective group cross sections from heterogeneous GENEX/SDR Doppler calculation

FIGURE 3.2
NEUTRON SPECTRUM OF VIPER REACTOR

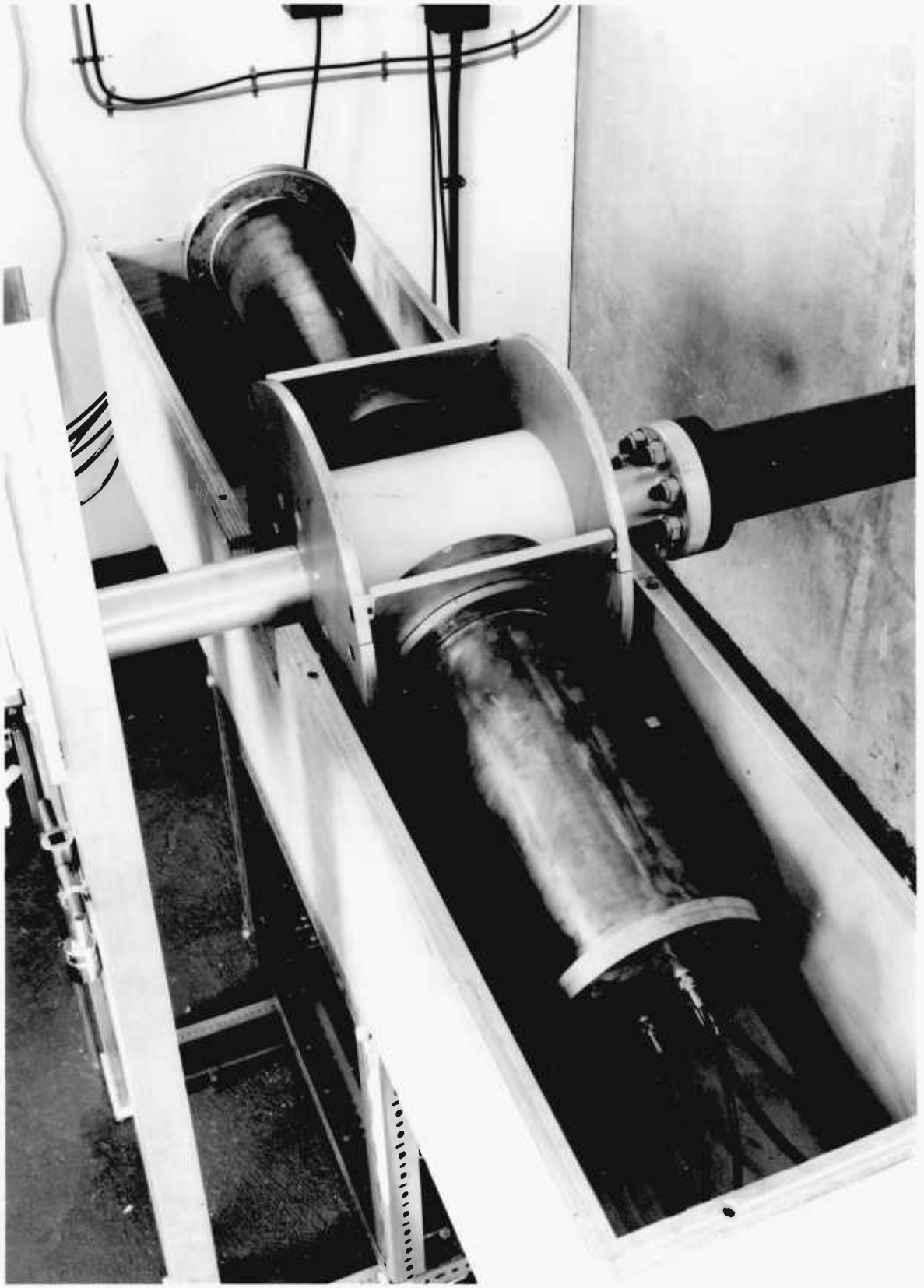

FIGURE 3.3

Detectors installed around flight tube.

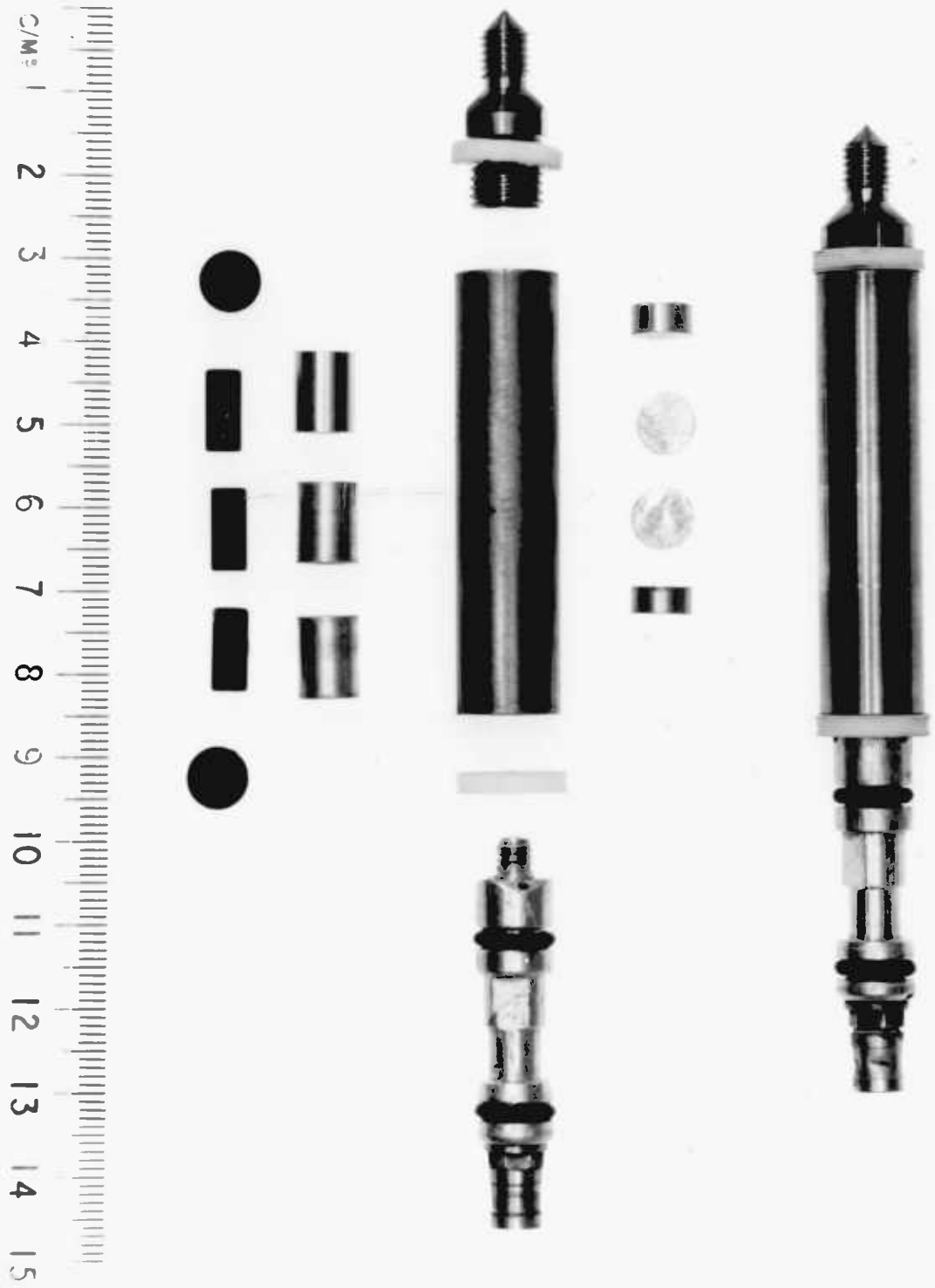

FIGURE 3.4

View of dismantled rabbit, showing samples and aluminium spacers.

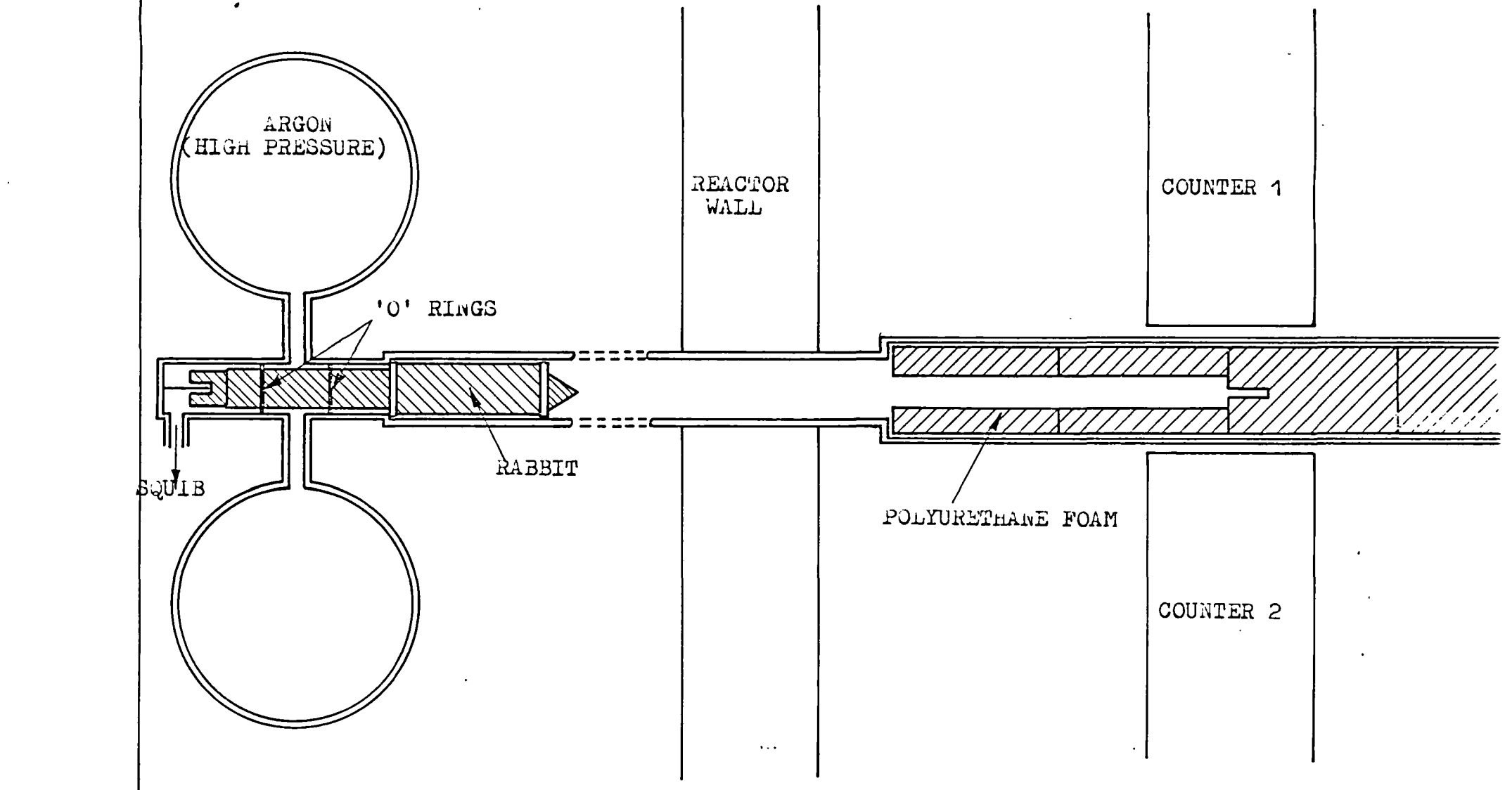

FIGURE 3.5 RABBIT IN THE FIRING POSITION OF THE FLIGHT TUBE

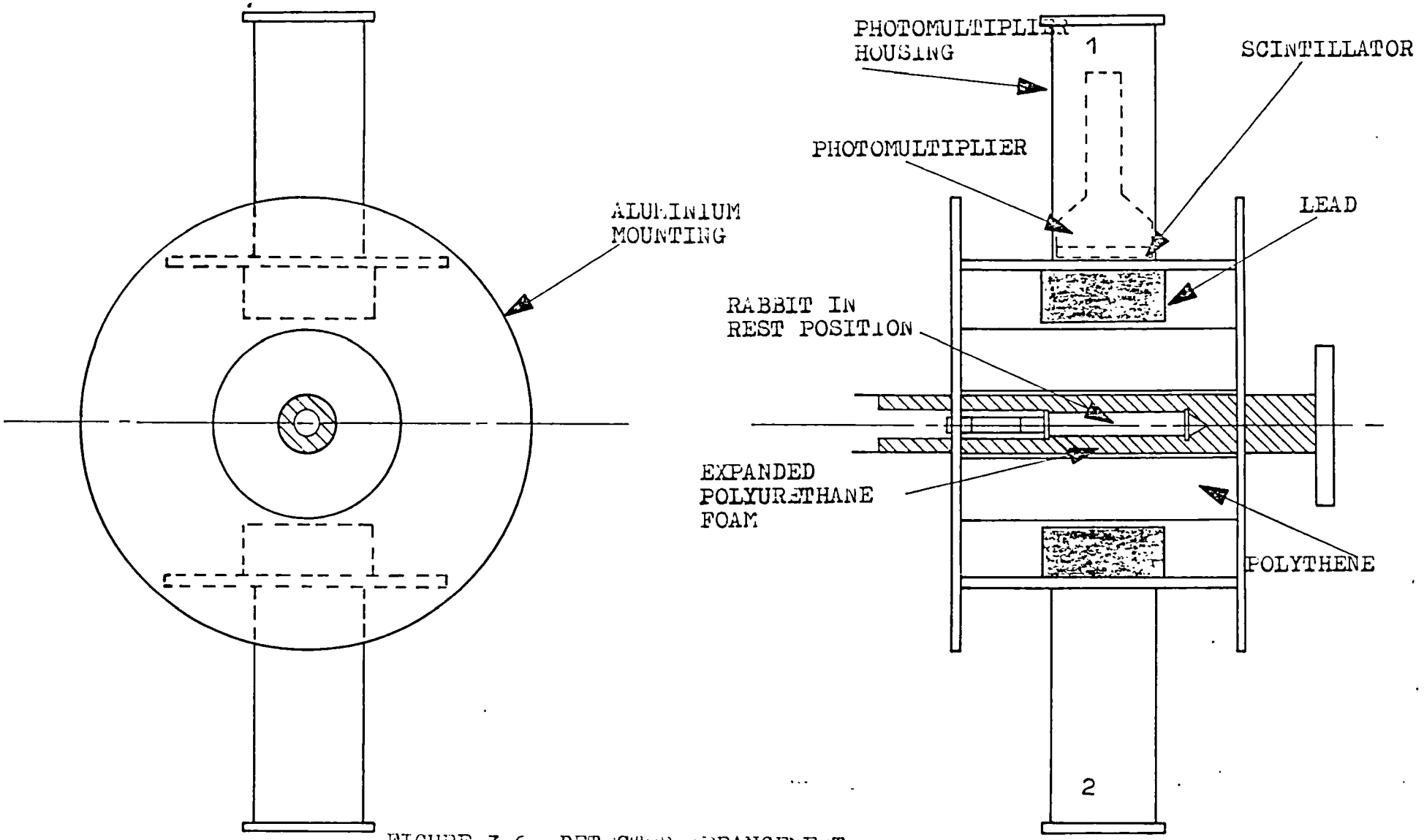

FIGURE 3.6 DETECTOR ARRANGEMENT

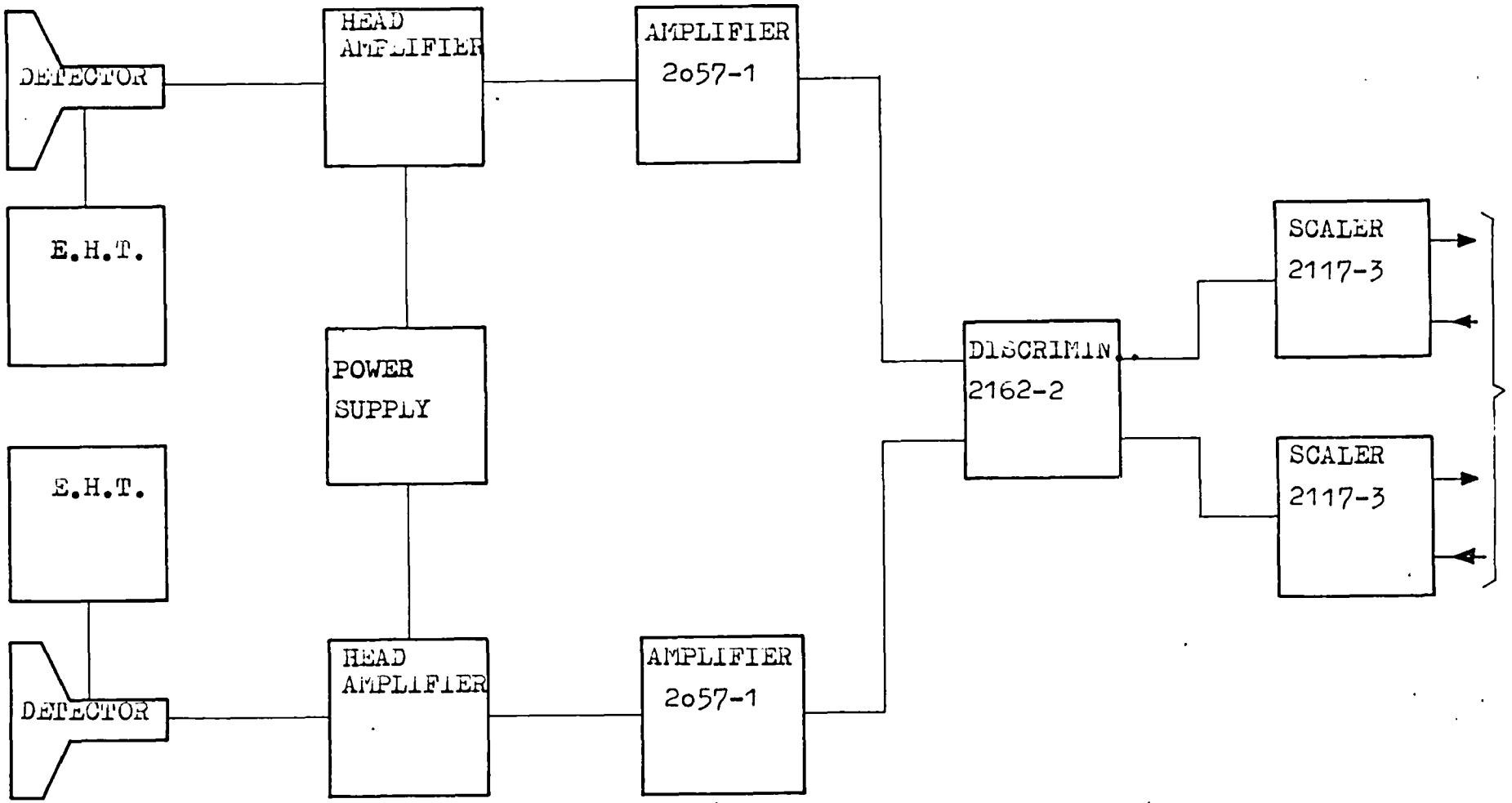

FIGURE 3.7 ELECTRONICS OF THE NEUTRON DETECTORS

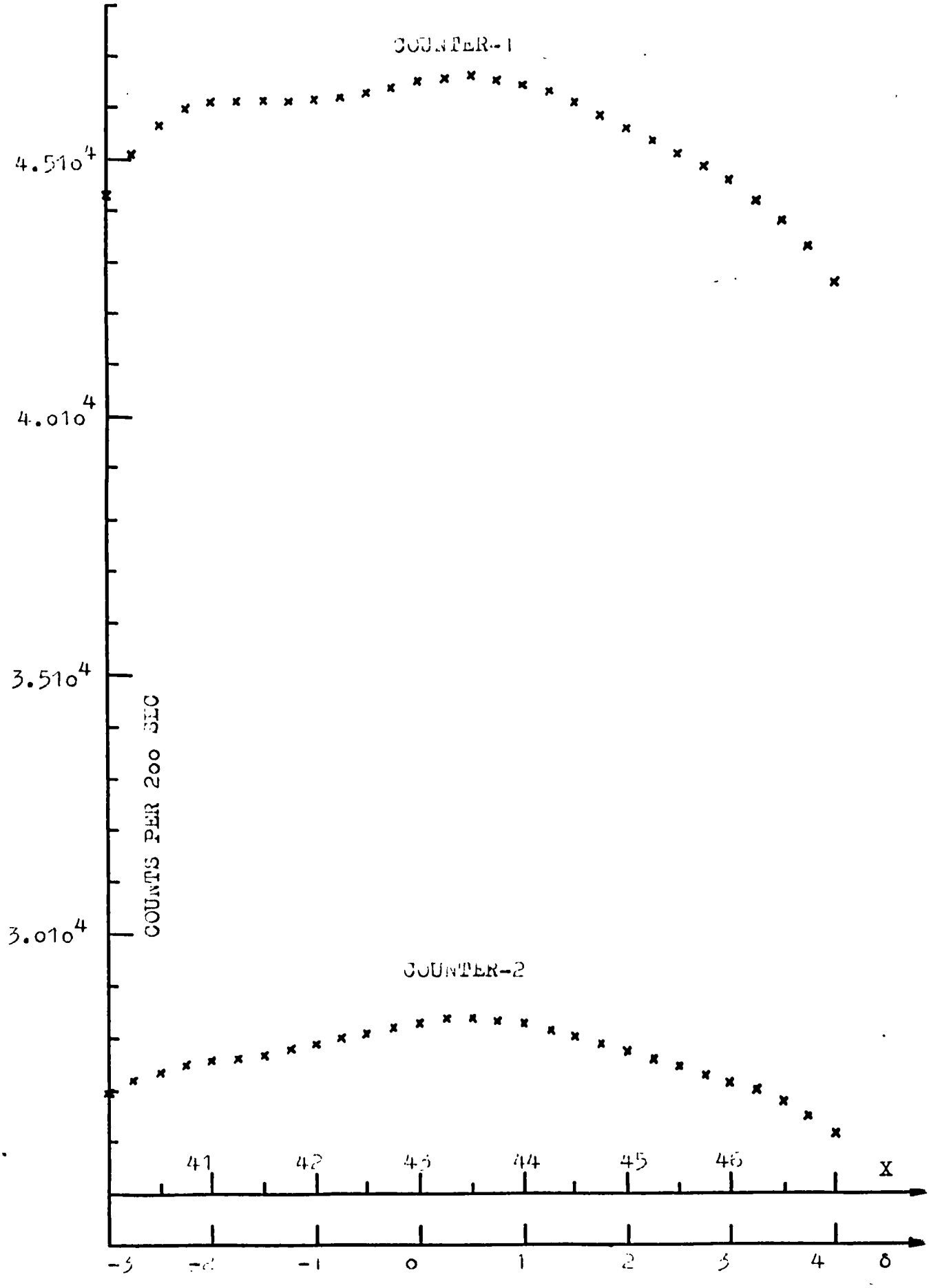

FIGURE 3.8 ESTIMATED AXIAL EFFICIENCY VARIATION

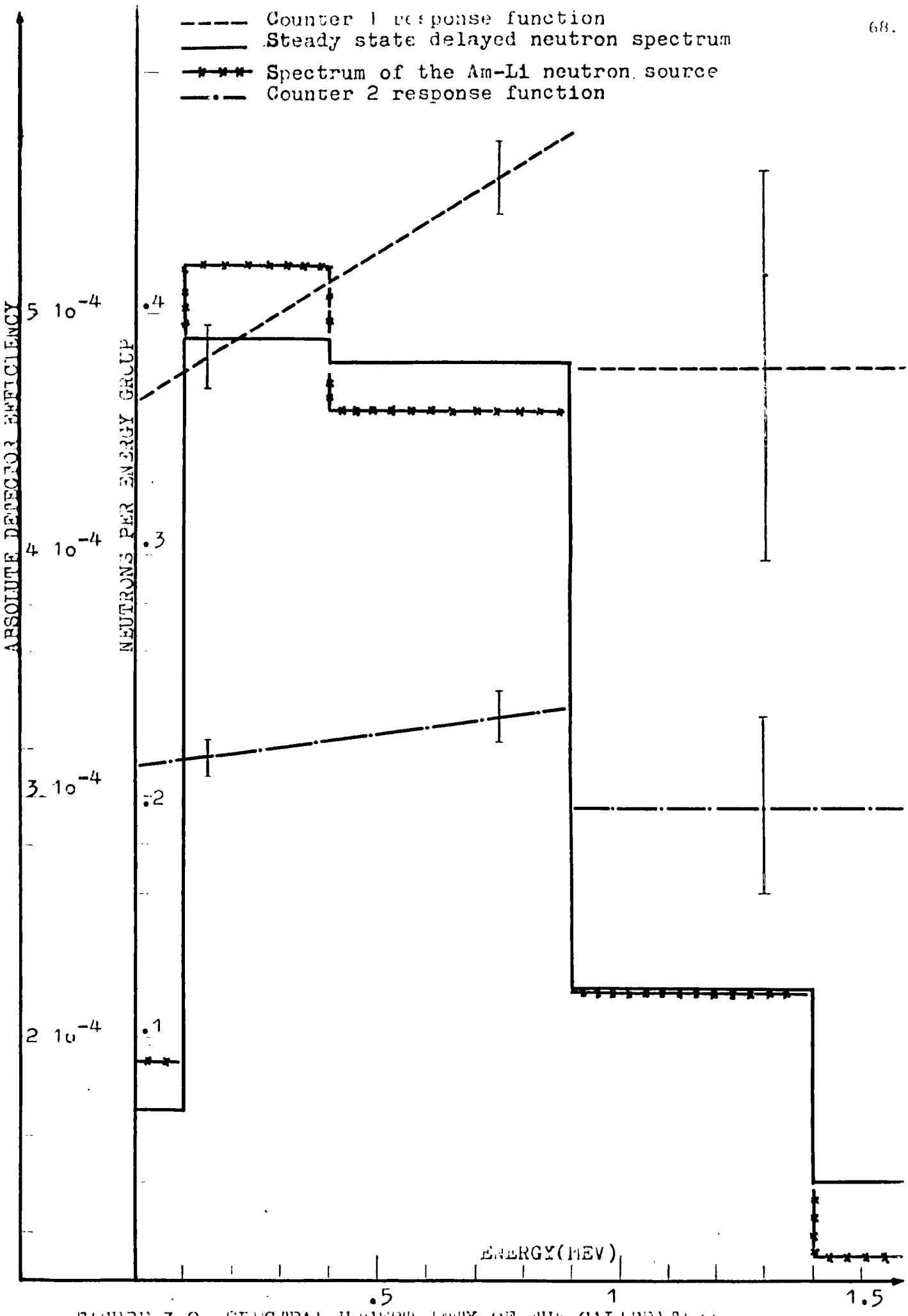

FIGURE 3.9 SPECTRAL UNCERTAINTY OF THE CALIBRATION.

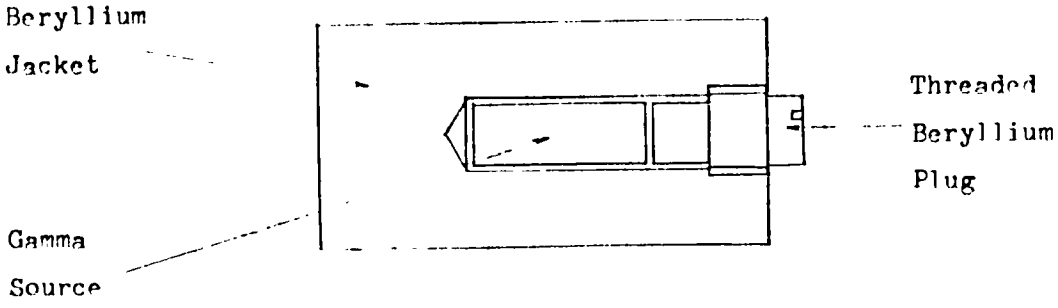

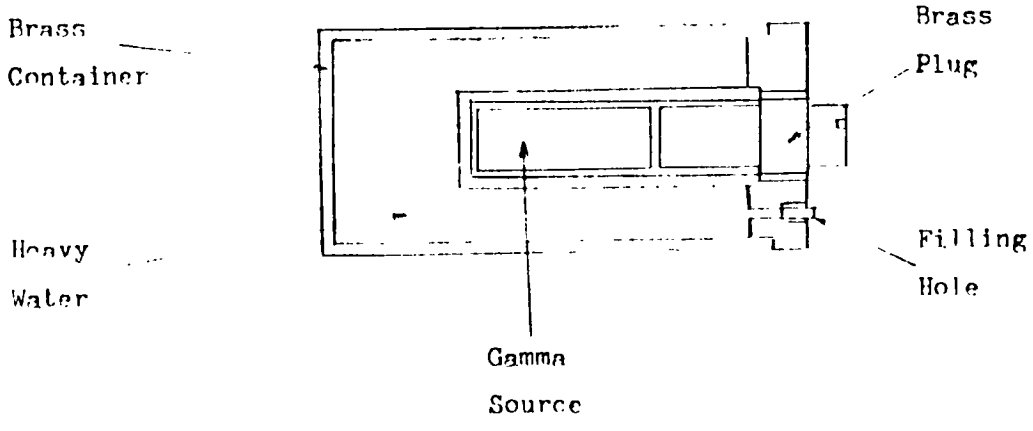

FIGURE 3.1o SCHEMATIC REPRESENTATION OF (γ,n) NEUTRON SOURCES.

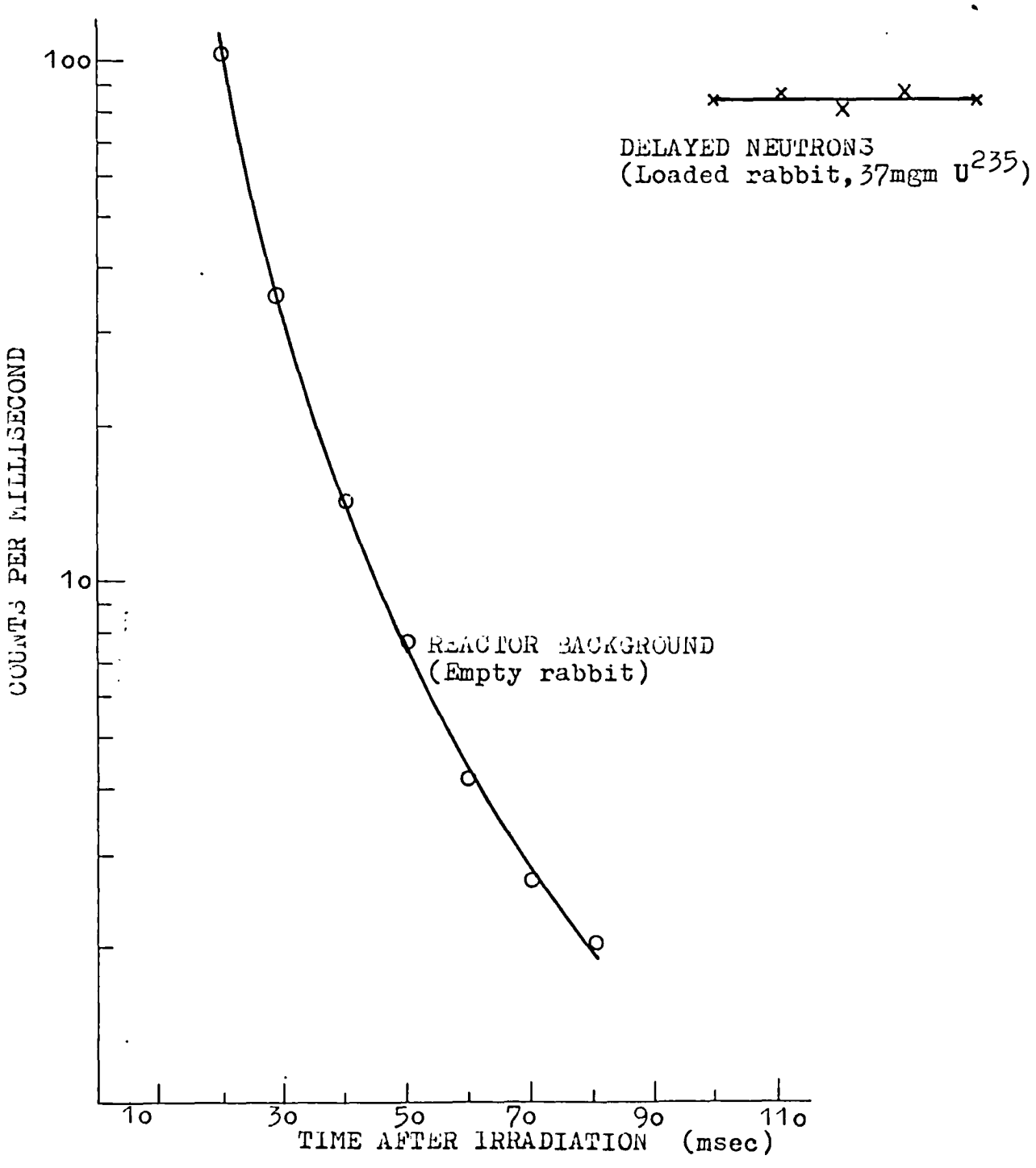

FIGURE 3.11 DETECTOR COUNT RATE DUE TO REACTOR BACKGROUND

TABLE 3.1 ENERGY DEPENDENCE OF AXIAL SCANNING OF EFFICIENCY

SOURCE POSITION (X,CM)	RELATIVE EFFICIENCY (Po-Be)		RELATIVE EFFICIENCY (Cf^{252})	
	COUNTER 1	COUNTER 2	COUNTER 1	COUNTER 2
40	.954 ± .49%	.951 ± .63%	.953 ± .58%	.946 ± .75%
41	.993	.974	.981	.969
42	.994	.985	1.002	.998
43	1.000	1.000	1.000	1.000
44	1.001	.998	.991	.995
45	.981	.980	.976	.984
46	.960	.961	.947	.965
47	.918	.924	.905	.926

Counters placed at 43 cm (Reference).

TABLE 3.2 AXIAL VARIATION OF THE EFFICIENCY*

SOURCE POSITION (X,CM)	COUNTER 1 (COUNTS/200 SEC)		COUNTER 2 (COUNTS/200 SEC)	
	EXPERIMENTAL VALUE	FITTED VALUE	EXPERIMENTAL VALUE	FITTED VALUE
38.5	41375.5 ± .35%	41374.4	25142 ± .45%	25141.5
40	44279.5	44275.4	26911	26910.7
41	46053.5	46061.4	27543.5	27542.4
42	46135.0	46103.9	27863.5	27864.1
43	46400.5	46440.4	28284	28281.4
44	46440	46391.6	28234	28235.6
45	45539	45564.0	27721	27719.3
46	44537	44520.7	27171.5	27171.9
47	42590.5	42589.6	26142.5	26141.2
48	40729	40724.2	25074.0	25073.4

*Counters placed at 43 cm (Reference)

TABLE 3.3 RADIAL SCANNING OF THE EFFICIENCY *

ANGLE θ DEGREES	RELATIVE EFFICIENCY r = .85 cm		$\frac{\varepsilon_1(r,\theta) + \varepsilon_2(r,\theta)}{2}$	RELATIVE EFFICIENCY r = 1.20 cm		$\frac{\varepsilon_1(r,\theta) + \varepsilon_2(r,\theta)}{2}$
	COUNTER 1	COUNTER 2		COUNTER 1	COUNTER 2	
0	1.112	.893	.002	1.166	.874	.020
45	1.090	.887	-.011	1.163	.861	.012
90	1.026	.940	-.017	1.043	.907	-.025
135	.933	1.028	-.019	.923	1.039	-.019
180	.888	1.103	-.004	.853	1.170	.012
225	.875	1.135	.005	.858	1.167	.013
270	.949	1.061	.005	.916	1.091	.004
315	1.023	.962	-.007	1.029	.947	-.012
STATISTICAL ERROR	.009	.012		.009	.012	
MEAN	$.99 \pm .003$	$1.00 \pm .004$		$.99 \pm .003$	$1.01 \pm .004$	

The quantities are defined in section (3.3)

TABLE 3.4 THE EFFICIENCY OF THE COUNTERS FOR THE Am-Li SOURCE

SOURCE	ABSOLUTE EFFICIENCY COUNTS/NEUTRON	
	COUNTER 1	COUNTER 2
Pu^{240}	$3.992\ 10^{-4} \pm .7\%$ (1)	$2.575\ 10^{-4} \pm 1\%$ (1)
Am-Li	$5.072\ 10^{-4} \pm .5\%$ (2)	$3.156\ 10^{-4} \pm .5\%$ (2)

(1) Statistical error only

(2) Error includes statistical error, source strength uncertainty, axial correction uncertainty.

TABLE 3.5 SYSTEMATIC ERRORS IN EFFICIENCY (MEAN ABSOLUTE YIELD)

DESCRIPTION OF THE ERROR	VALUE
Radial variation of efficiency, Calibration source	.3%
Radial variation of efficiency, Sample position	1.4%
Non-flat energy response function	2%

total error 2.5%

TABLE 3.6 RESPONSE FUNCTION OF COUNTERS

SOURCE	ABSOLUTE EFFICIENCY COUNTS/NEUTRON	
	COUNTER 1	COUNTER 2
La-D_2O	$4.822\ 10^{-4} \pm 2.9\%$ (1)	$3.167\ 10^{-4} \pm 2.7\%$ (1)
La-Be	$5.575\ 10^{-4} \pm 2.9\%$ (1)	$3.323\ 10^{-4} \pm 2.8\%$ (1)
Pu^{240}	$3.992\ 10^{-4}$ (2)	$2.575\ 10^{-4}$ (2)

(1) Errors include, source strength uncertainties and radial and axial uncertainties ((γ,n) source, Pu^{240} source), statistics and gamma background uncertainties.

(2) Reference source

TABLE 3.7 CHARACTERISTICS OF THE EXPERIMENTS

AXIAL DETECTOR POSITION (CM)	PULSE I.D.	ISOTOPE	RTR (°C)	SAMPLE MASS (GM)	FIRING DELAY (SEC)	FLIGHT TIME (MSEC)	NUMBER OF CHANNELS			RELATIVE STOPPING POSITION (CM)	Pu^{240} EFFICIENCY COUNTS/NEUTRON		BACKGROUND COUNTS/SEC		SAMPLE DESCRIPTION
							.01 SEC	.1 SEC	1 SEC		COUNTER 1	COUNTER 2	COUNTER 1	COUNTER 2	
43	571	U^{235}	197.5	.0366	.070	33	300	300	300	1.2		$2.706\ 10^{-4}$		1.60	1 FOIL
43	661	U^{235}	70.9	.0351	.067	35	300	300	300	0	$4.536\ 10^{-4}$	$2.525\ 10^{-4}$	.612	.693	1 FOIL
43	588	U^{235}	197.4	.3484	8	33	0	300	500	-3.3		$2.417\ 10^{-4}$		1.49	10 FOILS
43	572	U^{235}	199.2	8.2728	50	40	0	0	900	-2.5		$2.627\ 10^{-4}$		1.65	3 PELLETS
45	636	U^{238}	200.6	.2598	.060	37	300	300	300	-1.6	$4.036\ 10^{-4}$	$2.528\ 10^{-4}$	.680	1.22	7 FOILS
43	598	U^{238}	207	.2646	.068	41	300	300	300	0	$3.929\ 10^{-4}$	$2.606\ 10^{-4}$	.542	1.37	7 FOILS
42	597	U^{238}	207	2.8824	2	40	300	300	300	-1.9		$2.563\ 10^{-4}$		1.30	1 PELLET
40	596	U^{238}	202	11.2032	10	41	0	0	900	-0.6		$2.604\ 10^{-4}$		1.30	4 PELLETS
43	634	Pu^{239}	90.6	.0599	.060	39	300	300	300	2.4	$3.905\ 10^{-4}$	$2.447\ 10^{-4}$	.682	1.15	1 FOIL
45.5	668	Pu^{239}	97.2	.0600	.070	37	300	300	300	-3.8	$3.552\ 10^{-4}$	$2.743\ 10^{-4}$	.580	.888	1 FOIL
43	617	Pu^{239}	207	.1780	3	38	0	300	500	-0.5		$2.518\ 10^{-4}$		1.20	3 FOILS
	615	Pu^{239}	203.3	12.390	50	48	0	0	900					1.23	

CHAPTER 4

FISSION MEASUREMENTS

The number of fissions in a sample, irradiated in a VIPER pulse, was measured by a foil activation technique. A foil, which was irradiated along with the sample in a VIPER pulse, was subsequently gamma counted. The activity of the 1596 Kev gamma, which accompanies the β-decay of the La^{140} fission product, was measured using a high resolution Ge(Li) detector. A calibration experiment, to determine the conversion factor of the measured activity into fissions, was done. Foils, similar to the ones used in the sample, were irradiated in a double fission chamber loaded with deposits of known masses. The measurement of the gamma activity of the foils and the number of fissions in the deposits determined the necessary conversion factor.

4.1.1 Description of the sample

The sample, which was irradiated in a VIPER pulse (figure 3.4), consisted of a number of cylindrical pieces (pellets) and/or a number of foils. The isotopic composition of the pellets and the foils was the same and it is given in table (4.1).

The diameter and length of a pellet was equal to .43cm and 1cm respectively. The absolute yield of the delayed neutrons, from all the isotopes, has been based on samples made of foils only because,we could not (in general) measure the number of fissions in these long pellets. The diameter and thickness of the uranium foils was7.5mm and .05 - .075 mm, respectively. The diameter and thickness of the plutonium foils were equal to 6 mm and .12 mm respectively. The diameter of the foils matched the internal diameter of the rabbit (plutonium foils enclosed in steel capsules for contamination reasons).

The foils of the sample, which would be gamma counted, were sandwiched between two aluminium foils, so that, fission fragments (particularly those of mass number 140) which were produced in adjacent fissionable material could not enter the foil. The aluminium holders (figure 3.4) were used to mount the sample inside the rabbit rigidly.

4.1.2 The calibration experiment

In order to measure the number of fissions in the sample, irradiated in a pulse, the conversion factor of the measured gamma activity into fissions must be measured. The object of this experiment was to measure the number of fissions in a foil, which will be subsequently gamma counted, to determine the conversion factor of gamma activity into fissions. This experiment is similar to the one used in chapter-2 which has already been described in detail.

The double fission chamber was loaded with the calibrated deposits. One or more foils, similar to the ones used in the sample, were sandwiched between the platinum backings of the deposits. Thus, the number of fissions per gm of an isotope will be the same for the deposit (measured by the fission chamber) and the foil.

For this experiment, the VIPER reactor operated in the steady-state mode. Figure (3.1) shows the irradiation position of the double fission chamber. Initially, the reactor operated at low power (less than 30W). During this short time interval the setting of the discriminator levels described in chapter 2, was done. Then, the power was increased to 600W and the irradiation time was chosen, so that, the fissions per gm of the foil will be roughly the same with the fissions per gm of the appropriate small sample mass VIPER pulse. So, the foils which will be gamma counted (calibration experiment, pulsed irradiation) will be equally (approximately) gamma active.

Two monitor fission chambers (namely the VG 124 and VG 126) which were used to check the long term stability of the experiment, were not stable.

For the calibration experiment of the U^{235} and U^{238} isotope, both fission chambers were loaded with the deposits, so that, the U^{238}/U^{235} per atom fission ratio could be measured at the irradiation position of the samples. For the Pu^{239} calibration experiment, the double fission chamber operated as a single fission chamber effectively.

For each side of the double fission chamber, there were two scalers counting pulses above the V_L and V_V discriminator levels which were not controlled by the timer unit (figure 2.3). These scalers were used to avoid the errors because of the printing time of the differential (in time) scalers (which were used to check the long term stability of the experiment). These scalers were started before the increase of the power to the 600W level and they collected counts until the shut down of the reactor.

The necessary corrections for the steady-state experiment are listed below;

1) The extrapolation to zero bias and the fission fragment absorption corrections have been discussed in chapter-2.

2) The impurity fissions of the deposits (other than U^{235} or U^{238} in a U^{238} or U^{235} deposit, respectively) have been calculated using the per atom fission ratios of Table 4.2. The values of these ratios have been calculated using the reactor neutron energy spectrum in the cavity and point-wise cross-sections.

3) The dead time of the electronics was $0.3\mu s$ [16].

4) Since the foils were irradiated during the electronics setting

time interval, without a subsequent count collection by the scalers, a correction was done based on the time integrated reactor power during the setting period and counting period.

Table 4.3 summarises the corrections of a typical experiment and table 4.4 summarises the results of this experiment . Table 4.5 summarises the results of the experiments and table 4.6 gives the associated errors.

Two calibration experiments have been used for the U^{235} study (1133, 25/4/75) and U^{238} study (25/4/75, 1233) and a single one for the Pu^{239} study (11/11/75).

It has not been possible to reproduce the U^{238}/U^{235} per atom fission ratio and the value assumed, 0.0212 $\pm$ 4.3%, is the mean of the four measurements, the error being the standard deviation of the four measurements. The non-reproducibility of this ratio is probably due to spectrum changes in the cavity (non threshold, threshold reaction ratio) and the repositioning of the fission chamber. At any rate, this ratio corresponds to a small correction to the final result, so that, this error is acceptable.

TABLE 4.1 ISOTOPIC COMPOSITION OF SAMPLES

CONSTITUENT ISOTOPE	ATOMIC COMPOSITION		
	U^{235}	U^{238}	Pu^{239}
U^{234}	.012	—	
U^{235}	.9554	.0039	
U^{236}	.0017	—	
U^{238}	.0310	.9961	
Pu^{239}			.9385
Pu^{240}			.0579
Pu^{241}			.0036

Uncertainty .7%

TABLE 4.2 PER ATOM FISSION RATIO

Isotopes	Ratio
U^{234}/U^{235}	$.26 \pm .03$
U^{236}/U^{235}	$.08 \pm .008$
Pu^{240}/Pu^{239}	$.23 \pm .05$
Pu^{241}/Pu^{239}	$1 \pm .15$

TABLE 4.3 ANALYSIS OF STEADY-STATE CALIBRATION EXPERIMENT 1233

	U^{235} CHAMBER	U^{238} CHAMBER
COUNTED COUNTS	130629372	25238012
Extrapolation to zero bias	1.004	1.014
Fission Fragment absorption	1.0014	1.015
Dead Time	1.002	1.0004
Impurity fissions (other than U^{235}, U^{238})	.996	1.000
Fissions during Setting	1.0022	1.0022
Total fissions	$1.312\ 10^{8}$	$2.604\ 10^{7}$

TABLE 4.4 RESULTS OF STEADY-STATE EXPERIMENT 1233

U^{235} fissions/gm of U^{235} = $1.015\ 10^{12}$

U^{238} fissions/gm of U^{238} = $2.016\ 10^{10}$

U^{238}/U^{235} per atom fission ratio = .02011

U^{235} fission/gm of U^{235} sample = $.9697\ 10^{12}$

U^{238} fission/gm of U^{238} sample = $2.008\ 10^{10}$

TABLE 4.5 SUMMARY OF STEADY-STATE EXPERIMENTS

STEADY STATE RUN	U^{238}/U^{235} PER ATOM FISSION RATIO	U^{235} FISSIONS PER GM OF U^{235} SAMPLE	U^{238} FISSIONS PER GM OF U^{238} SAMPLE	Pu^{239} FISSIONS PER GM OF Pu^{239} SAMPLE
25/4/75	.02085	$.9604\ 10^{12}$	$.02062\ 10^{12}$	-
1233	.02011	$.9697\ 10^{12}$	$.02008\ 10^{12}$	-
1133	.02225	$1.066\ 10^{12}$	$.02444\ 10^{12}$	-
1139	.02155	-	-	-
11/11/75	-	-	-	$3.865\ 10^{11}$

TABLE 4.6 ERRORS OF THE STEADY STATE RESULTS

ERROR	VALUE FOR U^{235}	VALUE FOR U^{238}	VALUE FOR Pu^{239}
Random error	.01%	.02%	.01%
Extrapolation to zero bias	.1%	.3%	.1%
Fission Fragment Absorption	.35%	.35%	.35%
Mass uncertainty	1.3%	1.5%	1.3%
Isotopic Composition	.7%	.7%	.7%
Dead time	.1%	.0%	.1%
Impurity fission	.1%	.1%	.0%
Fissions during setting	.1%	.1%	.1%
Total error	1.53%	1.72%	1.53%

4.2.1 The Ba-140 technique

The La-140 isotope, apart from being produced directly by fission, it is produced by the below β-chain as well.

$$Xe^{140} \rightarrow Cs^{140} \rightarrow Ba^{140} \rightarrow La^{140} \rightarrow Ce^{140}$$
$$16sec \quad 66sec \quad 12.789d \quad 40.2h \quad stable$$

Since the half-lives of Xe-140 and Cs-140 are much less than the half-life of Ba-140, we assume that the Ba-140 is produced at the moment of the fission with a yield Ba(0) equal to the sum of the fission yields of Xe^{140}, Cs^{140} and Ba^{140}.

We allowed thirteen days to elapse between the irradiation and onset of counting, so that, any La^{140} formed directly from fission will decay out. Then, the La^{140} activity at time t after the fission is

$$R = Ba(0) \frac{\lambda_{Ba}\lambda_{La}}{\lambda_{La} - \lambda_{Ba}} (e^{-\lambda_{Ba}t} - e^{-\lambda_{La}t})$$

where λ_{Ba}, λ_{La}, R is the decay constant of Ba-140, La-140 and the La-140 activity per fission, respectively.

The reference time chosen for normalisation of the activity was 15 days after the irradiation, and in this case, we can use the following equation for the decay of R

$$R = Ba(0) \frac{\lambda_{Ba}\lambda_{La}}{\lambda_{La} - \lambda_{Ba}} e^{-\lambda_{Ba}t} \qquad (4.1)$$

within $\pm$ 0.5%.

The β-decay of La-140 is accompanied by a large number of gamma rays, the most prominent one (≈95%) being of energy 1596 Kev. The activity of the 1596 kev gamma was measured. The half-life of Ba-140 is given[27] equal to 12.789 $\pm$ .006d.

Equation (4,1) is correct for instantaneous irradiation. For the steady-state irradiations, the middle of the irradiation period was accepted as t = 0 and the resulting second order error is negligibly small,since the irradiation time has never exceeded six hours.

4.2.2 The Lithium drifted Germanium detector.

In order to measure the activity of the 1596 kev gamma which accompanies the La-140 β-decay, we must use a high resolution (energy) detector. The semiconductor detectors have the best resolution because the energy required for the production of a pair of charge carriers is less by a factor of 8-10 in semiconductors than in gases, and less by a factor of a 100 (approximately) than that required to produce a photo-electron in a scintillation counter.

Deme[28] has described the characteristics of the semiconductor detectors, while Gibbons et al[29] have described the features of the gamma-ray spectroscopy using lithium drifted germanium detectors, Ge(Li). We will give a brief description of this spectroscopy technique.

The operation of a semiconductor detector is similar to the operation of an ionisation chamber. When an ionising radiation goes through a semiconductor material, electron-hole pairs are generated; an electric signal appears on the anode because of the collection of these charges (by a polarizing high voltage). There are two main problems which must be solved (not met in the ionisation chambers) in order to achieve the good expected resolution.

(i) Impurity atoms and lattice defects in the monocrystal may trap charge carriers. The trapping of two charge carriers of opposite sign leads to their recombination. So, changes in the recombination rate

will lead to fluctuations in the amplitude of the output pulse. Generally, crystals with small concentration of traps (and effectively high free carrier lifetime) must be used. Also, high polarizing voltages, short distances between anode-cathode and crystals of high carrier mobility must be used to minimise the transit time of the electron-hole pairs, within the crystal.

(ii) The conductivity of semiconductor materials is not zero. Since we must use high polarizing voltages, a large direct current (fluctuating) will flow through the crystal which will impair the resolution of the detector.

There are two techniques which are used to manufacture semiconductor detectors of high resistivity.

(i) The junction semiconductor detectors utilize the high resistivity of the depletion layer of a p-n junction. Since the thickness of the depletion layer is very small, these detectors are unsuitable for gamma-ray spectroscopy.

(ii) Large sensitive volume semiconductor detectors, suitable for gamma-ray spectrometry, are manufactured using the Li-drift technique. Germanium is preferred to Silicon, because the density and atomic number of Germanium are higher than those of silicon. Lithium is diffused in a p-type purified germanium monocrystal and a p-n junction is formed. Under high temperature and reverse bias (of the junction) conditions the Lithium atoms drift inside the p-core, compensating the acceptor atoms. So, an intrinsic high resistivity detector is formed. Higher sensitive volume detectors are manufactured using the coaxial geometry than the earlier planar one, because of limitations in the maximum

drift distance and maximum diameter of a monocrystal.

The detector used has been manufactured by Canberra[30] (model 7219). It is a true coaxial detector and the dimensions are given below,

diameter of the crystal = 36 mm

length of the crystal = 43 mm

volume of detector = 43 cc

diameter of p-core = 6 mm

thickness of the diffused η layer = .3 mm

The detector is located within a vacuum chamber, so that, its surface will be protected from water vapours. The foils to be counted are placed in front of the flat surface of the detector, the thickness of the aluminium window (end cap of the vacuum chamber) being .5 mm. The cylindrical surface of the detector is surrounded by a cylindrical lead gamma-shield, so that, the natural background will be reduced.

In order to improve the resolution of the Ge(Li) detectors, they must be operated at low temperatures (reduce the reverse current). Also, the detectors must be stored at low temperatures to avoid drifting of the Lithium atoms. The present detector is cooled using liquid nitrogen stored in a dewar. The detector is mounted on the one end of a copper cold finger, the other end being immersed into the liquid nitrogen.

The preamplifier used was manufactured by Canberra[30] (model 1408C). The capacity of this detector is approximately 22 pF. The preamplifier used has a charge sensitive input stage so that, the overall gain will be insensitive to variations of the high voltage. The charge-sensitive stage consists of a high gain voltage amplifier (gain higher than 8000) with a negative feedback via a 1pF capacitor. The input FET stage of the preamplifier is mounted on the cryostat (so that it will be cooled).

Delaney[31] has described the noise sources associated with the previously described amplifier system. The shot noise of the reverse current of the detector and of the current of the gate of the FET and the thermal noise of the transistor, are the main noise sources.

Cooling the detector and the input FET will reduce the shot noise of the reverse current of the detector and the gate. In order to reduce the thermal noise of the input FET we have to reduce the input capacitance (including feedback) and increase the transconductance (cooling the FET increases the transconductance, DEME[28]).

The preamplifier is split into two parts, the input FET being mounted onto the cryostat for the previously mentioned reasons.

4.2.3 The 1596 KEV photopeak

The electronics associated with the measurements, using the Ge(Li) detector are given in Figure (4.1). The energy calibration of the detection system was done using a pulser and standard sources.

The linearity of the electronics and the back-bias of the multi-channel analyser was found using a pulser. The pulser was feeding the test input of the preamplifier and the shaping was adjusted, so that, the output pulses of the amplifier (observed with an oscilloscope) had a similar shape with the pulses due to gamma rays. Using this pulser shaping, the output voltage of the pulser was varied and the correspond ing channel of the multichannel analyser was read off. Table (4.7) gives part of the obtained results (a more fine division was used).

Two standard sources were used to calibrate the energy scale. Table (4.8) gives the energy of the counted photopeak. The observed peak was the only peak (within the statistics) over an energy interval of 60 Kev from either side. (Figure (4.2)).

The Pu^{239} foils emitted a high activity low energy x-ray, the 1596 kev photopeak had a very bad resolution. It was thought that the analysis of the photopeak would be inaccurate because of the bad resolution. It was thought that excessive pulse-pile up in the electronics was responsible for this bad resolution of the 1596 Kev photopeak. It is apparent that the reduction of the count rate would improve the resolution of the spectrometer. It is important to reduce the efficiency of the detection system at low gamma energies without a significant reduction of the efficiency at 1596 Kev, otherwise the statistical accuracy of the measurements will be low. This uneven reduction in the efficiency can be achieved using a gamma shield because of the large photoelectric cross-section at low energies. It was found that three millimetres of Cd gamma shield were adequate, to obtain an acceptable resolution. The detector flat face was completely shielded and a typical observed spectrum is given in Figure (4.2).

TABLE 4.7 The back-bias of the analyser was found 74ch (Tenellec amplifier)

VOLTAGE OF PULSE	PEAK CHANNEL NUMBER
.05	1005
.10	1931
.15	2861
.20	3790
.25	4720
.30	5649
.35	6578

TABLE 4.8 Energy of counted Peak (Tenellec Amplifier)

STANDARD SOURCE	ENERGY (KEV)
Yt-88 1836 kev	1596 kev
Yt-88 898 kev	1593 kev
Co-60 1173 kev	1594 kev
Co-60 1332 kev	1595 kev

AVERAGE 1595 kev

FIGURE 4.1 ELECTRONICS OF THE Ge(Li) DETECTOR

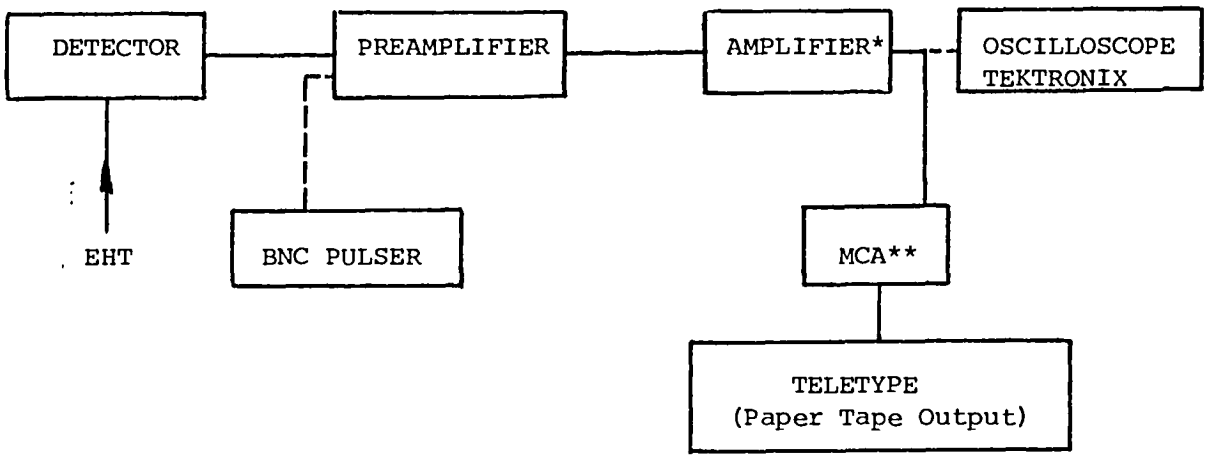

* Amplifier Canberra 1412. A few U^{235} measurements with Tenellec.

** MCA U-measurements with Northern Scientific

Pu-measurements with Laben-8000

FIGURE 4.2 TYPICAL COUNTED PHOTOPEAK
(1596 Kev photopeak, Pu-239 isotcpe, 0.500 kev/channel)

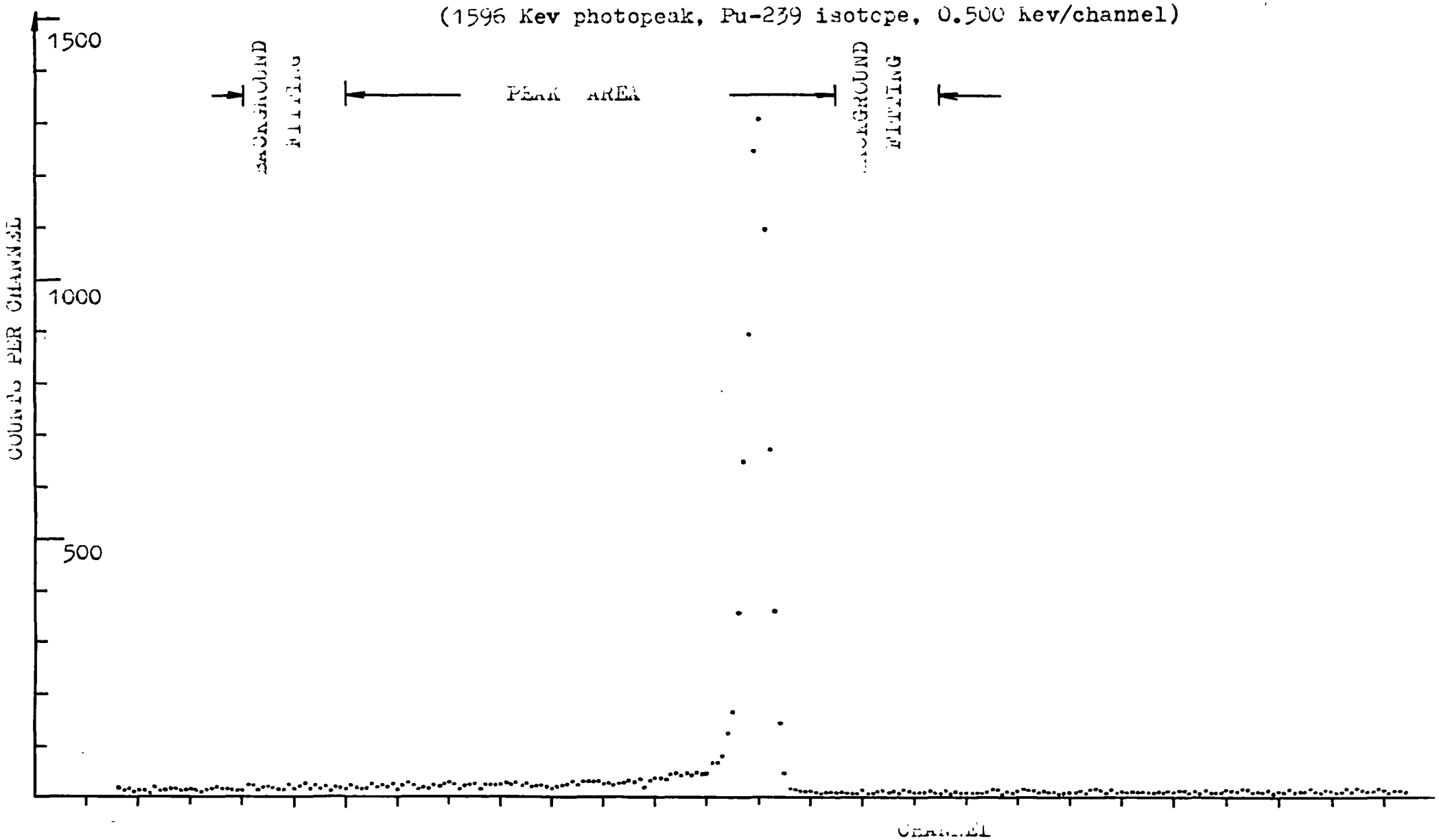

4.2.4 The photopeak analysis

Generally, the spectrum obtained by a Ge(Li) detector consists of well resolved peaks superimposed onto a compton continuum. The observed peaks may be single escape, double escape or full-energy (absorption) peaks. Different methods have been proposed for the analysis of these peaks.

HELMER et al[32] represented a peak by a Gaussian function and the compton contimuum by a straight line. VARNELL et al[33] represented a peak by a Gaussian plus low and high energy exponential tailings and the compton continuum by a quadratic function. The least squares method was used by both workers, to fit the postulated shapes to the experimental points. The disadvantage of these methods is that bias is being introduced because of the postulation of the shape of the peak but, these are the only methods which can be used for the analysis of multiplets.

For single peaks, a base line is constructed in the peak region and the number of counts above this line is a measure of the intensity of the particular activity. COVELL[34] calculates the peak area as the number of counts above a straight line drawn from two boundary points on either side of the peak. YULE[35] examined this method and concluded that the width of the peak area is critical. He devised an automatic way of determining the width working on a smoothed spectrum, the smoothing being done by a polynomial least squares fitting. QUITTNER[36] suggested a non-linear base line using smoothed values and derivatives for the Compton-continuum, outside the peak region.

The observed full-energy peak (Figure 4.2) is a single peak. Since the compton background is low, a straight line was used as base line. We used a smoothing technique to improve the statistical error of the

measurements. The technique is described below and the necessary calculations were performed by the code FISSION.

The channel number, K, corresponding to the peak channel was found and a predetermined number of channels on the left (ML) and on the right (MH) of the peak channel, determined the peak area (Figure 4.2). Then, a predetermined number of channels on the left of the peak area (M1) and on the right of the peak area (M2), determined the intervals where the linear base line will be fitted. Let us assume that C(I) is the measured number of counts in channel I and that $\alpha I + \beta$ is the base line. We estimate α,β using the equations (4.2).

$$\sum_{I=K-ML-M1}^{K-ML} (C(I)-\alpha I -\beta) = 0 \qquad \sum_{I=K+MH}^{K+MH+M2} (C(I)-\alpha I-\beta) = 0 \,, \tag{4.2}$$

The statistical error of the parameters α,β was found assuming that the standard deviation of C(I) is $\sqrt{C(I)}$. The intensity of the peak was found as the number of counts, above the linear base line, in the previously defined peak area. The statistical error of the intensity was found too, the trivial calculations not being reported.

The values of ML, MH were chosen, so that, the peak is covered completely thus, the calculated intensity being insensitive to small changes in resolution (e.g. because of decay). The values of M1,M2 were chosen, so that, smoothing was achieved and the linearity assumption would not give false results. The same values have been used for the foils of the pulses and the foils of the appropriate steady state runs, for each isotope.

The values of the previous parameters were chosen using the graphical representation of the peak (figure 4.2). The decay of the intensity was checked, over the time interval of the measurements, using published values (section 4.2.1) and typical result is presented in Table 4.9. The

good agreement of the measurements (Table 4.9) shows that the assumptions are valid.

4.2.5 The stability of the efficiency of the Ge(Li) detectors

Since the measurements are comparative ones, we are interested in the stability of the efficiency of the Ge(Li) detector, only.

The foils were placed within the slot of a demountable aluminium holder; the dimensions of the slot matched those of the foil so that repositioning was ensured.

Two different spectrometry systems were used for the uranium and plutonium foils, because of the necessary gamma shield for the plutonium measurements (section 4.2.3).

The aluminium holder, containing the uranium foil, was mounted into a hole of a vertically rotating sample changer. Then, the sample changer was rotated by an electric motor, which automatically placed the sample in front of the detector. It was necessary to check the short term stability (repositioning of the sample) of the efficiency, and the long term stability of the efficiency because of the previously described mode of sample positioning and possible variation in the detector characteristics.

The short term stability was studied using a Cs-137 standard source. Table 4.10.1 gives twelve measurements of the same source (live time equal to 300 sec) obtained within a few hours. The sample changer was rotated 360 degrees before each measurement, the source being permanently mounted on the sample changer. The error of each measurement is equal (assuming Poisson distribution) to .10% while it is calculated (using the twelve measurements) equal to .08%. We conclude that the short term stability is very good.

TABLE 4.9 The Decay of the 1596 Kev Photopeak

Irradiated 11/11/75 13.20 Reference 26/11/75 13.20

START OF COUNTING 7/12/75 13.45
La^{140} counts per gm per 7000 Live Secs at reference = 132409 ± 799

START OF COUNTING 24/11/75 16.08
La^{140} counts per gm per 7000 Live Secs at reference = 131611 ± 527

AVERAGE 132010 ± 479

Errors given are only statistical errors (1σ).

TABLE 4.10 Stability of the Detector Efficiency

TABLE 4.10.1 Short Term Stability

NO	COUNTS	NO	COUNTS	NO	COUNTS
1	1007212	5	1007543	9	1006990
2	1007018	6	1009026	10	1007950
3	1008701	7	1006755	11	1007051
4	1008256	8	1006635	12	1008597

TABLE 4.10.2 Long Term Stability

NO	TIME (DAYS)	COUNTS/300LIVE SECS (corrected for decay)
1	0	1054448
2	-4	1052020
3	-7	1050882
4	-10	1050795

4.10.3 REPOSITIONING OF THE GAMMA SHIELD

NO	COUNTS/100 SEC LIVE TIME	NO	COUNTS/100 SEC LIVE TIME	NO	COUNTS/100 SEC LIVE TIME
1	107689	11	107625	21	108077
2	108136	12	107938	22	107938
3	107773	13	108739	23	108089
4	107260	14	107656	24	107438
5	107199	15	108069	25	107824
6	107616	16	108058	26	107954
7	107664	17	108211	27	107511
8	107411	18	108033	28	108393
9	107569	19	107928	29	107638
10	108510	20	107963	30	107768

The long term stability of the sample changer was studied using a long lived standard source (Cs-137). Table (4.10.2) gives four measurements, uniformly distributed over a period of ten days. The error of each measurement is .10% while it is calculated equal to .16% using the four measurements. We conclude that the long term stability of the efficiency is good. A standard Cs-137 source was counted, before each measurement, to take into account any variation of the efficiency and the maximum correction applied was .8%, over a period of eight months.

The aluminium end-cap (section 4.2.2) of the Ge(Li) detector, used for the plutonium measurements, is vertical and it has a cylindrical slot. The foil holder was mounted onto the gamma-shield and the shield was placed onto the aluminium end-cap. The gamma shield was designed, so that, it could fit into the slot of the end-cap to ensure repositioning.

In order to check the repositioning of the shield, a standard Cs-137 source was mounted permanently onto the shield and thirty measurements (table 4.10.3) were obtained, the gamma shield being removed completely and repositioned onto the end-cap before each measurement. The error of each measurement is .30% and it is calculated equal to .33%. So, we conclude that the repositioning of the shield is very good.

For each isotope, the foil of at least one steady-state VIPER run and at least one small (the important)VIPER pulse have been counted simultaneously to avoid any long term drift in the electronics.

4.3 Measurements-Results-Errors-Discussion

The counting of a foil was completed within two weeks after its reference time (15 days after irradiation). Tables 4.11, 4.12 and 4.13 summarise the results of the gamma counting of the foils.

A Tenellec amplifier was used for the U^{235} measurements (table 4.11) because, the fine gain switch of the Canberra amplifier was loose, this electronic gain instability resulted in multipeaks in the energy region of the 1596 kev gamma. A new Canberra amplifier was obtained at a later stage (table 4.12) and the U^{235} study was repeated (steady state 25/4/75, Pulse 661) using this amplifier. Since the measurements are comparative ones, we have kept the counting conditions of the foil of a pulse and its corresponding steady state run identical.

The measurements were obtained over a predetermined live time of the analyser, so that the dead time correction was applied electronically. The real time between two consecutive Pu^{239} countings was fixed (Periodic-mode of the analyser operation), so that, the decay correction was calculated correctly. The real time between two consecutive uranium foil countings depends on the analyser dead time (read off) and the printing time of the teletype (measured). The maximum number of consecutive countings and the maximum continuous counting time were determined, so that, the maximum average (over a continuous counting) correction applied was .23% and .34% for the U^{235} and U^{238} foil counting, respectively. Since these corrections are small, no error has been assigned.

Table 4.15 summarises the systematic errors of foil counting, the random errors given in tables 4.11, 4.12 and 4.13.

The foil thickness was not constant (masses of foils, tables 4.11, 4.12, 4.13), so that, errors were introduced. The estimated absorption of the 1596 kev gamma within the foil is less than .6% so that, the variation of the foil thickness will introduce negligibly small errors. The fraction of uniformly produced fission fragments of range R which escape an infinite area foil of thickness t is R/2t ; so, large errors

may be introduced because of variable foil thickness (table 4.15).

The tables 4.14 and 4.16 summarise the fission measurement results and their errors.

The technique, which has already been used for the fission measurements, assumes that the Ba-140 cumulative fission yield is the same for the two irradiation environments (pulse, steady state run). Clifford[12] measured the U^{238}/U^{235} per atom fission ratio of these two irradiation environments and he did not observe any change outside the errors. Larsen et al[37] measured the Ba-140 fission yield of U^{235} and Pu^{239} for thermal neutrons and different fast neutron spectra (up to .072 U^{238}/U^{235} per atom fission ratio,McElroy et al[38]) and he did not observe any change in the yield, outside its errors. McElroy et al[38] have summarised the Ba-140 cumulative fission yield of U^{238} for assemblies with different degrees of hardness. It is apparent that all the measurements are in agreement within the errors. So, we argue that there is no difference in the Ba-140 fission yield, between these two irradiation environments.

Since the diameter of the foils is much less than the diameter of the deposits, a non linear flux gradient along the deposit will give false results. Four U^{235} foils were irradiated within the chamber (Figure 4.3) at the positions A, B, C and R simulataneously, and they were gamma counted subsequently (table 4.17). The two foils of the steady state run 1133 (table 4.11) were placed at two different vertical positions (normal to the figure 4.3).

We conclude that (tables 4.11, 4.17) the flux varies only in the direction normal to the reactor face, and this variation is linear. Since the foils were sandwiched vertically at the position R (figure 4.3) no error has been assigned because of flux gradient.

It is apparent that the fission density may vary along the sample irradiated in a VIPER pulse, too. The samples of the small U^{235} and Pu^{239} pulse consist of one foil only, which was gamma counted subsequently; so, the fissions are calculated properly for these pulses. The sample of the small U^{238} pulse (pulse 636) consists of seven foils; three foils, uniformly distributed over the length ofthe sample, were gamma counted (table 4.12) and no flux variation was observed along the sample. So, the average value was accepted as the number of fissions.

The U^{238} calibration factor (activity/fission) is reproduced by the experiments 1233 and (25/4/75). The U^{235} calibration factor calculated by the calibration experiments (25/4/75) and 1133 is not reproduced because, we have used different amplifiers. It will be apparent (chapter 6) that the number of fissions of the appropriate pulses has been calculated correctly by these calibration experiments.

A cross-check between the U^{238} calibration experiment (1233) and the U^{235} calibration experiment (25/4/75) is the Ba-140 fission yield ratio (identical foil counting conditions have been used for both experiments) for U^{235} and U^{238} isotopes. The Ba-140 fission yield ratio is calculated equal to

$$\frac{\text{Ba-140 fission yield } (U^{235})}{\text{Ba-140 fission yield } (U^{238})} = .991 \pm 2.8\%$$

The value reported for this ratio (CFRMF assembly, McElroy et al[38], the most accurate presented values in the tables) is $1.010 \pm 4.2\%$. Note that the latter error is high because it includes the error in the efficiency calibration of the detector which is irrelevant in the ratio.

TABLE 4.11 U^{235} Foil Counting

I.D.	1596 Kev gamma counts per 10000 live secs per gm of sample at reference(normalised*)	FOIL MASS (gm)
PULSE 661	$2.331\ 10^5 \pm .51\%$ (1)	.03505
STEADY STATE (25/4/75)	$6.501\ 10^5 \pm .49\%$ (1)	.03352
PULSE 588	$6.659\ 10^5 \pm .27\%$ (2)	.03849
STEADY STATE 1133	$6.958\ 10^5 \pm .23\%$ (2)	.03579
PULSE 571	$6.936\ 10^5 \pm .29\%$ (3)	.03672
STEADY STATE 1133	$7.050\ 10^5 \pm .46\%$ (3)	.03579
STEADY STATE 1133	$7.046\ 10^5 \pm .39\%$ (3)	.03526
PULSE 572	$6.558\ 10^5 \pm .27\%$ (4)	.03577
STEADY STATE 1133	$6.964\ 10^5 \pm .34\%$ (4)	TWO FOILS
PULSE 572	$6.524\ 10^5 \pm .25\%$ (5)	.04177
STEADY STATE 1133	$6.969\ 10^5 \pm .32\%$ (5)	TWO FOILS

* Cs-137 normalisation (section 4.2.5)

(1) Canberra amplifier. Position 1 on the sample changer. No other foil on the sample changer.

(2) Tenellec amplifier. Position 1 on the sample changer. No other foil on the sample changer.

(3) Tenellec amplifier. Position 4 on the sample changer. Three foils on the sample changer.

(4) Tenellec amplifier. Position 7 on the sample changer. Three foils on the sample changer.

(5) Tenellec amplifier. Position 1 on the sample changer. Three foils on the sample changer.

TABLE 4.12 U^{238} Foil Counting(1)

I.D.	1596 kev gamma counts per 40000 Live Secs per gm of sample at reference (Normalised*)	FOIL MASS (gm)
STEADY STATE 1233	$6.504\ 10^4 \pm 1.1\%$	.03332
STEADY STATE 25/4/75	$6.516\ 10^4 \pm 2.2\%$ (REFERENCE*)	.03693
PULSE 598	$4.431\ 10^4 \pm 1.2\%$	.03725
Pulse 596	$4.396\ 10^4 \pm 1.2\%$	.03715
Pulse 597	$4.388\ 10^4 \pm 1.3\%$	.03779
Pulse 636 -1	$4.441\ 10^4 \pm 1.2\%$	.03698
PULSE 636 -4	$4.537\ 10^4 \pm 1.3\%$	.03719
PULSE 636 -7	$4.465\ 10^4 \pm 1.5\%$	.03443

* Cs-137 normalisation (section 4.2.5)

(1) Canberra Amplifier. Position 1 on the sample changer.
No other foil on the sample changer.

TABLE 4.13 Pu^{239} FOIL COUNTING

I.D.	1596 kev gamma counts per 7000 live Secs per gm of sample at reference.	FOIL MASS (gm)
STEADY STATE 11/11/75	$1.324\ 10^5 \pm .60\%$	.0595
PULSE 634	$1.451\ 10^5 \pm .40\%$	.0599
PULSE 668	$1.583\ 10^5 \pm .48\%$	.0600
PULSE 617	$3.255\ 10^5 \pm .36\%$	.0597

TABLE 4.14 TOTAL NUMBER OF FISSIONS OF MAIN ISOTOPE

PULSE I.D.	SAMPLE MASS (gm)	NUMBER OF FISSIONS
571	.0366	$3.840\ 10^{10}$
661	.0351	$1.205\ 10^{10}$
588	.3484	$3.555\ 10^{11}$
572	8.2728	$8.281\ 10^{12}$
598	.2646	$3.620\ 10^{9}$
596	11.2032	$1.520\ 10^{11}$
597	2.8824	$3.905\ 10^{10}$
636	.2598	$3.594\ 10^{9}$
634	.0599	$2.537\ 10^{10}$
668	.0600	$2.773\ 10^{10}$
617	.1780	$1.691\ 10^{11}$

TABLE 4.15 SYSTEMATIC ERRORS IN FOIL COUNTING

SOURCE OF ERROR	U^{235}	U^{238}	Pu^{239}
Cs-137 normalisation	.20%	.20%	.20%
Decay of photopeak	.50%	.50%	.50%
Mass uncertainty	.03%	.03%	.20%
Fission Fragment Escape	.20%	.50%	—
total error	.57%	.74%	.57%

TABLE 4.16 ERRORS IN NUMBER OF FISSIONS

SOURCE OF ERROR	U^{235}	U^{238}	Pu^{239}
Calibration Experiment	1.53%	1.72%	1.53%
Foil Counting Statistics	.71%	1.34%	.72%
Systematic Errors in foil counting	.81%	1.04%	.81%
Mass uncertainty	.3%	.3%	.2%
total error .	1.91%	2.44%	1.88%

FIGURE 4.3 STUDY OF THE FLUX GRADIENT FOR THE CALIBRATION EXPERIMENT

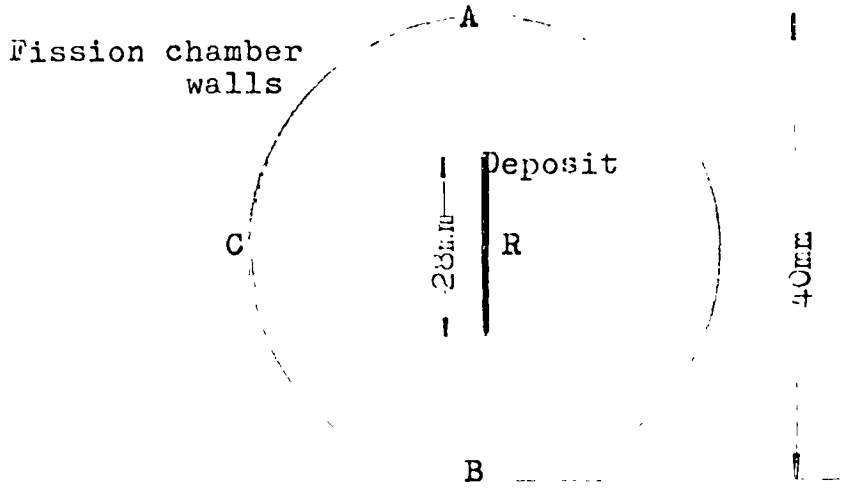

TABLE 4.17 FLUX GRADIENT

POINT (figure 4.3)	RELATIVE FLUX (Reference point R, figure 4.3)
A	1.036 ± 0.02
B	0.965 ± 0.02
C	0.995 ± 0.02

CHAPTER 5

ANALYSIS OF THE DATA

In this chapter, we describe the theories used for the analysis of the data. A complete set of data consists of the measurements of three VIPER pulses using one neutron counter only. The basic features of the codes, used for the analysis of the data, are described, too.

5.1 The codes DATA, JOIN, FINAL

The raw data, obtained from a set of three VIPER pulses, were transferred on a permanent file of the CDC-6400 machine, using paper tape as the intermediate storage medium between the ARGUS computer and the CDC machine.

The program DATA reads the raw data of each pulse, and it calculates the discrete function of delayed neutron emission rate per fission versus time t after the irradiation, for each pulse of the VIPER reactor separately. The program performs the following corrections;

1. Computer (ARGUS) and detection system dead time correction
2. Detector background (laboratory) correction.
3. Impurity delayed neutron correction from U^{235} or U^{238} in a U^{238} or U^{235} sample, respectively. The isotopic composition of the sample, the U^{238}/U^{235} per atom fission ratio and the group constants of Keepin et al[4] were used for the impurity delayed neutron correction, performed at each point of the three discrete functions. This is a significant correction for the U^{238} sample.

The basic steps of the code DATA are described below. If n is the number of delayed neutrons collected over a time channel of duration T, the delayed neutron count rate is

$$n/(T-D) \qquad (5.1)$$

where, D is the computer dead time. We assume that the count rate, given by equation (5.1), corresponds to the middle of the collection time interval (i.e. (T-D)/2), so that the count rate given by eq. (5.1) has a systematic error, approximately equal to

$$\frac{T^2}{8} \sum_i \alpha_i \lambda_i^3 e^{-\lambda_i t} \Big/ \sum_i \alpha_i \lambda_i e^{-\lambda_i t} \qquad (5.2)$$

where, α_i, λ_i are the group constants of the delayed neutrons, and t is the time after the irradiation corresponding to the time channel under consideration.

It is apparent that, the time t after the irradiation and the channel width T must be selected, so that, the error given by equation (5.2), will be negligibly small. Although a single short channel width T could be used to cover the whole time interval, where measurements must be accumulated, the multiscaling of the measurements (variable T) is necessary for computational reasons (reduce the number of points of the discrete function which must be fitted).

We have assumed that the random error of n is given (Poisson distribution) by

$$\pm \sqrt{n} \quad (1 \text{ standard deviation}) \qquad (5.3)$$

The delayed neutron count rate is corrected for the previously mentioned reasons, and it is converted into the delayed neutron emission rate per fission, using the number of fissions of the main isotope in the sample of the particular pulse and the detector efficiency. The detector efficiency, which was used, is the efficiency of the Pu^{240} neutron source the date the experiment was done at the axial arrest position of the sample.

The absolute time scale calibration of the measurements has been described in chapter-3.

The output of the program DATA consists of three discrete functions

(corresponding to each of the three VIPER pulses) of delayed neutron emission rate per fission versus time, each point associated with a random error because of the delayed neutron and background measurements. This output is written on a permanent file of the machine.

The program JOIN reads the output of the program DATA and it calculates the total number of delayed neutrons per fission emitted over a time interval. The trapezoidal rule is used for the numerical integration. In particular, the delayed neutrons emitted in the time interval (T'_1,T'_2) per fission, as it has been measured by the small and medium sample VIPER pulses, is calculated, provided that the time interval is within the overlapping time interval of these two pulses. Similar work is done for another time interval (T'_3,T'_4) and the medium and large sample VIPER pulses.

The program JOIN allows a strict check on the reproducibility or required adjustment of the measurements.

The program FINAL reads the output of the program DATA and joins the three pulses at different moments T_1, T_2, T_3, so that, the measurements of the small sample VIPER pulse are used in the time interval $(0,T_1)$, the measurements of the medium sample VIPER pulse are used in the time interval (T_1,T_2) and the measurements of the large sample VIPER pulse are used in (T_2,T_3). Furthermore, the data of each pulse can be multiplied by a normalisation factor, before joining the three discrete functions, so that the joined final discrete function will include the measurements of one or more pulses multiplied by a normalisation factor. The normalisation factors are calculated by the program JOIN.

The moments T_1 and T_2 are chosen, so that, the final discrete function will have the best statistical accuracy which can be obtained from the performed experiments, provided that the detected count rate will be less than 30000 c/sec at any moment after the irradiation and

the error given by equation (5.2) will be negligibly small.

The output of this program (single discrete function of delayed neutron emission rate per fission versus time along with a random error at each point) is stored onto a permenent file of the machine. This discrete function is the basis for the absolute delayed neutron yield and group constants calculation.

The group constants of the delayed neutrons (relative group abundance) and the reactivity (dollars)-period relationship depend only on the shape of the delayed neutron decay curve. The three VIPER pulses may be consistent, as far as the yield of the delayed neutrons is concerned, but, the joined discrete function may still have a systematic error in the shape of the delayed neutron decay curve if, the previously described normalisation will not be used. In particular, random errors in the efficiency measurement (Pu^{240} detector calibration) and random errors in the foil counting (fission measurements) will introduce systematic errors in the delayed neutron decay curve shape, if the previously described normalisation will not be used. The previously described normalisation allows a correction to be applied to the shape of the final discrete function, which is correct (as far as the shape is concerned) to within the random error of the delayed neutron measurements in the time interval where the normalisation factors are calculated.

5.2 Linear regression analysis

Let us consider that the random variable y is a linear function of the fixed (non random) variable x_i (i=1, .., k). So,

$$y = b_0 + b_1x_1 + \ldots\ldots + b_kx_k + u \qquad (5.4)$$

Equation (5.4) (linear regression model) implies that, for specified values of the variables x_i (i=1, ...,k) the observed value of the variable y will be different from the calculated, using the linear

combination, by the random quantity u.

Let us assume that at any point (x_i, i=1, ...,k), the random variable u has a mean equal to zero and a variance σ^2 independent of the point. Furthermore, let us assume that the discrepancies u, at any two different points (x_i, i=1, ..,k), are uncorrelated.

In practice, measurements of the variable Y are obtained at n different points and we require an estimate of the parameters b_i (i=0,1,..,k). The least squares method is used to calculate the parameters of a regression model.

Let us assume that x_{ij} is the value of the j^{th} variable at the i^{th}(=1,...,n) point of measurement and y_i(i=1,...,n) the value of the y variable at the i^{th} point of measurement. Then,

$$y_i = b_0 + b_1x_{i1} + ... + b_kx_{ik} + u_i \qquad (5.5)$$

According to the least squares technique, we require b_i(i=0,1, ..,k) so that

$$\sum_{i=1}^{n} u_i^2 = \sum_{i=1}^{n} (y_i - b_0 - b_1x_{i1} - .... - b_kx_{ik})^2 \qquad (5.6)$$

will be minimum.

If we consider the below matrix notation,

$$X = \begin{bmatrix} 1 & x_{11} & ..... & x_{1k} \\ & & & \\ & & & \\ 1 & x_{n1} & ..... & x_{nk} \end{bmatrix}$$

$B = [b_0, b_1, ..., b_k]^T$ and $Y = [y_1, ...,y_n]^T$

where T the transpose of a matrix then, Huang[39] shows that:

The parameter estimates are given by

$$B = (X^T X)^{-1} X^T Y \tag{5.7}$$

and the variance-covariance matrix of B is given by

$$\sigma^2 (X^T X)^{-1} \tag{5.8}$$

and an estimate of the variance σ^2 of the population is

$$S^2 = \frac{\sum_{i=1}^{n} u_i^2}{n-k-1} \tag{5.9}$$

where, (k+1) is the number of the estimated parameters.

5.3 The regression model. The least squares solution.

Assume that the delayed neutron group yield and decay constant is α_i and λ_i respectively. The number of delayed neutrons emitted per second per fission at time t after the irradiation is

$$y(t) = \sum_{i=1}^{M} \alpha_i \lambda_i e^{-\lambda_i t} + u(t) \tag{5.10}$$

We have assumed that the number of groups is M and that the irradiation is instantaneous. It is possible a delayed neutron precursor to be a member of a β-chain reaction, so that, growth and decay phenomena may be present[10]. Such phenomena have been neglected in formulating the regression model of equation (5.10).

The quantity u(t) is the statistical discrepancy because of the statistical nature of radioactivity. The mean of this quantity is zero and its variance, $\sigma^2(t)$, is a function of time. Futhermore, since the status of a precursor does not depend on the status of another precursor, the statistical discrepancies $u(t_1)$ and $u(t_2)$, at two different moments t_1 and t_2, are uncorrelated. So, the regression model of eq. (5.10) is a heteroskedastic one.

The heteroskedasticity can be removed, if the model is rewritten as

$$\frac{y(t)}{\sigma(t)} = \frac{\sum_{i=1}^{M} \alpha_i \lambda_i e^{-\lambda_i t}}{\sigma(t)} + \frac{u(t)}{\sigma(t)} \tag{5.11}$$

since, the new discrepancy $u(t)/\sigma(t)$ has the variance equal to unity.

The least squares solution of the model eq. (5.11) is

$$\text{MINIMISE} \qquad S = \sum_{j=1}^{J} \frac{1}{\sigma^2(tj)} \left[y(t_j) - \sum_{i=1}^{M} \alpha_i \lambda_i e^{-\lambda_i t_j} \right]^2 \qquad (5.12)$$

We have assumed that we have obtained J measurements of the delayed neutron count rate per fission at the moments $t_j (j=1, \ldots, J)$ and that an estimate of the variance is available at each point.

Powell[40] has examined the available techniques for non-linear least squares optimisation. Generally, the techniques using information on the derivatives of S are more efficienct than those using only function values. The former techniques are different versions of the steepest descent and the Gauss-Newton methods.

Let us assume that

$$f_j(\bar{X}) = \frac{1}{\sigma(tj)} \left[Y(tj) - \sum_{i=1}^{M} X(i) e^{-X(i+M)tj} \right]$$

where $X(i) = \alpha_i \lambda_i$, $X(i+M) = \lambda_i$ $\qquad i = 1, \ldots, M$

$$\bar{X} = \{X(1), \ldots., X(2M)\}^T$$

$$F = \{f_1, \ldots., f_J\}^T$$

$$P_{ij} = \frac{\partial f_i(\bar{X})}{\partial X(j)} \quad \text{and} \quad P = \{P_{ij}\} \qquad (5.13)$$

In the steepest-descent method, the step per iteration δ is chosen along the direction $-P^T F$. So, if $\bar{X}^k$ is the iteration point of the k^{th} iteration then,

$$\delta = \bar{X}^{k+1} - \bar{X}^k = \lambda(-P^T F) \qquad \lambda>0 \qquad (5.14)$$

The quantity λ must be chosen, so that, a decrease in the function S will be assured (e.g. small λ). The quantities P^T and F are evaluated at the $\bar{X}^k$ iteration point.

In the Gauss-Newton method, we assume linearity of $F(\bar{X})$ around the current iteration point $\bar{X}^k$, and the solution of the linear model according to the least squares technique is

$$\bar{X}^{k+1} - \bar{X}^k = -(P^T P)^{-1} P^T F \tag{5.15}$$

where, all the quantities are evaluated at the point $\bar{X}^k$.

It is known that the steepest descent method is reliable but slow and the Gauss-Newton method is unreliable (it may diverge) but fast.

Marquardt[41] suggested a hybrid method; the step per iteration δ is given by

$$(P^T P + \lambda I)\delta = -P^T F \tag{5.16}$$

where I is the unity matrix and λ a positive quantity controlled by the method.

It is apparent that for $\lambda \to 0$ we obtain the Gauss-Newton method and for $\lambda \to \infty$ we obtain the steepest descent method, with a very small step. So,it is possible, by the λ adjustment, to use the reliability of the steepest descent method and the fast convergence of the Gauss-Newton method.

Assuming linearity of the function $F(\bar{X})$ at the optimal point, the variance-covariance matrix of the parameters is (section 5.2)

$$(P^T P)^{-1} \tag{5.17}$$

where the matrix P is evaluated at the optimal point.

We have said that the variance of the random discrepancy of the regression model given by eq. (5.11) is equal to one. In section 5.2 we have given an estimate of the variance of a regression model (eq.(5.9)).

So, we conclude that the quantity

$$\frac{S}{J-2M} \tag{5.18}$$

S = optimal value of the quantity defined by eq. (5.12).

is an estimate of one. It is apparent that, the optimal value of the quantity given by eq. (5.12) should be equal (statistically) to the number of experimental points ($J \gg 2M$). Any large discrepancy between these two quantities should be due to inaccurate modelling and/or data contaminated with systematic bias (error).

5.4 The code FITEXP

This code will fit up to six exponentials to the data points, according to the Marquardt method. It will calculate the error of the parameters, as well. The mathematical library NAG[42] has been used mainly for all the matrix operations required and for the optimisation routine based on the Marquardt technique. The later routine requires two subroutines (FUNCT and DERIV) for the evaluation of $f_j(\bar{X})$, (P^TP) and $-P^TF$. In order to avoid multiple calculation of the exponentials (6000 typically, per iteration) special common blocks were used (described in the N.A.G. library manual) and the total time has never exceeded 2 min on the CDC-6400 machine.

Generally, the minimum of the function was achieved after a few iterations but the partial derivatives of S were very high, especially for the linear terms $(\alpha_i\lambda_i)$ of the two longest lived groups. So, we required the relative accuracy of the variables to be 10^{-10}, so that, the partial derivatives would be zero (numerically).

Furthermore, we required all the variables to be positive, so that, strictly speaking, the optimisation is constrained as one would expect from physical considerations.

It was very difficult to check these routines (especially since they are in binary, at present) so that, a test example was used to check the routines and the programming. It is given in Table (5.1).

5.5 The code YIELD

From equation (5.10), we obtain that the absolute delayed neutron yield is

$$\sum_{i=1}^{M} \alpha_i = \int_0^{\infty} y(t)\,dt$$

The program YIELD reads the output of the program FINAL and it performs the integration. The delayed neutrons missing, because of incomplete data (at very early times and very late times), are estimated using the group constants of Keepin[4]. The numerical integration is performed using the trapezoidal rule.

TABLE 5.1 TEST OF THE FITTING ROUTINES

In order to check the least squares routine the following test data have been used. The total number of channels used was 1000. The first 300 channels had a .01 sec step. The next 270 channels had a .1sec step. The remaining channels had a 1 sec step. The data had no statistical error.

DATA USED		INITIAL SOLUTION		RESULT OF THE MINIMIZATION	
DECAY CONST.	ABUNDANCE	DECAY CONST.	ABUNDANCE	DECAY CONST.	ABUNDANCE
.0127	.00063	.0127	.000472	.012700	.0006300
.0317	.003508	.0310	.003258	.031700	.00350800
.115	.00310	.110	.00318	.11500	.0031000
.311	.00672	.315	.00635	.31100	.0067200
1.4	.00211	1.35	.00222	1.4000	.0021100
3.87	.00043	4	.00040	3.8700	.0004300
Gradient $.19\ 10^{-14}$	$.19\ 10^{-14}$	$.17\ 10^{-14}$	$.14\ 10^{-14}$	$.68\ 10^{-15}$	$.30\ 10^{-19}$
$-.18\ 10^{-19}$	$-.25\ 10^{-18}$	$-.70\ 10^{-18}$	$-.28\ 10^{-17}$	$-.10\ 10^{-17}$	$-.12\ 10^{-18}$

Function value at the minimum = $.49\ 10^{-31}$

5.6 Gardner's method

The least squares method requires an initial estimate of the group constants and the number of groups has to be determined in advance. It is known that, the optimum solution will be a local minimum in the neighbourhood of the initial estimate.

Gardner[43] proposed a technique which does not require any initial estimate of the parameters and no advance knowledge of the number of exponential terms.

According to this technique, if we have experimental points $(t_j, f(t_j))$, where

$$f(t) = \sum_{i=1}^{I} \alpha_i e^{-\lambda_i t} \tag{5.19}$$

we want to determine the function $g(\lambda)$, where

$$g(\lambda) = \sum_{i=1}^{I} \alpha_i \delta(\lambda-\lambda_i) \tag{5.20}$$

$\delta(\lambda)$ = dirac function

It is apparent that the function $g(\lambda)$ is a discrete function having non-zero values at the points λ_i $(i=1,\ldots,I)$. The function $g(\lambda)$, calculated by this technique, has broad peaks because of numerical inaccuracies in the calculation. The number of peaks is equal to the number of exponential terms and the position of the peaks determines the decay constants λ_i.

Gardner[43] shows that

$$\int_{-\infty}^{\infty} g(e^{-y}) e^{i\mu y} dy = \frac{\int_{-\infty}^{\infty} e^{x} f(e^{x}) e^{i\mu x} dx}{\int_{-\infty}^{\infty} \exp(-e^{s}) e^{s} e^{i\mu s} ds} \tag{5.21}$$

where the obvious transformations are $\lambda = e^{-y}$ and $t = e^{x}$.

It is apparent that we have to calculate the Fourier Transform of $e^{x}f(e^{x})$ and $e^{s}\exp(-e^{s})$ and the inverse Fourier Transform of their ratio will be the required function $g(e^{-y})$. It is not possible for the integrations to be carried out over an infinite range and this approximation is responsible for the error ripples appearing in the function $g(e^{-y})$.

Since the classical integration theory is time consuming, Schlessinger[44] proposed the use of the Fast Fourier Transform for the evaluation of the Fourier Transform.

If we consider the discrete function A(j),

$$A(j),\ j = 0,1,.....,N-1 \tag{5.22}$$

its discrete Fourier Transform is defined by

$$X(n) = \frac{1}{\sqrt{N}} \sum_{j=0}^{N-1} A(j) e^{-2\pi i \frac{jn}{N}} \qquad n=0,\ 1,\ ...,N-1 \tag{5.23}$$

The Fast Fourier Algorithm allows the calculation of X(n), (n = 0,1,...,N-1) with a considerable reduction in computing time than the straightforward calculation. This algorithm is based on the fact that, the discrete Fourier Transform of the discrete function A(j), (j = 0, 1, ..., N-1) can be easily calculated from the discrete Fourier Transforms of the discrete functions B(k), C(k) where

$$\begin{aligned} B(K) &= A(2K) \\ C(K) &= A(2K+1) \end{aligned} \qquad K = 0,\ 1,\ ...,\ \frac{N}{2} - 1 \tag{5.24}$$

The necessary calculations have been described by Kerlin.[46] So, it is necessary the number of elements, N, of the discrete function A(j) to be a power of two.

The aliased function $Z_p(t)$, of a function Z(t) is defined by

$$Z_p(t) = \sum_{l=-\infty}^{\infty} Z(t + lT) \qquad (5.25)$$

where T is any period. If we assume that the function Z(t) is non-zero over a finite time interval only, then, if the period T is chosen larger than this time interval the aliased function $Z_p(t)$ will be a periodic function, with period T, the basic function being the original function Z(t).

Cooley[45] has proven that, if

$$Q(f) = \int_{-\infty}^{\infty} Z(t) e^{-2\pi i f t} dt$$

then,

$$Q_p(n\Delta F) = \frac{1}{F} \sum_{j=0}^{N-1} Z_p(j\Delta T) W_N^{-jn} \qquad (5.26)$$

where,

$$W_N = e^{\frac{2\pi i}{N}}, \quad F = N\Delta F = \frac{1}{\Delta T} = \frac{N}{T}$$

It is apparent that, if the function $Z_p(t)$ will be sampled at the points $t_j = j\Delta T$ (j = 0, 1, ..., N-1) then, the values of the function $Q_p(f)$ are calculated at the points $f_n = n\Delta F = n/(N\Delta T)$ (n = 0, 1, ..., N-1) using equation (5.26). The functions $Q_p(f)$ and $Z_p(t)$ are the aliased functions of a Fourier Transform pair. It is apparent that (equations (5.26) and (5.23)) the Fast Fourier Algorithm can be used for the calculation of the discrete function $Q_p(n\Delta F)$, provided that we know the discrete function $Z_p(j\Delta T)$. Similar results exist and for positive sign for the exponent of e (Cooley[45]).

This technique was used for the analysis of the decay curve of the delayed neutron emission rate, f(t). We assume that this function, f(t), is zero outside the time interval $(0, T_3)$ where, T_3 is the largest time for which experimental measurements exist.

We want to calculate the Fourier Transform of the quantity $e^x f(e^x)$

(equation 5.21). It is apparent that

$$e^x f(e^x) = 0 \qquad t = e^x > T_3$$

We arbitrarily assume that

$$e^x f(e^x) = 0 \qquad x \notin (-\ln T_3, \ln T_3) \tag{5.27}$$

and according to Gardner[43] this is the reason for the error ripples of the function $g(\lambda)$.

Let us assume that N (power of two) is the size of the sample and X_0 is the sampling interval. Let us assume that the sampling interval X_0, is a value (near the lowest one), which satisfies

$$NX_0 > 2\ln T_3 \tag{5.28}$$

for the chosen value of N.

Let us assume that the period of the aliased function of $e^x f(e^x)$ is NX_0. According to the assumption in equation (5.27) the aliased function of $e^x f(e^x)$ will be a periodic function, with the function $e^x f(e^x)$ being the basic function. The sampling of the aliased function of $e^x f(e^x)$ (equation 5.26) at the points $x_j = jX_0 (j = 0, 1, \ldots, N-1)$ gives the following results

$$\begin{aligned} &e^x f(e^x) \text{ at } X = jX_0 , \quad j = 0, 1, \ldots, N/2 \\ &e^x f(e^x) \text{ at } X = (-N + j)X_0 , \quad j = \frac{N}{2} + 1, \ldots, N-1 \end{aligned} \tag{5.29}$$

The aliased function of the Fourier Transform of $e^x f(e^x)$ is calculated (equation 5.26) at the points

$$\mu'_j = j/NX_o \qquad j = 0, 1, \ldots, N-1$$
$$\mu = 2\pi\mu'$$

Similar work was done for the function $e^s \exp(-e^s)$. We used the same sample size, N, and the sampling interval s_0 was chosen equal to X_0. So, the aliased function of the Fourier Transform of the function $e^s \exp(-e^s)$ is calculated at the points

FIGURE 5.1 TEST EXAMPLE OF THE GARDNER METHOD.

Exact data of the exponential

$$100 \exp(-0.01\ t)$$

at the points $t=0,1,2,\ldots,1499$.

The result presented is for the below parameter values;

$N=512 \qquad X_0=0.029$

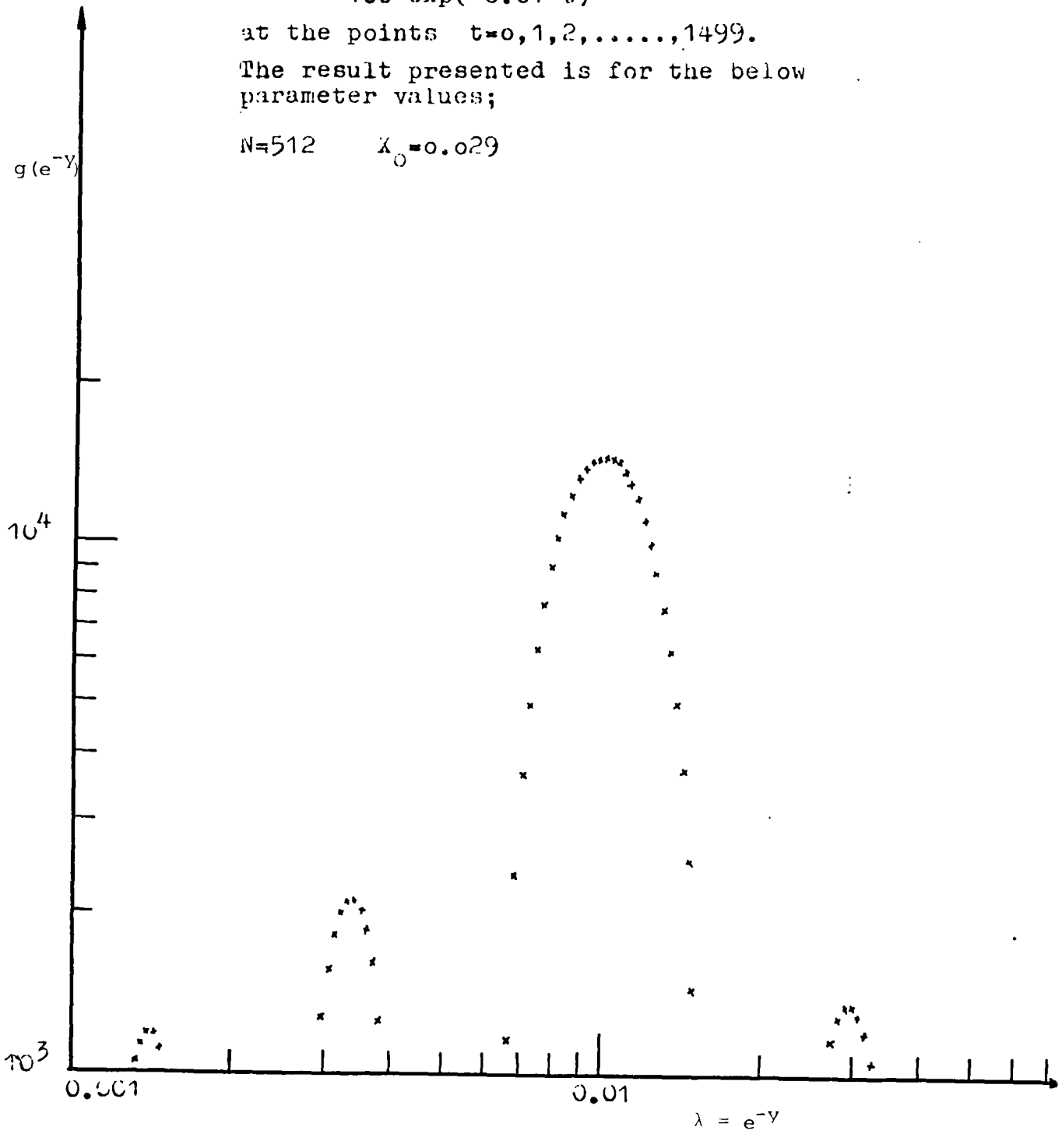

$$\mu'_j = j/Ns_0 = j/NX_0 \qquad j = 0, 1, \ldots, N-1$$

Since both aliased functions have been calculated at the same points of the frequency axis μ, the ratio given by equation (5.21) can be calculated at these points too.

A parameter, FCUT, was used and the ratio of the aliased functions was set equal to zero in the frequency interval

$$\mu' \varepsilon (FCUT, (1/X_0) - FCUT)$$

Gardner[43] has shown that, a progressive decrease of the value of the FCUT parameter removes the error ripples of the result, $g(\lambda)$, but the observed peaks have worse resolution.

The aliased function of $g(e^{-y})$ is calculated, from the previously described ratio, at the points

$$y_j = jX_0 \qquad j = 0, 1, \ldots, N-1$$

Thus the sampling interval X_0 of the function $e^x f(e^x)$ determines the sampling interval in the result, $g(\lambda)$, and for this reason it has to be short and compatible with the sample size (equation 5.28).

It is apparent that the function f(t) must be calculated at some arbitrary points (equation 5.29). Since f(t) is a discrete function (experimental points) we have used a polynomial fitting to estimate the function f(t) at any point t.

A third order polynomial was fitted to the experimental points in the interval $(t - T_0, t + T_0)$ where the interval T_0 was allowed to vary with t, so that, the polynomial representation of the exponentials would be accurate and so that, enough points would be included, in the interval, to achieve smoothing. The group constants of Keepin[10] were used for the estimation of the width T_0 as a function of t.

The method was programmed and the mathematical routines needed (Fast Fourier Transform, polynomial fitting) were obtained from the NAG[42] library. The method was checked using a test example (fig.5.1).

It is apparent that this method is worse, as far as accuracy is concerned, than the least squares method. Note that the test example shows one exponential (plus the error ripples) at $\lambda = .01$ sec^{-1}. The present example (and the work of Schlessinger[44] generally) indicates that our requirements from this method should be rather modest.

5.7 Peeling off method

This is the classical method for determining exponentials. The data are plotted on a semilogarithmic paper and the straight line for large times is determined. The resulting exponential is subtracted from the data and the process is continued until no further straight line can be identified.

This method is inaccurate and the subtraction of exponentials causes large errors in the residuals.

CHAPTER 6

RESULTS

6.1 The U^{235} isotope results

The pulses 661, 588, 572 have been used to study the U^{235} isotope. The absolute decay curves (delayed neutron emission rate per fission based on the efficiency of the Pu^{240} neutron source) measured by the three pulses has been studied in the overlapping time intervals. Table 6.1.1 summarises the results of this study, using the measurements of COUNTER 2. We have summed the measurements over different time intervals in the overlapping region, so that, the statistical errors will be reduced (smoothing of the measurements).

The previously described ratios should have the same value, for a particular pair of pulses, for all the time intervals in the overlapping time region. Table 6.1.1 shows that the delayed neutron count rate per fission is overpredicted progressively with increasing detection count rate. Furthermore, the shape of the curves is reproduced by all three pulses, within the statistical error of the delayed neutron measurements, for detection count rates lower than 30,000 c/sec. So, we have decided that we will never exceed this count rate at any phase of the study of the delayed neutron characteristics.

The statistically most accurate ratios predicted for pulses 661/588 and 588/572 (table 6.1.1) are $1.002 \pm .0085$ and $.990 \pm .004$ (delayed neutron statistical errors only), respectively. The study has been based on the small (661) VIPER pulse, the other pulses being renormalised to the small one. Table 6.1.2 gives the normalisation factors used and the time interval where the measurements of a particular pulse are being used (the remaining of the measurements being disregarded).

These normalisation factors should be equal to one, provided that allowance is made for the self-multiplication of the delayed neutrons in the samples. The self-multiplication in cylindrical samples has been examined in Appendix A. The sample of the pulse 661 is made of one foil only, and the self-multiplication of the delayed neutrons is equal to .07%. The sample of the pulse 588 is made of ten foils, the self-multiplication being .38%. The sample of the pulse 572 is made of three cylindrical pieces of ^{235}U. The two foils which have been gamma counted (table 4.11) have been placed on either side of the central cylindrical piece. The gamma counting of these foils shows that there is no variation of the fission density along the long sample. The self-multiplication of this sample is equal to 1.3%

The previous examination of the self-multiplication of the delayed neutrons shows that the pulse ratios 661/588 and 588/572, predicted by the decay curves of the delayed neutrons, should be equal to .997 and .991 respectively. These values are in good agreement with the experimentally determined ones.

The pulse 571 is an earlier experiment, where a full-size VIPER pulse was used. The measurements of this pulse can not be used because, the delayed neutron count rate exceeds 30,000 c/sec at short times after the irradiation.

Table 6.1.3 compares the absolute decay curves of the delayed neutrons predicted by the pulses 571 and 588. The ratio of the two curves is equal to .996 $\pm$ 1.4%.

The previous results show that the experiment is reproducible. It has been stated (section 3.3) that large discrepancies should be expected because of the large radial variation of the efficiency of a single detector and possible variation in the radial arrest position of the rabbit. The previous agreement of the pulses can be justified only if

we assume that the sample is being arrested at the same radial position, always.

We have said that, the width of the time channel must be chosen as a function of time after the irradiation, so that, the error in predicting the count rate (eq. 5.2) will be negligibly small. This work was done for the final (table 6.1.2) distribution of the measurements and the error was less than .04% at any point.

The data were subsequently analysed by the peeling-off method. Figure 6.1.1 gives the results obtained by this technique. We did not attempt to separate the residuals into further groups, because of their large statistical error. Table 6.1.4 summarises the results of the peeling-off method.

These group constants, along with the group constants of Keepin et al[4] for the fifth and sixth group, were used as the initial estimate required by the least squares fitting routine. Table 6.1.5 summarises the results of this work. A second fit was done, using the group constants of Keepin et al[4] as the initial estimate; the result obtained was identical to the one given in Table 6.1.5.

The Gardner method was used, as well. We used N = 1024 and X_o = .013 and since the result was oscillating we have set the parameter FCUT equal to 1. Figure 6.1.2 gives the result, in the decay constant interval $\lambda\varepsilon(.01, 4\ sec^{-1})$. This technique shows that there are six groups of delayed neutrons and the decay constants predicted are in agreement with those of the least squares method, to within 40%. Because of the poor results of this technique, we have not applied it for the other isotopes.

Table 6.1.6 gives the comparison of the reactivity ($)- period relationship calculated by the new group constants, Keepin et al[4] group constants and directly from the data (Laplace method). Table 6.1.7 summarises the results of the yield measurements. The dead time and the U^{238} impurity delayed neutron corrections are made in the programs, the values given being calculated separately, so that, an error will be estimated. The absolute yield of .01993 delayed neutrons per fission is based on the efficiency of COUNTER 2 using the Pu^{240} source. The self-multiplication correction is examined in Appendix A.

We have said (section 3.3.5) that we have to use the mean yield of the two counters in order to reduce the error in the yield because of the radial efficiency variation of a single counter. Since the pulses 588 and 572 have been normalised to the pulse 661, the arrest position of the sample (section (3.3.5), arrest position of the sample S) will be the arrest position of the sample of the pulse 661. Therefore, it is necessary to compare the yield measurements of the two counters considering only the measurements of the pulse 661.

Table 6.1.8 gives the comparison of the yield of the delayed neutrons based on the two counters (pulse 661). In order to limit the count rate below 30,000 c/sec for both counters, the shortest time of comparison was .4 sec. The detected counts by the two counters (same number of fissions) were corrected for dead time and background and added in the time interval (.4, 73 sec) where 83% of the total number of delayed neutrons is emitted. So, it has been found that the mean yield of the two counters should be $1.023 \pm .9\%$ times the yield based on COUNTER 2 measurements only.

The limiting count rate of 30,000 c/sec has been shown for COUNTER 2. In order to check that this limit is applied into the count rate of counter 1 as well, we have repeated the previous work in different time intervals. Table 6.1.9 summarises the results obtained from this work. We argue that count rates below 30,000 c/sec can be used for COUNTER 1 too. Table 6.1.9 shows that the measured shape of

FIGURE 6.1.1 TEST OF OFF METHOD RESULTS (Continued)

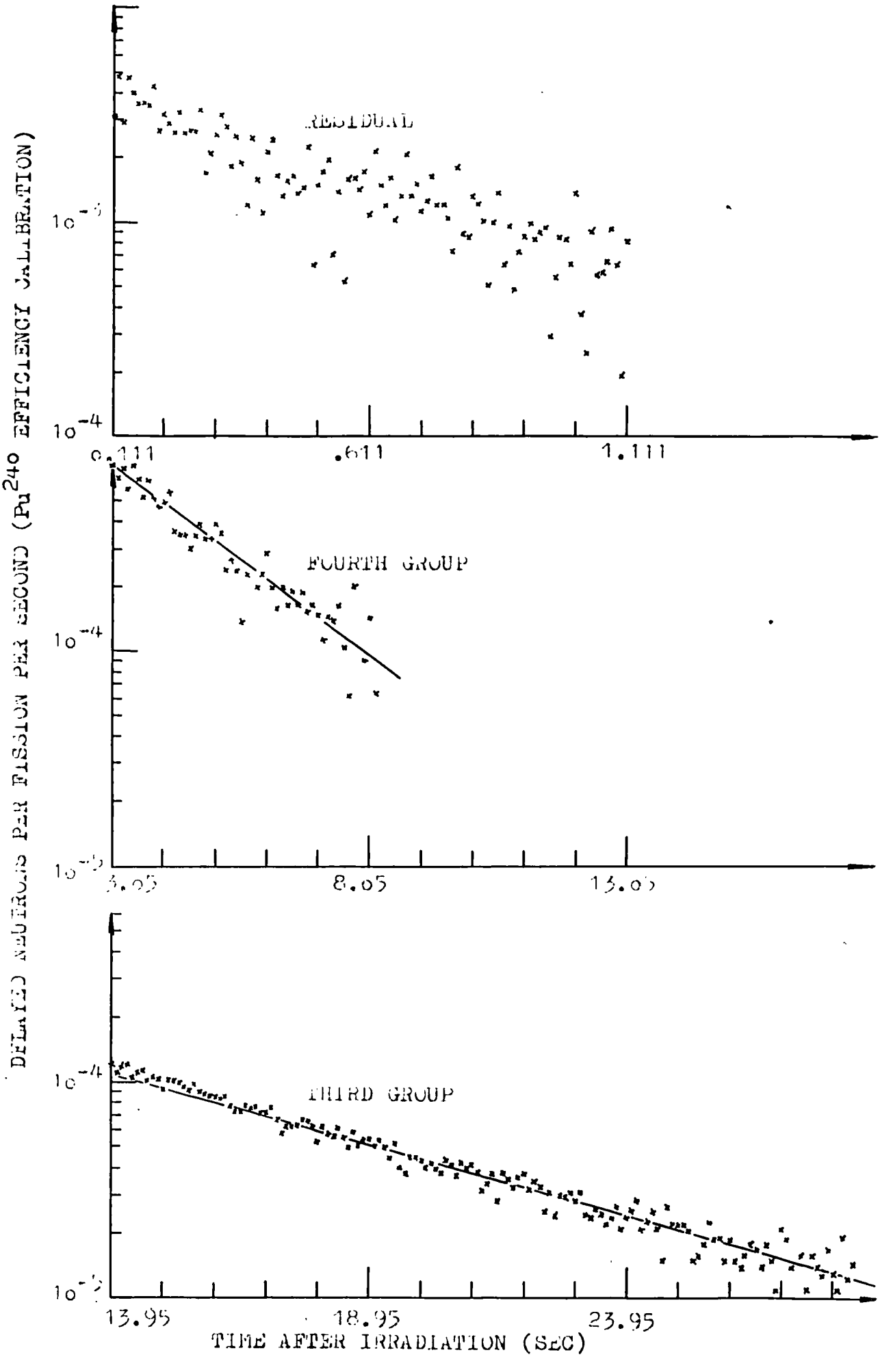

FIGURE 6.1.1 PEELING OFF METHOD RESULTS

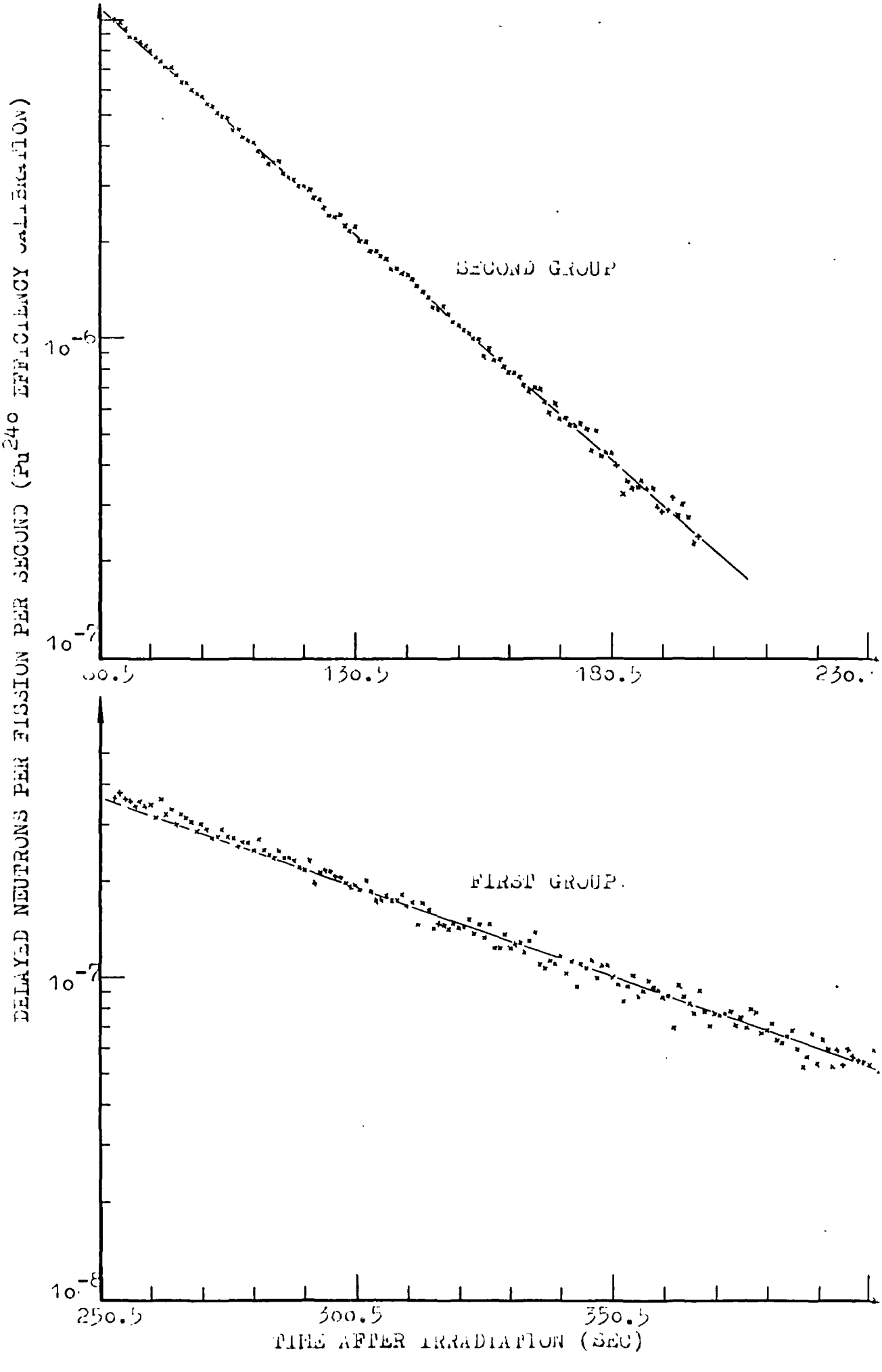

FIGURE 6.1.2 U^{235} GROUP STRUCTURE
THE GARDNER METHOD

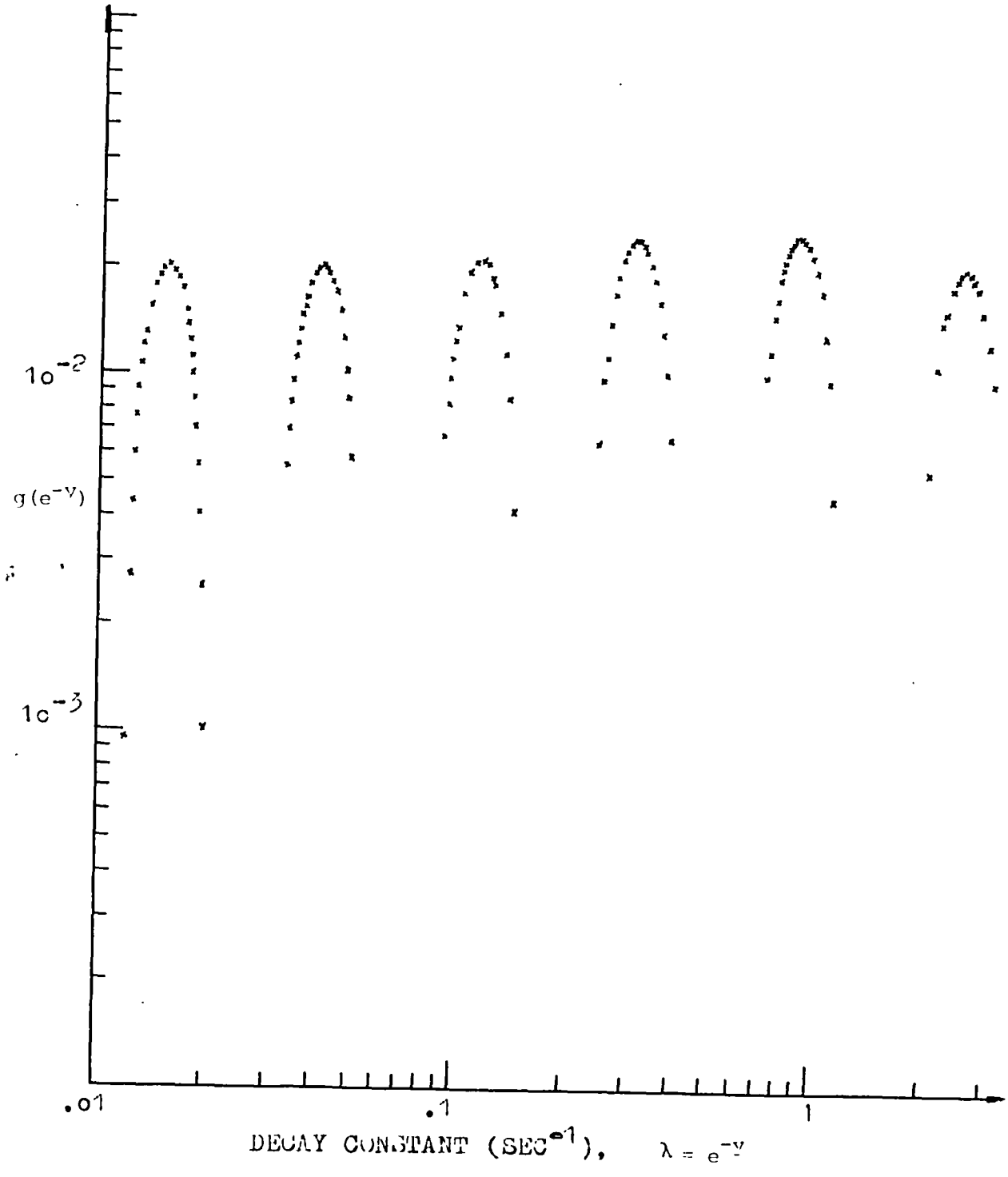

TABLE 6.1.1 Comparison of the Absolute Decay Curves of the Delayed Neutrons Predicted by the Three U^{235} Pulses.**

OVERLAPPING TIME INTERVAL (SEC)	RATIO OF TOTAL DELAYED NEUTRONS EMITTED IN OVERLAPPING TIME INTERVAL	OVERLAPPING TIME INTERVAL (SEC)	RATIO OF TOTAL DELAYED NEUTRONS EMITTED IN OVERLAPPING TIME INTERVAL
	PULSE 661/PULSE 588		PULSE 588/PULSE 572
8.3 - 10	.955 ± .021	53 - 60	.910 ± .007
10.0 - 15	.992 ± .016 *	60 - 70	.938 ± .007
15.0 - 25	.993 ± .016 *	70 - 80	.970 ± .008
25.0 - 40	.995 ± .018 *	80 - 100	.980 ± .007 *
40.0 - 100	1.026 ± .016 *	100 - 200	.995 ± .006 *
100.0 - 330	.999 ± .033 *	200 - 330	1.004 ± .016 *
12.0 - 330	1.002 ± .0085 *	80 - 330	.990 ± .004 *

* COUNT RATE LESS THAN 30,000 c/sec

** ERRORS GIVEN ARE ONLY STATISTICAL ERRORS BECAUSE OF THE DELAYED NEUTRON MEASUREMENTS

TABLE 6.1.2 Pulse Joining. Normalisation Factors. U^{235} Isotope

PULSE	TIME INTERVAL WHERE THE DATA ARE BEING USED	NORMALISATION FACTOR	PER CENT CONTRIBUTION IN THE YIELD
661	0 - 12 sec	1	76.5
588	12 - 80 sec	$1 \pm 1.6\%$	20.5
572	80 - 450 sec	$.990 \pm 1.6\%$	3

TABLE 6.1.3 Comparison of the Absolute Decay Curves of the Delayed Neutrons Predicted by Two U^{235} Pulses**

OVERLAPPING TIME INTERVAL (SEC)	RATIO OF TOTAL NUMBER OF DELAYED NEUTRONS EMITTED IN OVERLAPPING TIME INTERVAL. PULSE 571/PULSE 588
8.3 - 10	.921 ± .012
10.0 - 15	.955 ± .009 *
15.0 - 25	.983 ± .009 *
25.0 - 40	1.011 ± .01 *
40.0 -100	1.002 ± .009 *
100.0 -330	1.038 ± .018 *
12.0 -330	.996 ± .005 *

* COUNT RATE LESS THAN 30,000 C/SEC

** ERRORS GIVEN ARE ONLY STATISTICAL ERRORS BECAUSE OF THE DELAYED NEUTRON MEASUREMENTS

TABLE 6.1.4 Peeling-Off Method Group Constants. U^{235} Isotope.

	Decay Constant SEC^{-1}	Relative Abundance
1	.0128	.035
2	.0328	.237
3	.151	.300
4	.389	.304

TABLE 6.1.5 Least Squares Method Group Constants.
U^{235} isotope. Six Group Structure.

	KEEPIN'S WORK		PRESENT WORK	
	Relative Abundance	Decay Constant SEC^{-1}	Relative Abundance	Decay Constant SEC^{-1}
1	0.038 ± 0.004	0.0127 ± 0.0003	0.035 ± 0.002	0.0130 ± 0.0001
2	0.213 ± 0.007	0.0317 ± 0.0012	0.234 ± 0.003	0.0326 ± 0.0002
3	0.188 ± 0.024	0.115 ± 0.004	0.216 ± 0.069	0.135 ± 0.010
4	0.407 ± 0.010	0.311 ± 0.012	0.290 ± 0.055	0.275 ± 0.038
5	0.128 ± 0.012	1.40 ± 0.12	0.178 ± 0.038	0.836 ± 0.151
6	0.026 ± 0.004	3.87 ± 0.55	0.047 ± 0.013	3.74 ± 0.91

Number of points fitted = 981
Minimum value of the function = 977.9

GRADIENT AT THE MINIMUM						
Variable	i = 1	i = 2	i = 3	i = 4	i = 5	i = 6
$\alpha_i\lambda_i$	$.10\ 10^{-3}$	$.75\ 10^{-5}$	$.56\ 10^{-6}$	$.50\ 10^{-6}$	$.29\ 10^{-6}$	$.53\ 10^{-7}$
λ_i	$.54\ 10^{-4}$	$.44\ 10^{-4}$	$-.36\ 10^{-5}$	$.83\ 10^{-6}$	$.19\ 10^{-6}$	$-.11\ 10^{-5}$

TABLE 6.1.6 U^{235} Reactivity Comparison. Six Group Structure.

PERIOD (SEC)	REACTIVITY $ USING GROUP CONSTANTS FROM KEEPIN'S DATA	REACTIVITY $ USING GROUP CONSTANTS FROM PRESENT DATA	RATIO OF REACTIVITY FROM PRESENT TO KEEPIN'S DATA	REACTIVITY $ USING LAPLACE TRANSFORM WITH PRESENT DATA	RATIO OF REACTIVITY FROM LAPLACE TO KEEPIN'S DATA
.2	.9312	.9320	1.0009	.9318	1.0006
.5	.8616	.8642	1.0030	.8637	1.0024
1	.7817	.7858	1.0052	.7849	1.0041
3	.6081	.6141	1.0099	.6126	1.0074
7	.4543	.4605	1.0136	.4590	1.0103
10	.3911	.3969	1.0148	.3955	1.0113
30	.2215	.2248	1.0149	.2239	1.0108
70	.1263	.1278	1.0119	.1273	1.0079
100	.09651	.09745	1.0097	.09708	1.0059
300	.03810	.03828	1.0047	.03815	1.0013
700	.01734	.01737	1.0017	.01732	0.9988
900	.01363	.01365	1.0015	.01361	0.9985
-900	-.01478	-.01475	0.9980	-.01471	0.9953
-500	-.02760	-.02748	0.9957	-.02742	0.9935
-200	-.08025	-.07908	0.9854 *	-.07901	0.9845
-100	-.2713	-.2507	0.9241 *	-.2527	0.9314

The random error of the reactivity based on the Laplace method is better than .4% for all periods.

* Contribution of missing data is higher than 1%. The contribution for all the other periods is less than 1%.

TABLE 6.1.7 U^{235} Delayed Neutron Yield. Corrections. Uncertainties

ABSOLUTE YIELD OF DELAYED NEUTRONS	CORRECTION APPLIED TO THE DELAYED NEUTRON YIELD	VALUE OF THE CORRECTION	UNCERTAINTY OF THE YIELD BECAUSE OF THE CORRECTION
.01993	Contribution of Missing Time Interval Data	4.3%	.45%
	Dead Time Correction	1.7%	.2%
	U^{238} Impurity Delayed Neutrons	.17%	-
	Relative efficiency of the Am-Li source to the Pu^{240} source	1.226	1.1%
	U^{234}-U^{236} Impurity delayed neutrons	.998	.1%
	Self Multiplication	.999	.1%
	Counter-1 yield correction	1.023	.9%

total error 1.5%

UNCERTAINTIES	VALUE
Fission measurements	1.91%
Efficiency systematic errors	2.5%
Correction uncertainties	1.5%
Pu^{240} Efficiency calibration	.7%
Delayed neutron statistics	.3%
Normalisation of decay curves	.4%

U^{235} ABSOLUTE DELAYED NEUTRON YIELD = $0.0166 \pm 3.6\%$

the delayed neutron decay curve is the same for the two detectors.

In order to check the effect of the number of groups in the reactivity ($)-period relationship, a five group least squares fit was done, too. Table 6.1.10 gives the results of this work and table 6.1.11 gives the reactivity ($)-period relationship predicted by this five group structure and Keepin et al[4] group structure. The initial solution of the five group fit is that of table 6.1.4, along with the fifth group constants of Keepin et al[4].

TABLE 6.1.8 Comparison of the Delayed Neutron Yield Measured by the Two Counters

	COUNTER 1	COUNTER 2
Delayed Neutrons Measured in (.4,73 secs) interval "Dead time correction applied"	98650 ± .3%	50661 ± .45%
Total Background in (.4,73 secs)	44.4	50.3
Pu^{240} Efficiency of counters	$(4.536 \pm .54\%)10^{-4}$	$(2.525 \pm .7\%)10^{-4}$
Relative efficiency of the Am-Li source to the Pu^{240} source	1.270 ± .9%	1.226 ± 1.1%

COUNTER 1 CORRECTION = 1.023 ± 0.9%

TABLE 6.1.9 Effect of Count Rate on the Measurements of Counter 1

TIME INTERVAL (SEC)	RATIO OF TOTAL DELAYED NEUTRONS IN TIME INTERVAL (BACKGROUND AND DEAD TIME CORRECTIONS APPLIED) COUNTER 1/COUNTER 2	MAXIMUM COUNT RATE C/SEC
.4 - 3	1.976 ± 1%	30000
3.0 - 15	1.936 ± 1%	9000
15.0 - 33	1.943 ± 1.6%	1200

TABLE 6.1.10 Least Squares Method Group Constants. U^{235} Isotope. Five Group Structure

GROUP	DECAY CONSTANT SEC^{-1}	RELATIVE ABUNDANCE
1	.0130 ± .0001	.036 ± .002
2	.0328 ± .0001	.237 ± .002
3	.156 ± .003	.327 ± .020
4	.437 ± .025	.297 ± .024
5	2.08 ± .19	.103 ± .010

Number of points fitted = 981

Minimum value of the function = 995.7

GRADIENT AT MINIMUM					
VARIABLE	i = 1	i = 2	i = 3	i = 4	i = 5
$\alpha_i\lambda_i$	$.81\ 10^{-4}$	$.71\ 10^{-5}$	$.13\ 10^{-5}$	$.22\ 10^{-6}$	$.36\ 10^{-7}$
λ_i	$-.33\ 10^{-3}$	$-.29\ 10^{-3}$	$-.10\ 10^{-3}$	$-.69\ 10^{-4}$	$-.92\ 10^{-5}$

TABLE 6.1.11U^{235} Reactivity Comparison. Five Group Structure.

PERIOD (SEC)	REACTIVITY ($)		% DISCREPANCY
	NEW GROUP STRUCTURE	KEEPIN GROUP STRUCTURE	
.01	.9960	.9957	.03
.1	.9640	.9619	.22
.3	.9089	.9050	.4
.5	.8665	.8616	.6
1	.7880	.7817	.8
3	.6159	.6081	1.3
5	.5234	.5155	1.5
10	.3981	.3911	1.8
30	.2256	.2215	1.8
50	.1627	.1600	1.7
100	.09786	.09651	1.4
300	.03846	.03810	.9
500	.02401	.02382	.8
900	.01372	.01363	.7
-900	-.01483	-.01478	.3
-500	-.02764	-.02760	.1
-200	-.0796	-.0803	-.7

6.2 The U^{238} isotope results

The absolute delayed neutron yield of U^{238} has been studied using the pulses 636-597-596 and 598-597-596.

Table 6.2.1 compares the three pulses of each set, in the overlapping time interval. Table 6.2.2 gives the resulting normalisation factors used for pulses 597 and 596.

The sample of the pulse 597 is made of one cylindrical piece of U^{238} (along with foils). The self-multiplication (actually self-absorption) was calculated (appendix A) for this pellet and it was less than .2%. So, the large discrepancies in the table 6.2.1 can not be explained by the self-multiplication of the sample.

Table 6.2.1 shows that the number of fissions of the pulse 597 has been overestimated, and that the actual number of fissions is .920 $\pm$ 2.5% times the measured value. The sample of the pulse 597 was reconstructed, the pellet being simulated by a number of foils along with a foil at the same position with the one used to determine the number of fissions of the pulse 597. This sample was irradiated, and all the foils were gamma counted, subsequently. This experiment showed that the number of fissions per gm of the sample is .94 $\pm$ .04 times the number of fissions per gm calculated by the single foil of the pulse 597. So, the observed discrepancies of table 6.2.1 are genuine, the variation of the fission density along the sample being the reason. Similar work gave a value of .95 $\pm$ .04 for the pulse 596.

Table 6.2.3 summarises the results of the yield measurement. The yield of the delayed neutrons, based on the measurements of COUNTER 2, was found equal to 0.05037 and 0.05057 (uncorrected values,

table 6.2.3) for the sets of pulses 636-597-596 and 598-597-596, respectively. The yield of the delayed neutrons was compared (COUNTER 1-COUNTER 2 comparison) in the time interval (.42 sec - 73 sec) where 75.5% of the total number of delayed neutrons is emitted. The correction found was 1.047 and 1.037 for the pulses 636 and 598 respectively.

The correction for the missing time interval was checked using the present six group structure, and it was found that the yield should be higher by 1%.

The pulses 636-597-596 have been used for the study of the group structure of the delayed neutrons.

It was not possible to determine the longest lived group by the peeling-off method, because of the bad statistical error of the data for times higher than 200 sec after the irradiation (figure 6.2.1). For this reason, the data of Keepin et al[4] have been used for this group. Table 6.2.4 gives the results of the peeling-off method.

We attempted a six group fit using the previously described results (along with Keepin's[4] sixth group constants) as the initial solution but, the decay constant of the longest lived group was equal to .017 sec^{-1}, which is unacceptably high.

So, the first (longest lived) group was subtracted from the data, using Keepin et al[4] group constants and the residuals were fitted to five groups. Table 6.2.4 summarises the results of this work.

Table 6.2.5 compares the reactivity ($)- period relationship, using the present group constants, Keepin et al[4] group constants and calculated directly from the data (Laplace method).

TABLE 6.2.1 Comparison of the Decay Curves in Overlapping Time Intervals U^{238} Isotope

OVERLAPPING TIME INTERVAL (SEC)	RELATIVE NUMBER OF DELAYED NEUTRONS PER FISSION IN OVERLAPPING TIME INTERVAL	
	Pulse 636/Pulse 597	Pulse 597/Pulse 596
5 - 300	1.078 ± 1.1%	
15 - 300		1.030 ± .5%

OVERLAPPING TIME INTERVAL (SEC)	RELATIVE NUMBER OF DELAYED NEUTRONS PER FISSION IN OVERLAPPING TIME INTERVAL	
	Pulse 598/Pulse 597	Pulse 597/Pulse 596
5 - 300	1.096 ± 1.1%	
15 - 300		1.030 ± .5%

Errors given are only statistical errors because of the delayed neutron emission.

TABLE 6.2.2 Pulse Joining. Normalisation Factors. U^{238} Isotope

PULSE I.D.	TIME INTERVAL WHERE THE DATA ARE BEING USED	NORMALISATION FACTOR	PER CENT CONTRIBUTION IN THE YIELD
636	0 - 5	1	72.5
597	5 - 40	1.078 ± 2.4%	22.8
596	40 - 420	1.110 ± 2.5%	4.6

PULSE I.D.	TIME INTERVAL WHERE THE DATA ARE BEING USED	NORMALISATION FACTOR	PER CENT CONTRIBUTION IN THE YIELD
598	0 - 5	1	72.5
597	5 - 40	1.096 ± 2.5%	22.8
596	40 - 420	1.128 ± 2.5%	4.6

TABLE 6.2.3 U^{238} Delayed Neutron Yield.Corrections.Uncertainties

ABSOLUTE YIELD OF DELAYED NEUTRONS	CORRECTION APPLIED TO THE DELAYED NEUTRON YIELD	VALUE OF THE CORRECTION	UNCERTAINTY ON THE YIELD BECAUSE OF THE CORRECTION
.05047	Contribution of Missing Time Interval Data	7.6%	.8%
	Dead Time Correction		.2%
	U^{235} Impurity Delayed Neutrons	6.9%	.75%
	Relative efficiency of the Am-Li source to the Pu^{240} source	1.226	1.1%
	Self Multiplication	1.000	.1%
	Counter 1 yield correction	1.042	.7%
		total error	1.72%

UNCERTAINTIES	VALUE
Fission measurements	2.44%
Efficiency systematic errors	2.5%
Correction uncertainties	1.72%
Pu^{240} efficiency calibration statistics	.7%
Delayed neutron statistics	.3%
Normalisation of decay curves	.55%

U^{238} absolute delayed neutron yield = 0.0429 ± 4.0%

TABLE 6.2.4 U^{238} Group Structure

PEELING OFF METHOD RESULTS

	Relative abundance	Decay Constant SEC^{-1}
2	.130	.0306
3	.204	.134
4	.385	.397
5	.220	1.63

LEAST SQUARES METHOD RESULT

	KEEPIN'S WORK		PRESENT WORK	
	Relative Abundance	Decay Constant SEC^{-1}	Relative Abundance	Decay Constant SEC^{-1}
1	0.013 ± 0.001	0.0132 ± 0.0004	0.013	0.0132
2	0.137 ± 0.003	0.0321 ± 0.0009	0.144 ± 0.003	$0.0316 \pm 0.000?$
3	0.162 ± 0.030	0.139 ± 0.007	0.182 ± 0.031	0.148 ± 0.008
4	0.388 ± 0.018	0.358 ± 0.021	0.372 ± 0.024	0.369 ± 0.018
5	0.225 ± 0.019	1.41 ± 0.10	0.257 ± 0.026	1.83 ± 0.12
6	0.075 ± 0.007	4.02 ± 0.32	0.032 ± 0.030	11.2 ± 6.6

Number of points fitted = 976
Minimum value of the function = 801.7

GRADIENT AT THE MINIMUM					
Variable	i = 2	i = 3	i = 4	i = 5	i = 6
$\alpha_i\lambda_i$	$.36\ 10^{-4}$	$.20\ 10^{-4}$	$.88\ 10^{-7}$	$.18\ 10^{-7}$	$.14\ 10^{-7}$
λ_i	$.21\ 10^{-5}$	$.11\ 10^{-5}$	$.92\ 10^{-7}$	$-.12\ 10^{-7}$	$.20\ 10^{-9}$

TABLE 6.2.5 U^{238} Reactivity Comparison

PERIOD (SEC)	REACTIVITY $ USING GROUP CONSTANTS FROM KEEPIN'S DATA	REACTIVITY $ USING GROUP CONSTANTS FROM PRESENT DATA	RATIO OF REACTIVITY FROM PRESENT TO KEEPIN'S DATA	REACTIVITY $ USING LAPLACE TRANSFORM WITH PRESENT DATA	RATIO OF REACTIVITY FROM LAPLACE TO KEEPIN'S DATA
.2	.8859	.8773	0.9903	.8783 *	0.9914
.5	.7852	.7772	0.9898	.7784 *	0.9913
1	.6818	.6761	0.9916	.6771	0.9931
3	.4876	.4871	0.9990	.4873	0.9994
7	.3398	.3420	1.0065	.3419	1.0062
10	.2844	.2872	1.0098	.2870	1.0091
30	.1493	.1522	1.0194	.1520	1.0181
70	.08146	.08351	1.0252	.08341	1.0239
100	.06133	.06298	1.0269	.06291	1.0258
300	.02348	.02418	1.0298	.02416	1.0290
700	.01055	.01088	1.0313	.01087	1.0303
900	.00828	.00853	1.0302	.00853	1.0302
-900	-.00882	-.00910	1.0317	-.00910	1.0317
-500	-.01633	-.01686	1.0325	-.01686	1.0325
-200	-.04564	-.04719	1.0340	-.04722 *	1.0346
-100	-.1281	-.1323	1.0328	-.1325 *	1.0343

The random error of the reactivity based on the Laplace method is better than .5% for all presented periods.

* Missing data contribution is higher than 1%. For all the other periods, less than 1%.

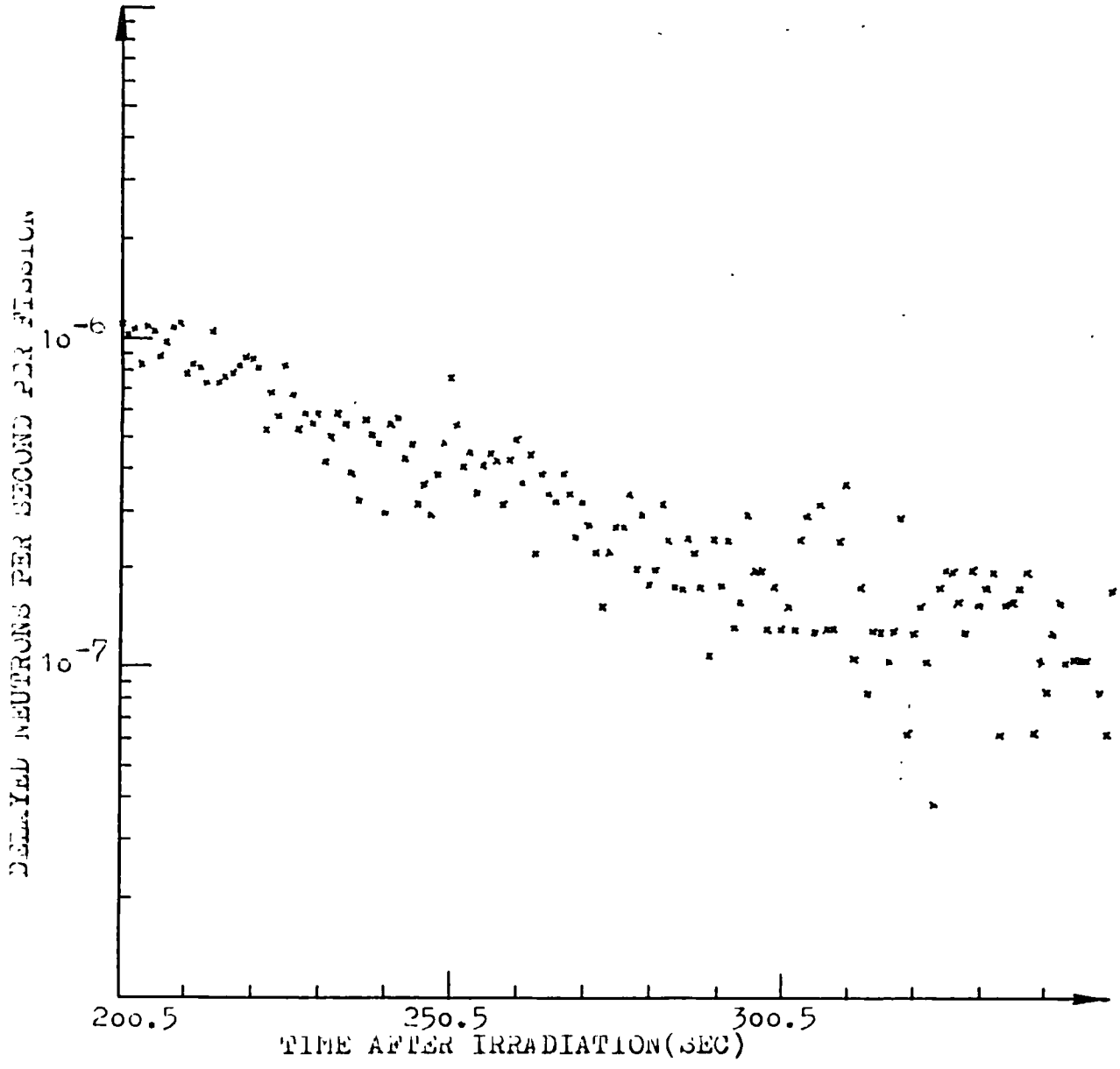

FIGURE 6.2.1 U^{238} LONGEST LIVED GROUP
(Results based on Pu-240 calibration)

6.3 The Pu^{239} isotope results

The absolute delayed neutron yield of Pu^{239} has been measured using the pulses 668-617-615 and 634-617-615.

Two Pu^{239} foils of the pulse 615 were gamma counted and they disagreed by 12%. These foils were placed on either side of the cylindrical Pu^{239} long sample and it was decided that we can not determine the number of fissions in the sample of the 615 pulse. For this reason, the efficiency of the counter 2 (Pu^{240}source) and the number of fissions have been arbitrarily set equal to one and this pulse has been eventually normalised to the small Pu^{239} pulse.

The two previously defined sets of pulses have been used to study the delayed neutron characteristics (absolute yield, group constants) based on the measurements of COUNTER 2.

Table (6.3.1) compares the decay curves of the delayed neutrons in the overlapping time intervals and table (6.3.2) gives the normalisation factors used for the pulses 617 and 615. Since these pulses are eventually normalised to the 668 and 634 pulses, the absolute yield measurements by the two sets of VIPER pulses are partially independent.

We should point out that since the sample of the pulse 617 consists of three foils while the samples of pulses 668 and 634 consist of only one foil, the expected normalisation factors (Pulse 668/Pulse 617, Pulse 634/Pulse 617) should be equal to·992 because of the self-multiplication of the sample (Appendix A). We note that the measured normalisation factors are in very good agreement with the expected value.

The uncorrected absolute yield (calculated by the programs) are .007288 and .007353 based on the pulses 668-617-615 and 634-617-615, respectively.

TABLE 6.3.1 Comparison of the Decay Curves in Overlapping Time Interval Pu^{239} Isotope

OVERLAPPING TIME INTERVAL (SEC)	RELATIVE NUMBER OF DELAYED NEUTRONS PER FISSION IN OVERLAPPING INTERVAL	
	Pulse 668/Pulse 617	Pulse 617/Pulse 615
3.4 - 150 102 - 230	.9799 ± .62%	.3336 10^{-9} ± 1.29%

OVERLAPPING TIME INTERVAL (SEC)	RELATIVE NUMBER OF DELAYED NEUTRONS PER FISSION IN OVERLAPPING INTERVAL	
	Pulse 634/Pulse 617	Pulse 617/Pulse 615
3.4 - 150 102 - 230	.9909 ± .68%	.3336 10^{-9} ± 1.29%

Errors given are only statistical errors because of the delayed neutron emission.

TABLE 6.3.2 Pulse Joining. Normalisation Factors. Pu^{239} Isotope

PULSE	TIME INTERVAL WHERE THE DATA ARE BEING USED	NORMALISATION FACTOR	PER CENT CONTRIBUTION IN THE YIELD
668	0 - 3.5 sec	1	47.3
617	3.5 - 105 sec	.9799 $\pm$ 1.6%	50.6
615	105 - 440 sec	.3269 10^{-9} $\pm$ 1.8%	2.0

PULSE	TIME INTERVAL WHERE THE DATA ARE BEING USED	NORMALISATION FACTOR	PER CENT CONTRIBUTION IN THE YIELD
634	0 - 3.5 sec	1	47.3
617	3.5 - 105 sec	.9909 $\pm$ 1.6%	50.6
615	105 - 440 sec	.3306 10^{-9} $\pm$ 1.8%	2.0

TABLE 6.3.3 Pu^{239} Delayed Neutron Yield. Corrections. Uncertainties

ABSOLUTE YIELD OF DELAYED NEUTRONS	CORRECTION APPLIED TO THE DELAYED NEUTRON YIELD	VALUE OF THE CORRECTION	UNCERTAINTY ON THE YIELD BECAUSE OF THE CORRECTION
.007321	Contribution of missing time interval data	3.83%	.4%
	Dead Time Correction		.1%
	Relative efficiency of the Am-Li source to the Pu^{240} source	1.226	1.1%
	Self multiplication	.996	.4%
	Pu^{240}-Pu^{241} impurity delayed neutrons	.971	.7%
	Counter 1 Yield correction	1.037	.9%

Total error 1.68%

UNCERTAINTIES	VALUE
Fission measurements	1.88%
Efficiency systematic errors	2.5%
Correction uncertainties	1.68%
Pu^{240} Efficiency calibration	.7%
Delayed neutron statistics	.24%
Normalisation of decay curves	.80%

Pu^{239} absolute delayed neutron yield= 0.00599 ± 3.7%

TABLE 6.3.4 Pu^{239} Least Squares Six Group Structure

	KEEPIN'S WORK		PRESENT WORK	
	Relative Abundance	Decay Constant SEC^{-1}	Relative Abundance	Decay Constant SEC^{-1}
1	0.038 ± 0.004	0.0129 ± 0.0003	0.030 ± 0.002	0.0126 ± 0.0002
2	0.280 ± 0.006	0.0311 ± 0.0007	0.294 ± 0.006	0.0301 ± 0.0003
3	0.216 ± 0.027	0.134 ± 0.004	0.181 ± 0.039	0.118 ± 0.010
4	0.328 ± 0.015	0.331 ± 0.018	0.373 ± 0.025	0.316 ± 0.018
5	0.103 ± 0.013	1.26 ± 0.17	0.108 ± 0.091	1.63 ± 0.53
6	0.035 ± 0.007	3.21 ± 0.38	0.014 ± 0.042	3.66 ± 3.66

Number of points fitted = 971

Minimum value of the function = 953.3

GRADIENT AT THE MINIMUM						
Variable	i = 1	i = 2	i = 3	i = 4	i = 5	i = 6
$\alpha_i \lambda_i$	.23	.01	$.46\ 10^{-2}$	$.58\ 10^{-3}$	$.30\ 10^{-2}$	$.43\ 10^{-3}$
λ_i	$.14\ 10^{-3}$	$.16\ 10^{-3}$	$.27\ 10^{-4}$	$.14\ 10^{-4}$	$-.56\ 10^{-6}$	$-.16\ 10^{-5}$

Table 6.3.3 summarises the corrections and uncertainties of the absolute delayed neutron yield of Pu^{239}. The maximum count rate of both counters was less than 30000 counts/sec for the whole time interval covered by the Pulses 668 and 634. So, the yield of counter 1 and counter 2 measurements was compared in the time interval (.1 sec - 73 sec). Since only 4.5% of the total delayed neutrons are emitted for times higher than 73 sec, we argue that this is a strict comparison of the yield of delayed neutrons calculated by the two counters. The mean yield of the two counters was 1.037 times the yield calculated by the counter 2, for both pulses 634 and 668, indicating that the samples of these experiments were arrested at the same radial distance.

The yield presented in table 6.3.3 is the mean yield of the two sets of data, based on the measurements of both counters.

The contribution of the missing data at very early and very long times (3.83%) is calculated using the group constants of Keepin et al[4]. The self-multiplication correction is examined in Appendix A. The impurity delayed neutrons have been calculated by the isotopic composition (table 4.1) of the sample, the per atom fission ratio (table 4.2) and the absolute yields presented by Keepin[10].

Table 6.3.4 gives the six group constants of the delayed neutrons emitted by Pu^{239}. This six group structure is examined in detail in Appendix B.

6.4 The effect of the radial efficiency variation on the yield measurement

In section (3.3.5) we studied the radial efficiency variation of a single neutron detector and it was shown that this variation was very high. It is apparent (sections 6.1, 6.2, 6.3) that the delayed neutron yield measurement based on the COUNTER 2 measurements is reproducible. Therefore, we concluded that the rabbit (sample) is arrested at the same

radial position within the flight tube. This is consistent with the experimental evidence that the rabbit was arrested along the axis of the polyurethane catcher. This reproducibility of the yield measurement shows that the efficiency calibration of the COUNTER 2 was performed in a reproducible position. The reproducibility of the Pu^{240} counting is supported by the reproducibility of the before and after the pulse counting of this source which was obtained during this work.

We have argued (section 3.3.6) that axially symmetric sources with large cross-sections can be used to calibrate the counters and the efficiency which will be measured will correspond to a small source placed at the Cf reference position, provided that the axis of the extended source coincides with the axis of the flight tube at the counting position. Therefore, if the Am-Li source had been inserted in the flight tube so that its axis coincided with the axis of the flight tube, the values of the delayed neutron yield measured separately by each neutron counter would be the same, provided that the Cf reference position coincided with the arrest position of the sample (apart from an error because of the spectral responses of the detectors). These requirements are very strict because of the large radial efficiency variation. If we assume that the sample is arrested three millimetres away from the Cf reference position towards the detectors then the difference between the yield values obtained separately by the two neutron counters, would be 8%. Discrepancies of this order should be expected because of small eccentricities of the Am-Li counting position, too. Both these reasons may be responsible for the different yield values obtained by the two counters.

We have shown (section 3.3.5) that the mean yield (calculated by the two neutron counters) is the actual delayed neutron yield for any arrest position of the sample and any small eccentricity of the Am-Li counting position, to within 1.4%. This argument substantiates the use of the mean value of the two measurements.

CHAPTER 7

SUMMARY AND DISCUSSION

The object of this work was to measure the absolute yield and group constants of the delayed neutrons from the fast fission of U^{235}, U^{238} and Pu^{239}.

7.1 Group structure of the delayed neutrons

The delayed neutron emission rate per fission, following an instantaneous irradiation, was measured typically in the time interval (.11 sec, 450 sec) after the irradiation. Three irradiations were used to cover the time interval of interest, so that measurements of improved statistical accuracy were obtained without exceeding the maximum allowed detection count rate. These three decay curves were subsequently joined and normalisation factors were used, so that we could eliminate systematic errors in the shape of the joined decay curve. Typically, a thousand points were obtained which were fitted by a linear combination of exponentials, using the least squares technique. A number of other techniques were also used to support the least squares analysis.

A complete study of the group structure of the delayed neutrons emitted from the fast fission of U^{235}, U^{238} and Pu^{239} has only been published by Keepin et al[4]. Keepin et al[4] argue that the optimum number of groups is six and this data are extensively used in the dynamic study of the fast assemblies. Keepin[10] claims that a five (or fewer) group fit did not give satisfactory convergence and that a seven (or higher) group fit gave a higher value for the quantity given by equation (5.18), which implied a worse fit. Keepin et al[4] used two types of irradiation to determine the group constants, namely, saturation irradiations were used to determine the group constants of the two longest

lived groups and instantaneous irradiations were used to determine the group constants of the four shortest lived groups.

The U^{235} delayed neutron decay curve was analysed using the peeling-off method and four groups could be definitely identified. The residuals could not be resolved into any further groups because of their bad accuracy. In order to determine the number of groups we used Gardner's method. The result was highly oscillating and it was necessary to use the FCUT parameter (chapter 5) to remove the unwanted error ripples. The use of this parameter worsens the resolution of the observed peaks, so that genuine peaks (exponential terms) may be lost. It is known that the delayed neutron decay curve is due to a large (more than 38) number of exponential terms. So, the FCUT parameter is responsible for the grouping of the different precursors into a smaller number of fictitious ones. This technique showed that there were six groups of delayed neutrons, at least in the case of the U^{235} isotope.

In order to examine the effect of the number of groups a six group and a five group least squares fit was done (tables 6.1.5, 6.1.10). We observe that the group constants of the two longest lived groups did not change significantly, as was expected. We observe that the decay constant of the fifth group of the five group fit (2.08 sec^{-1}) is approximately equal to the mean of the decay constants of the fifth and sixth group of the six group fit (λ_5 = .836 sec^{-1}, λ_6 = 3.74 sec^{-1}). This is consistent with the fact that the amplitudes, $\alpha_i\lambda_i$, of the exponential terms of the fifth and sixth group of the six group fit are approximately equal ($\alpha_5\lambda_5$ = .149 sec^{-1}, $\alpha_6\lambda_6$ = .176 sec^{-1}). So, these two different fits are consistent.

We have argued that the quantity given by equation (5.18) should be approximately equal to one. This quantity has the values of 1.009 and 1.025 for the six and five group structure, respectively. So, we argue that the six group structure is better than the five group structure and it is near the optimum. This result is consistent with the result of Gardner's method which showed that there were six groups.

The Pu^{239} delayed neutron decay curve was analysed by the peeling-off method and four groups were positively identified. The residuals could not be resolved into any further groups because of their bad accuracy. The decay curve was approximated by a five and a six group structure, using the least squares technique (tables 6.3.4 and B2).

Again, we observe that the group constants of the longest lived groups are approximately the same and the fifth group decay constant of the five group fit is between the fifth and sixth group decay constants of the six group fit.

The quality of the fit (eg(5.18)) is equal to 0.994 and 1.038 for the six group and five group structure, respectively. So, the six group fit is better than the five group fit and near the optimum one. The main objection of the six group structure is the fact that, the relative abundance of the sixth group is statistically zero.

The study of the U^{238} delayed neutron group structure is rather incomplete. In particular, the efficiency of the detector was not compatible with the maximum achieved delayed neutron emission rate, so that, the longest lived group could not be identified. It is known[1] that the longest lived group is due to the Br^{87} precursor, which has a half-life of 55.7 sec. This half-life is inconsistent with the half-life of the longest lived group (41 sec) predicted by the six group fit. So, a five group fit was done, subtracting the longest lived group contribution from the decay curve. The quality of the fit (eg. (5.18)) is equal to

0.83,which shows that it is not a particularly good fit.

There are two possible reasons for this bad fit, namely the bias introduced by the arbitrary fixing of the group constants of the longest lived group and/or inadequacy of the regression model because of the small number of counts collected per time channel at large times after the irradiation. The simultaneous six group fit (which gave $\lambda_1 = 0.017$ sec^{-1}) shows that, the quality of the fit is equal to 0.81, indicating that, the poor quality of the fit is due to inaccurate modelling. This is due to the assumption of equation (5.3). It is apparent that the smaller the number of counts collected per time channel, the larger will be the error in estimating the standard deviation of the counts. So, the poor quality of the fit is due to inaccurate estimates of the weights $1/\sigma^2(t_j)$ for long times t_j after the irradiation.

According to the theoretical arguments of Keepin[10], we will have precursors, and especially short lived ones, which will be important contributors in U^{238}, U^{235} cases but minor contributors in the case of Pu^{239}. So, the existence of a six group structure for the delayed neutrons from U^{235} and U^{238}, and a five group structure (statistically zero sixth group abundance) for the delayed neutrons from Pu^{239} is consistent with this theoretical prediction.

Table (7.1) summarises the half-lives of the three longest-lived groups, which were measured in this work, along with the presently accepted group separation of the known precursors.[1] There is a large number of precursors associated with the fourth group and the knowledge of the precursor contribution to the other groups is incomplete. So, the presently measured group half lives of the three longest lived groups are consistent with the half-lives of the known delayed neutron precursors (table 7.1).

TABLE 7.1 Half lives of the groups (present work) and identified Precursors of Delayed Neutrons.

GROUP	PRECURSOR		HALF-LIFE OF GROUP (SEC). PRESENT WORK		
	IDENTIFICATION	HALF-LIFE (SEC)	U^{235}	U^{238}	Pu^{239}
1	Br^{87}	55.7	53.32 ± .8%	—	55.01 ± 1.6%
2	Br^{88} Te^{136} I^{137}	15.9 20 24.4	21.3 ± .6%	21.9 ± .6%	23.0 ± 1.0%
3	Se^{87} Br^{89} Rb^{93} I^{138}	5.6 4.5 5.9 6.0	5.13 ± 7.4%	4.68 ± 5.4%	5.87 ± 8.5%

TABLE 7.2 Errors in period-reactivity ($) calculations

SOURCE OF ERROR	VALUE
Statistical error	.5%
Contribution of missing data error	1%
Non-flat response of the the detector error	.6%

Acton[47] has discussed the problem of the least squares fitting of exponentials . He argues that the problem of fitting even two exponentials to accurate data has not got a unique solution; the data can be approximated (up to four digits) with different sets of exponentials and the problem becomes more complicated if statistical errors exist. The present six group constants are in agreement with the group constants of Keepin et al[4], to within the large errors of the present work. But the large differences could also be explained by the previous argument of Acton.[47]

Not only are the statistical errors of the group constants too large but, their direct use to calculate the error of any quantity (eg reactivity given by the inhour equation) will be incorrect because these group constants are correlated. Therefore, a more careful examination of the significance of the errors is needed.

To summarise the results of the analysis of the delayed neutron decay curves, we can state that:

(1) We found that we should use six groups to represent the decay curve of the delayed neutrons emitted by U^{235}, using Gardner's method.

(2) A six group fit was done to the decay curves of the delayed neutrons emitted by U^{235}, U^{238} and Pu^{239}, using the least squares technique. The U^{235} and Pu^{239} fit is near optimum, but for the U^{238} fit we do not have any definite indication about the quality of the fit because of inaccuracies in the regression model. The U^{238} longest lived delayed neutron group could not be resolved successfully, because of statistically inaccurate data, and for this reason it was fixed. The existence of the sixth shortest lived group in the Pu^{239} case is questionable and the non-existence of such a group can be justified theoretically. The decay constants of the three longest lived groups are consistent with the decay constants of the known delayed neutron precursors.

(3) The six group structure of the delayed neutrons emitted by U^{235}, U^{238} and Pu^{239} is different from the currently used one (Keepin et al[4]). These differences can be explained by the large errors of the present group constants and/or by the fact that the solved problem does not have a unique solution.

Because of these doubts about the group structure of the delayed neutrons, we examined the period-reactivity relationship (in dollars) in detail. In particular, this relationship was calculated directly from the delayed neutron measurements (Laplace method) and the error of the reactivity was estimated. Then, we checked if the present group structure is capable in reproducing this relationship, using the inhour equation.

The period-reactivity relationship was calculated directly from the data, using the Laplace technique (chapter 1), i.e.

$$\rho(T) = \frac{\int_0^\infty (1-e^{-t/T}) y(t)\,dt}{\int_0^\infty y(t)\,dt} \qquad (7.1)$$

where

$\rho(T)$ = reactivity in dollars corresponding to a period T

$y(t)$ = delayed neutron count rate at time t after an instantaneous irradiation.

The integrations were carried out numerically (using the trapezoidal rule) and a correction was applied, using the present six group structure, for the time intervals where no measurements exist. The results of this work were presented in tables (6.1.6), (6.2.5) and (B3) (B3 in appendix B) for the U^{235}, U^{238} and Pu^{239} isotopes, respectively. The errors in the period-reactivity (in dollars) relationship are given in table (7.2).

The contribution of the missing measurements in the calculation of the denominator of equation (7.1) was examined in the yield measure-

ments (chapter 6). It was found that, the maximum discrepancy in the calculation of the integral was 1% (U^{238} isotope) using the present or Keepin et al[4] group constants. Since for all practical periods (chapter 1) the contribution of the missing data in the numerator of equation (7.1) is less than 1% (tables 6.1.6), (6.2.5) and (B3)), we argue that the error caused by the missing data, in calculating the reactivity by the Laplace method, is less than 1%.

The systematic error introduced because of the non-flatness of the detector response is examined in appendix C.

Thus, the error of the period-reactivity (in dollars) relationship calculated by the Laplace method, is less than 1.3%.

Examination of the period-reactivity values (in tables (6.1.6),(6.2.5) and (B3)) shows that the present six group structure is capable of preserving this information to better than 0.4%, for any practical period. So, the reactivity error is less than 1.5% for any practical period.

The statistical errors of the group constants are too large and the very good agreement between the two methods of evaluating the period-reactivity ($) relationship can be explained by the fact that, the substitution of the group constants into the inhour equation has a smoothing effect[10]. Therefore, these errors should be ignored in control rod calibrations and the previously mentioned error should be used.

Except for the group constants of the two longest lived groups of the five-group and six-group structure of the delayed neutrons from U^{235}, the other group constants have large differences. The period-reactivity relationship, evaluated by these two sets of data, has a difference of less than 0.5% for any practical period. We conclude that it is possible for two group structures, which appear to be different, to contain identical information. Thus, the best way of comparing the present group

structure with the group structure suggested by Keepin et al[4] is by utilising the inhour equation. We observe that the period-reactivity ($) relationships, evaluated by the present group structure and the group structure of Keepin et al[4], are in agreement to better than 3% for any isotope and practically used period. Large discrepancies were found for periods $T \to -1/\lambda_1$ which are never used in practice for control rod calibrations.

7.2 Absolute yield of the delayed neutrons.

The absolute yield of the delayed neutrons was measured by instantaneous irradiations. There are two main quantities which must be measured, in order to measure the absolute yield of the delayed neutrons, namely, the absolute efficiency of the detector and the number of fissions in the sample. A number of corrections (dead time, impurity delayed neutrons and missing neutron measurements) must also be applied, in order to obtain the absolute yield of the delayed neutrons from the present measurements.

The efficiency of the two neutron detectors was measured using the $La(\gamma,n)Be$, $La(\gamma,n)D$ and Pu^{240} neutron sources. It was found that the detection efficiency was not independent of the energy of the neutrons. Therefore, a neutron source with a neutron spectrum similar to the steady state delayed neutron spectrum should be used for the absolute calibration of the efficiency of the detectors for the delayed neutron yield measurements. The Am-Li neutron source was used to determine the efficiency of the detectors for the delayed neutron yield measurements because, the spectrum of this source satisfies the previous requirement. It was found (section 3.3.6) that the energy response function of the detectors is adequately flat, so that, the absolute efficiency determination of the detectors, using the Am-Li source, to be correct to within 2%.

The variation of the efficiency of the detectors with the source position was studied using a small Cf source. The axial efficiency

variation was reasonably small and the correction applied because of the stopping position of the sample, was small (section 3.3.7). The variation of the efficiency with the radial position of the Cf source was unacceptably high. Therefore, unacceptably large errors should be introduced because of the large difference of the diameters of the sample and the calibration source (Am-Li) and uncertainties in the radial stopping position of the sample and positioning of the calibration source within the flight tube. It was shown (section 3.3.5) that the use of the two neutron detectors eliminated these sources of error in the efficiency determination. In particular, the mean delayed neutron yield determined by the two neutron counters is the absolute delayed neutron yield to within 1.4% for any accidental eccentricity in the calibration experiment (Am-Li source) and any (up to 1.2cm) radial stopping position of the sample which could take place without notice.

The number of fissions in the samples was determined by a foil activation technique (chapter 4). In general, it was not possible to determine the number of fissions in samples made of pellets (sections 6.2, 6.3). Therefore, the measurement of the delayed neutron yield was based on irradiations using foils only as samples. The irradiations using samples made of pellets were normalised to the irradiations using samples made of foils only by the delayed neutron decay curve measurement .

It was shown (chapter 6) that the measurements were reproducible provided that we restrict the detected neutron count rate below 30000 c/sec and use samples made of foils only. Therefore, we concluded (section 6.4) that the Pu^{240} source was counted reproducibly and the radial stopping position of the sample was the same. Both these results were consistent with the experimental evidence (section 6.4).

Table 7.3 summarises the absolute delayed neutron yield measurements

which have been done up to now, along with the most recent evaluation of Tuttle[9]. The early measurements of Rose and Smith[3] are not included in the present discussion. The measurements of Masters et al[5], Krick and Evans[6] and Cox[8] have used accelerators as irradiation media, the neutron energies being below 5 Mev (where the delayed neutron yield starts decreasing). On the other hand, Tuttle[9] has corrected the values presented by Keepin et al[4] to take into account the neutron spectrum of the reactor Godiva, so that, the corrected yield corresponds to the plateau value of the delayed neutron yield. It was found necessary to increase only the U^{238} delayed neutron yield (threshold fission) by 1.6%, in order to take into account the decrease of the absolute delayed neutron yield for fissioning energies higher than 5 Mev (calculated correction for VIPER spectrum and measurements of Krick and Evans[6]). Therefore, the values presented in table 7.3 are compatible, except of the ones presented by Keepin[10].

The present measurements are the most accurate measurements, the error of the absolute yield of the delayed neutrons being less than 4%. Comparing the present experimental results with the other measurements, we can state that;

(1) The value for the U^{235} absolute delayed neutron yield, obtained in this work, is in agreement with all the other published results and the evaluated mean, to within the error of the present measurement(almost).

(2) The value for the U^{238} absolute delayed neutron yield, obtained in this work, is in agreement with all the other published results (except the one of Masters et al[5]) and the evaluated mean, to within the error of the present measurement.

(3) The value for the Pu^{239} absolute delayed neutron yield, obtained in this work, is in agreement with the measurements of Keepin et al[4], Masters et al[5] and Krick and Evans[6], to within (almost) one standard deviation of these measurements. The result published by Cox[8] is slightly

TABLE 7.3 COMPARISON OF THE PRESENT ABSOLUTE DELAYED NEUTRON YIELDS WITH PUBLISHED VALUES

REFERENCE	ABSOLUTE DELAYED NEUTRON YIELD			COMMENT
	U^{235}	U^{238}	Pu^{239}	
Rose and Smith[3] 1957	.0174 ± .0014	.037 ± .004	.0070 ± .0006	Yield based on five groups only
Keepin et al[4] 1957	.0165 ± .0005	.0412 ± .0017	.0063 ± .0003	Values reported by Keepin[10] Reported errors are probable errors
Keepin et al[4] 1957	.0167 ± .0016	.0421 ± .0043	.0064 ± .0007	Values reported by Tuttle[9] .Fast effect correction of Godiva spectrum applied.
Masters et al[5] 1969	.0172 ± .0013	.0484 ± .0036	.0066 ± .0005	
Krick and Evans[6] 1972	.0163 ± .0013	———	.0062 ± .0005	
Cox[8] 1974	.0167 ± .0010	.0434 ± .0026	.00661 ± .00043	Reported by Tuttle[9]
Tuttle[9] (Evaluation) 1975	.01714 ± .00022	.04510 ± .00061	.00664 ± .00013	Evaluated mean of reported measurements
Present Work 1976	.0164 ± .0006	.0439 ± .0017	.00599 ± .00022	Fast effect correction of VIPER spectrum applied*

* Yield values of present work corresponding to masses of U^{235}, U^{238}, Pu^{239} deposits 127.6 μgm, 1280 μgm, 112.8 μgm respectively (Williams[16] evaluation)

higher than the present measurement (the difference being 1.5 times the standard deviation of the Cox[8] measurement) and the evaluated mean is definitely higher than the present measurement.

7.3 Conclusions and recommendations.

In this work, we measured the absolute yield and group constants of the delayed neutrons from the fast fission of U^{235}, U^{238} and Pu^{239}.

The period-reactivity (in dollars) relationship was calculated directly from the delayed neutron decay curve and the error was less than 1.5% for any period which is used for control rod calibration experiments. The group structure, found in this work, preserves this relationship when the group constants will be substituted in the inhour equation. The present group structure reproduces the currently used (Keepin et al[4]) period-reactivity (in dollars) relationship to better than 3% for any practically used period for the control rod calibration.

The measured values for the absolute delayed neutron yield are the most accurate ones(error less than 4%) and these values are in agreement with most of the values which have been presented up to now.

We recommend the use of the present values, for the delayed neutron parameters, because they should give the most accurate control rod reactivity worth ($\Delta K/K$) calibrations.

More work is needed to find how the present values affect the control rod worth calibrations of existing fast assemblies and what is their significance in resolving the existing discrepancies between theoretically and experimentally predicted central reactivity worth of small samples, introduced into existing fast reactors. We believe that they will not probably resolve these discrepancies because of the large values which have been reported for these discrepancies and the good agreement of the present results with those of Keepin et al[4],which were thought

to be responsible for these discrepancies.

CHAPTER 8

PROGRESS REPORT ON THE DELAYED NEUTRON SPECTRA MEASUREMENTS

8.1 Introduction

Except of the absolute delayed neutron yield and the delayed neutron group constants, reactor kinetic calculations require the emission spectra of the delayed neutrons (Keepin[10]). According to the delayed neutron group notation, each delayed neutron group is characterised by a spectrum.

The delayed neutron group spectra have been measured up to now by the periodic irradiation-counting technique. The sample is irradiated over a period t_I and the delayed neutron spectrum is measured in a low background area over a counting period t_C, the cycle being repeated. Two cooling time intervals are used between the end of irradiation and onset of counting and between the end of counting and onset of the new cycle, and all the timings of a cycle are chosen so that the contribution of a particular group into the measured spectrum will be enhanced. It is apparent that the measurement of N spectra by N different cycles will be necessary and sufficient to determine the spectra of N groups. The group spectra will depend on the group structure assumed and they will depend on the actual timings of the cycles used (apart from the spectrum which is due entirely to Br^{87}). A number of measurements of the delayed neutron group spectra have been done and it is apparent that the information is not complete.

Batchelor and Hyder[24] used a He^3 spectrometer and they measured the U^{235} thermal fission group spectra of the four longest lived groups.

Shalev and Cuttler[48] used a He^3 spectrometer of better resolution

than the previously used one and they showed that the spectra of the delayed neutrons are structured ones.

Fieg[25] measured the four longest lived group spectra from the thermal U^{235} fission and the 14Mev fission of U^{235}, U^{238} and Pu^{239} using the proton recoil proportional counters spectrometry technique. The thermal fission measurements are essentially in agreement with the measurements of Batchelor and Hyder[24].

Sloan and Woodruff[49] measured the four longest lived group spectra from the thermal fission of U^{233}, U^{235} and Pu^{239} using the proton recoil proportional counters spectrometry technique. These measurements indicate that the thermal fission U^{235} steady state spectrum is softer than the one estimated by Batchelor and Hyder[24].

The steady state delayed neutron spectrum (sum of group spectra weighted by the group relative abundances) can be measured without any knowledge of the delayed neutron group structure. The irradiation and counting timings must be similar to the ones described in section 1.2 for the absolute delayed neutron yield measurements.

Evans and Krick[50] have recently measured the steady state delayed neutron spectra from the fast fission of U^{235}, U^{238} and Pu^{239} using a He^3 spectrometer and irradiation-counting timings similar to the ones used by Masters et al[5] (section 1.2) for the yield measurement.

8.2 The proton-recoil proportional counter spectroscopy technique

The spectrometer which will be used for the delayed neutron measurements must be usable in the energy interval (50 kev,1 Mev) at least, where most of the delayed neutrons are emitted. There are two spectrometry techniques which cover most of the required energy interval, namely, the He^3 spectrometry technique (proportional counters) and the proton recoil

spectrometry technique (proportional counters). The review of the measurements (section 8.1) shows that these are the only techniques which have been used.

The He^3 spectrometer is based on the reaction

$$He^3 + n \rightarrow T + p + 764 \text{ kev}$$

There are two main difficulties of this technique, namely the calculation of the wall effects and the He^3 recoils.

The hydrogen elastic scattering cross-section is smooth and one of the most accurately known. Therefore, the spectrometry technique based on the elastic scattering of neutrons by hydrogen is the most accurate fast neutron spectrometry technique employed nowadays. The simple proportional counter filled with hydrogen has been proved to be highly useful for the fast reactor neutron spectra measurements below 1.5 Mev and an extensive development work has been done. Therefore, it was decided to examine this technique for the delayed neutron spectra measurements. The basic features of this technique are reviewed below.

Since the elastic scattering of neutrons by hydrogen atoms is isotropic in the center of mass system, the neutron flux $\Phi(E)$ is

$$\Phi(E) = \frac{E}{N\sigma(E)} \quad \frac{dM(E)}{dE} \qquad (8.2.1)$$

where $M(E)$ is the proton recoil spectrum and $N,\sigma(E)$ the hydrogen atoms and hydrogen scattering cross-section. The equation (8.2.1) is correct provided that:

1) The multiplication factor of the proportional counter is constant along the anode wire.

2) The total recoil proton energy is deposited in the sensitive volume of the detector (wall effect).

3) The effect of the gamma background is negligibly small.

These are the main problems which must be solved so that, this spectrometry technique will be successfully employed. These three factors have also determined the three different counters which are currently in use, namely, the small cylindrical counters (Bennett[51]), the small spherical counters (Kemshall[52]) and the long cylindrical counters (up to 1 meter long, Werle[23]).

The principles of the proton recoil spectra analysis have been described by Benjamin et al[53]. If we assume that there is an upper limit (E_{MAX}) of the energy of the neutron flux $\Phi(E')$ then, the proton spectrum $M(E)$ is given by

$$M(E) = \int_0^{E_{MAX}} M_0(E,E')\ \Phi(E')dE' \qquad (8.2.2)$$

where the response function $M_0(E,E')dE$ is the number of proton pulses in $E \div E + dE$ per unit neutron flux of energy E'. Ideally, the response functions should be rectangular functions (extending in the energy interval $(0,E')$) but in practice they are sloping functions because of the wall effect. Therefore, it is necessary to calculate the response functions so that they will take into account the electric field distortion and the wall effect.

In practice (Benjamin et al[53]) equation (8.2.2) is differentiated with respect to the energy E and it is reduced to the conventional multigroup notation

$$\Delta M^i = \sum_{j=1}^{i} \Delta M_0{}^{ij}\ \Phi^j \qquad (8.2.3)$$

where the prefix Δ means small differences. The back substitution technique is used to calculate Φ^j from the differentiated proton spectrum. It is apparent that the response functions must be accurately calculated otherwise, the differention and backsubstitution noisy processes may lead to an oscillating flux.

In the case of the small cylindrical counters the response functions are calculated so that, they will take into account the electric field distortion and the wall effect. The small spherical counters have been designed (Benjamin et al[54]) so that the multiplication factor will be constant along the anode wire. Therefore, the response functions are calculated taking into account the wall effect only. In both cases, the wall effect is calculated according to the expressions of Snidow et al[55]. These expressions assume that the neutron flux is isotropic and constant throughout the volume of the counter. It is apparent that these conditions are correct for in-core measurements. In the case of the long cylindrical counters, the field distortion is negligibly small and the Monte-Carlo technique is used to calculate the response functions so that, they will take into account the wall effect.

For a proton recoil counter of specific pressure and dimensions, there is an upper limit (E_{MAX}) of the energy of the neutron flux which can be measured. The proton spectrum due to the neutron flux of energy higher than E_{MAX} is calculated using the response functions and the neutron flux (measured by proton recoil counters of higher pressure and/or estimated by another technique). The calculated proton spectrum is normalised to the measured one in the energy interval (E_{MAX}, 1.05 E_{MAX}) and it is subsequently subtracted from the measured spectrum. Then, equation (8.2.3) is used to calculate the neutron flux below E_{MAX} from the differentiated difference proton spectrum. It is known (Kemshall[52]) that if the wall correction is excessively high the unfolding technique gives oscillating answer. Therefore, each counter of specific pressure and dimensions is associated with an upper limit E_{MAX}.

For a counter of specific pressure and dimensions there is a maximum energy which can be dissipated into the sensitive volume of the counter due to the gamma rays. Therefore, there is an energy E_γ so that, all the

pulses of energy higher than E_γ are due to protons.

Therefore, for a counter of specific dimensions and pressure there is a useful range (E_γ, E_{MAX}) which can be used to measure the neutron flux. If we increase the pressure of the filling gas of a specific counter then both the E_γ and E_{MAX} energies increase. Therefore, the proton recoil spectroscipy technique employs a number of counters with different filling pressures to achieve measurements over a desired energy interval. It is apparent that the wall correction in this spectrometry technique is important especially for the low pressure counters since they still respond to high energy protons. The upper limit of this spectrometry technique is roughly 1.5 Mev, using the small spherical and cylindrical counters. This is determined by the wall correction of the counter filled with the maximum practically acceptable pressure.

Werle[23] used the long cylindrical counters to extend the upper limit of this spectrometry technique up to 10 Mev. These large counters are exclusively used in beam geometry measurements.

The lower limit of the proton recoil spectrometry technique is approximately 10 Kev and it is determined by the fact that below this energy the total ionisation produced is not proportional and independent of the dissipated energy in hydrogen.

The pulses due to gamma rays can be discriminated by the pulse shape discrimination technique, too (Kemshall[52]). The rise time of the pulse depends on the length of the ionisation track and its orientation with respect to the anode wire. The rise time of the pulses due to electrons (produced by gamma rays) is higher than the rise time of the pulses due to protons of the same energy as the electrons, because of the large difference of the specific ionisation (dissipated Kev/cm) of the electrons and protons. In order to obtain information on the rising time of the

pulse, the pulses are differentiated by a short clipping time (50 nsec typically). A two dimensions storage medium is required (Energy-rise time of pulses) because there is an overlapping region of rise times which are due to protons and gamma rays (i.e. no complete distinction).

The only advantage of the long cylindrical counters for the delayed neutron spectra measurements is their higher efficiency (compared with the small counters). Their disadvantage is the necessary pulse-shape discrimination (because of the large dimensions) and the fact that the Monte-Carlo technique is used for the generation of the response functions. Fieg[25] used this spectrometry technique for the delayed neutron spectra measurements.

Sloan and Woodruff[49] used the small cylindrical counters to measure the delayed neutron spectra. The expressions of Snidow et al[55] were used to generate the response functions and these expressions do not cover the anisotropy of the flux (point source) in the measurements.

We have decided to examine the spherical counters (simplest geometry) and calculate the response functions in the case of a beam neutron source. It is known (Kemshall[52]) that the number of pulses $C(E)dE$ obtained in the energy interval $E \div E+dE$, because of monoenergetic neutrons of energy E_n, are

$$\frac{C(E)}{C_T} = \frac{F(E)}{E_n} + \frac{1}{E_n} \int_E^{E_n} \frac{dR}{dE} (E'-E)\, N(R(E')-R(E'-E))\, dE' \qquad (8.2.4)$$

where C_T is the total number of recoil protons and $R(E)$ is the range-energy relationship. The $F(L)$ quantity is the probability that a particle will arrive at the detector wall having travelled a distance higher or equal to L (assuming zero stopping power of the gas) and

$$N(L)dL = \frac{-dF(L)}{dL} dL$$

is the probability that a particle will arrive at the walls having travelled a distance L : L + dL. The first term of equation (8.2.4) is the fraction of the recoil protons which are emitted with an energy E and they are stopped within the sensitive volume of the counter. The second term of equation (8.2.4) is the fraction of the recoil protons which are emitted with an energy E' > E and they arrive at the walls having dissipated an amount of energy equal to E within the sensitive volume.

8.3 The response functions of spherical proton recoil counters in the case of beam neutron source

8.3.1 Calculation of the probability function F(B,L)

Let S, B, R, α be the position of the neutron source, any point within the detector, the radius of the detector and the distance of the source from the detector center, respectively (Figure 8.3.1)

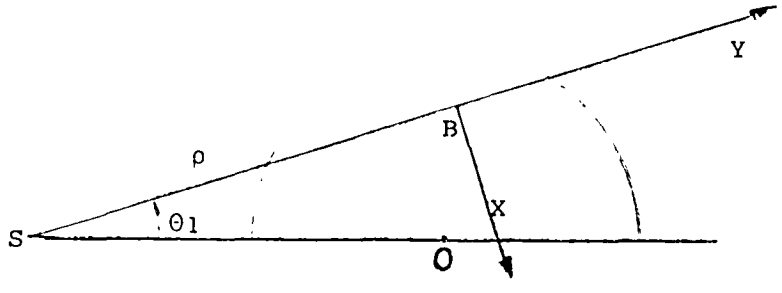

Figure 8.3.1 Geometry of the calculations.

At the point B we define a Cartesian system (X,Y,Z) so that, the axis Y will be on the extension of SB and the axis X will be on the plane determined by the points S,B,O and pointing towards the center of the detector. The coordinates of the center of the detector are

$$(X_0, Y_0, 0) \qquad X_0 \geq 0 \qquad (8.3.1)$$

We define F(B,L) as the probability that a proton which is produced at the point B because of a neutron elastic scattering at B, will arrive at the detector walls travelling a distance greater or equal to L (assuming zero gas stopping power). It is apparent that we may write

$$F(B,L) = F(X_0, Y_0, L) \tag{8.3.2}$$

Since the elastic scattering is isotropic in the center of mass system

$$p(\Theta,\Phi)\ d\Theta d\Phi = \frac{1}{2\Pi} \sin 2\Theta\ d\Theta d\Phi \tag{8.3.3}$$

is the probability that an elastically scattered proton will travel in $(\Theta, \Theta + d\Theta)$ and $(\Phi, \Phi + d\Phi)$. The angle between the path of the proton and the Y axis is Θ, and the solid angle between the plane determined by the points S, B, O and the plane determined by the Y axis and the path of the proton is Φ.

Let A be the set of all the directions (Φ, Θ) which intersect the detector wall at such a point so that its distance from the point B is greater or equal to L. Let C be the set defined by the intersections

$$C = A \cap \{\Phi/\Phi \in (0,2\Pi)\} \cap \{\Theta/\Theta \in (0,\Pi/2)\} \tag{8.3.4}$$

Then, the probability $F(X_0, Y_0, L)$ is

$$F(X_0, Y_0, L) = \frac{1}{2\Pi} \iint_C \sin 2\Theta d\Theta d\Phi \tag{8.3.5}$$

If (Θ,Φ) is an allowed direction of the integration the direction $(\Theta, 2\Pi-\Phi)$ is an allowed direction of the integration, too. Therefore,

$$F(X_0, Y_0, L) = \frac{1}{\Pi} \iint_D \sin 2\Theta\ d\Theta\ d\Phi \tag{8.3.6}$$

where the space D is determined by the intersections

$$D = A \cap \{\Phi/\Phi \in (0,\Pi)\} \cap \{\Theta/\Theta \in (0,\Pi/2)\}$$

Let M(X,Y,Z) be a point on the sphere (BM) = L. The direction BM belongs to the set D if and only if

$$Z = \sqrt{L^2 - X^2 - Y^2} \geq 0$$

$$Y \geq 0$$

$$X^2 + Y^2 \leq L^2 \qquad (8.3.9a)$$

$$-2XX_0 - 2YY_0 \leq R^2 - L^2 - (X_0^2 + Y_0^2) \qquad (8.3.9b)$$

The transformation of the variables is

$$X = L \sin\theta \cos\Phi$$

$$Y = L \cos\theta$$

and the integration (8.3.6) is equivalent to

$$F(X_0, Y_0, L) = \frac{2}{\pi L^2} \int \frac{Y dX dY}{\sqrt{L^2 - X^2 - Y^2}} \qquad (8.3.10)$$

The integration has been carried out analytically and the results are given in table 8.3.1. The symbols ofthe table 8.3.1 are explained below:

(1) The straight line given by equation (8.3.9b) intersects the axis X,Y at the points $(X_T, 0)$ and $(0, Y_T)$ respectively.

$$X_T = \frac{-\{R^2 - L^2 - (X_0^2 + Y_0^2)\}}{2X_0}, \quad Y_T = \frac{-\{R^2 - L^2 - (X_0^2 + Y_0^2)\}}{2Y_0} \qquad (8.3.11)$$

(2) The distance of the point (0,0) from the straight line given by equation (8.3.9b) is

$$V = \frac{|X_T| \, |Y_T|}{\sqrt{X_T^2 + Y_T^2}} \qquad (8.3.12)$$

(3) The straight line given by equation (8.3.9b) intersects the cycle given by equation (8.3.9a) at the points (X_1, Y_1) and (X_2, Y_2) where

$$X_{1,2} = \frac{-X_0\{R^2 - L^2 - (X_0^2 + Y_0^2)\} \pm \sqrt{4Y_0^2 L^2 (X_0^2 + Y_0^2) - Y_0^2 (R^2 - L^2 - (X_0^2 + Y_0^2))^2}}{2(X_0^2 + Y_0^2)} \qquad (8.3.13)$$

$$X_1 \leq X_2$$

8.3.2 Wall correction - Probability F(L)

Let F(L) be the probability that a proton will arrive on the detector walls travelling a distance greater or equal to L, per collision in the detector. Considering the geometry given in Figure (8.3.1) we write

$$F(L) = \frac{\iint \sin\theta_1 F(X_0, Y_0, L)\, d\theta_1 d\rho}{R - \frac{\alpha^2 - R^2}{2\alpha} \ln\frac{\alpha + R}{\alpha - R}} \qquad (8.3.14)$$

$$L \leqslant 2R$$

where

$$X_0 = \alpha\sin\theta_1$$

$$Y_0 = \alpha\cos\theta_1 - \rho$$

and the integration is carried out over the space

$$\rho \in \{\alpha - R,\ \alpha + R\}$$

$$\theta_1 \in \{0,\ \text{arc cos}\ \frac{\alpha^2 + \rho^2 - R^2}{2\alpha\rho}\}$$

We could not carry out the integration given by equation (8.3.14) analytically. Since the SPEC4[53] code which is used for the analysis of the proton recoil spectra requires the probability function F(L) (and N(L), section 8,3,2) to be easily calculable, the present numerical formulation is of little practical use.

A program WALL was written to perform the integration (8.3.14) numerically. In particular, the probability function F(L) was calculated for different values of the parameter L. We considered the SP2 proportional counters (Kemshall[52]) and the special case when the distance α is much longer than the radius of the detector (i.e. beam geometry). The results of the calculations are summarised in table 8.3.2 and they are compared with the analytical solution of Snidow et al[55].

We conclude that the spherical proton recoil spectrometers can be used in beam geometry and the analytical expressions suggested by Snidow et al[55], which are correct for isotropic and uniform neutron

flux,can be used for the calculation of the response functions.

8.4 Recommendations

The proton recoil proportional counters spectrometry technique, using the small spherical counters, is suggested for the delayed neutron spectra measurements because of the accuracy (5% error, Kemshall[52]) of this technique. The measurements should be performed in a beam geometry and in this special case the presently used (SPEC 4code) response functions are correct.

TABLE 8.3.1 INTEGRATION RESULTS

1. $X_0 = Y_0 = 0$

1.1 IF $L \leq R$ $\quad F(X_0, Y_0, L) = 1$

1.2 IF $L > R$ $\quad F(X_0, Y_0, L) = 0$

2. $X_0 = 0 \quad Y_0 \neq 0$

2.1 $R^2 - L^2 - (X_0^2 + Y_0^2) > 0$

2.1.1 $Y_0 > 0$ $\quad F(X_0, Y_0, L) = 1$

2.1.2.1 $Y_0 < 0$ and $\quad R^2 - L^2 - (X_0^2 + Y_0^2) \geq 2L\sqrt{X_0^2 + Y_0^2}$

$F(X_0, Y_0, L) = 1$

2.1.2.2 $Y_0 < 0$ and $\quad R^2 - L^2 - (X_0^2 + Y_0^2) \leq 2L\sqrt{X_0^2 + Y_0^2}$

$$F(X_0, Y_0, L) = 1 + \frac{4L^2 (X_0^2 + Y_0^2) - (R^2 - L^2 - (X_0^2 + Y_0^2))^2}{4L^2 (X_0^2 + Y_0^2)^{3/2}} Y_0$$

2.2 $R^2 - L^2 (X_0^2 + Y_0^2) < 0$

2.2.1 $Y_0 < 0$ $\quad F(X_0, Y_0, L) = 0$

2.2.2.1 $Y_0 > 0$ and $\quad \left|R^2 - L^2 - (X_0^2 + Y_0^2)\right| \geq 2L\sqrt{X_0^2 + Y_0^2}$

$F(X_0, Y_0, L) = 0$

2.2.2.2 $Y_0 > 0$ and $\quad \left|R^2 - L^2 - (X_0^2 + Y_0^2)\right| \leq 2L\sqrt{X_0^2 + Y_0^2}$

$$F(X_0, Y_0, L) = \frac{4L^2 (X_0^2 + Y_0^2) - (R^2 - L^2 - (X_0^2 + Y_0^2))^2}{4L^2 (X_0^2 + Y_0^2)^{3/2}} Y_0$$

2.3 $R^2 - L^2 - (X_0^2 + Y_0^2) = 0$

2.3.1 $Y_0 > 0$

$F(X_0, Y_0, L) = 1$

2.3.2 $Y_0 < 0$

$F(X_0, Y_0, L) = 0$

3. $X_0 \neq 0 \quad Y_0 = 0$

3.1 $X_T \geq L \quad F(X_0, Y_0, L) = 0$

3.2 $X_T \leq -L \quad F(X_0, Y_0, L) = 1$

3.3 $-L \leq X_T \leq L$

TABLE 8.3.1 Continued

$$F(X_0, Y_0, L) = \frac{2}{\Pi L^2}\left(\frac{\Pi L^2}{4} - \frac{X_T}{2}\sqrt{L^2 - X_T^2} - \frac{L^2}{2}\arcsin\frac{X_T}{L}\right)$$

4. $X_0 \neq 0 \qquad Y_0 \neq 0$

4.1 $Y_0 > 0$

4.1.1 $X_T \geq L$

4.1.1.1 $V \geq L \qquad F(X_0, Y_0, L) = 0$

4.1.1.2 $V \leq L \qquad F(X_0, Y_0, L) = \left[\dfrac{4L^2(X_0^2 + Y_0^2) - (R^2 - L^2 - (X_0^2 + Y_0^2))^2}{4L^2(X_0^2 + Y_0^2)^{3/2}}\right] Y_0$

4.1.2 $X_T \leq -L$

$F(X_0, Y_0, L) = 1$

4.1.3 $-L \leq X_T \leq L$

$$F(X_0, Y_0, L) = \frac{2}{\Pi L^2}\left(\frac{\Pi L^2}{4} - \frac{X_T}{2}\sqrt{L^2 - X_T^2} - \frac{L^2}{2}\arcsin\frac{X_T}{L}\right)$$

$$+ \frac{2}{\Pi L^2}\,\frac{\sqrt{X_0^2 + Y_0^2}}{Y_0}\left[\frac{2X_T - X_1 - X_2}{4}\sqrt{(X_T - X_1)(X_2 - X_T)} + \frac{(X_2 - X_1)^2}{8}\arcsin\frac{2X_T - X_1 - X_2}{X_2 - X_1} + \frac{\Pi(X_2 - X_1)^2}{16}\right]$$

4.2 $Y_0 < 0$

4.2.1 $X_T \geq L$

$F(X_0, Y_0, L) = 0$

4.2.2 $-L \leq X_T \leq L$

$$F(X_0, Y_0, L) = \frac{2}{\Pi L^2}\left(\frac{\Pi L^2}{4} - \frac{X_T}{2}\sqrt{L^2 - X_T^2} - \frac{L^2}{2}\arcsin\frac{X_T}{L}\right) - \frac{2}{\Pi L^2}\,\frac{\sqrt{X_0^2 + Y_0^2}}{Y_0}\left[\frac{2X_T - X_1 - X_2}{4}\sqrt{(X_T - X_1)(X_2 - X_T)} + \frac{(X_2 - X_1)^2}{8}\arcsin\frac{2X_T - X_1 - X_2}{X_2 - X_1} - \frac{\Pi(X_2 - X_1)^2}{16}\right]$$

4.2.3 $X_T \leq -L$

4.2.3.1 $V \geq L \qquad F(X_0, Y_0, L) = 1$

4.2.3.2 $V \leq L$

TABLE 8.3.1 Continued

$$F(X_0, Y_0, L) = 1 + \left[\frac{4L^2 (X_0^2+Y_0^2) - (R^2 - L^2 - (X_0^2+Y_0^2))^2}{4L^2 (X_0^2 + Y_0^2)^{3/2}} Y_0 \right]$$

TABLE 8.3.2 Comparison of probability functions

α = 40 cm R = 2 cm

Relative accuracy of the NEW F(L) is 10^{-4}.

L	F(L)		$N(L)=-\frac{F(L+\Delta L)-F(L)}{\Delta L}$	
(CM)	NEW	SNIDOW[55]	NEW	SNIDOW[55]
.01	.996267	.99625	.3753	.3750
.06	.977500	.97750	.3751	.3749
.11	.958744	.95876	.3746	.3747
.16	.940013	.94003	.3740	.3744
.21	.921313	.92132	.3740	.3740
.26	.902614	.90264	.3731	.3734
.31	.883960	.88398	.3725	.3727
.36	.865334	.86536	.3716	.3720
.41	.846756	.84679	.3707	.3711
.46	.828221	.82826	.3694	.3700
.51	.809750	.80979	.3683	.3689
.56	.791333	.79137	.3671	.3676
.61	.772980	.77302	.3658	.3663
.66	.754690	.75475	.3638	.3648
.71	.736499	.73655	.3623	.3632
.76	.718385	.71843	.3605	.3615
.81	.700359	.70040	.3587	.3596
.86	.682423	.68247	.3562	.3577
.91	.664613	.66464		
1.00	.632767	.63281		
1.06	.611762	.61180		
1.30	.529626	.52966		
1.50	.463832	.46387		
1.90	.341062	.34109		
2.30	.232544	.23255		
2.80	.121497	.12150		
3.50	.0224627	.022461		

REFERENCES

1. TOMLINSON L. "Theory of delayed neutron physics" AERE-R6596 (1970)

2. LAMARSH J. "Introduction to nuclear reactor theory" ADDISON-WESLEY Publ. Co. (1966)

3. ROSE H. and SMITH R.D. "The delayed neutrons arising from fast fission in U^{235}, U^{233}, U^{238}, Pu^{239} and Th^{232}" J. NUCL. ENERGY 4(1957) p141

4. KEEPIN G.R., WIMETT T.F. and ZEIGLER R.K. "Delayed neutrons from fissionable isotopes of Uranium, Plutonium and Thorium" J. NUCL. ENERGY 6(1957) p1

5. MASTERS C.F., THORPE M.M. and SMITH D.B. "The measurement of absolute delayed neutron yields from 3.1- and 14.9- Mev fission" NUCL. SCI. ENG. 36(1969) p202

6. KRICK M.S. and EVANS A.E. "The measurement of total delayed neutron yields as a function of the energy of the neutron inducing fission" NUCL. SCI. ENG. 47(1972) p311

7. EVANS A.E., THORPE M.M. and KRICK M.S. "Revised delayed neutron yield data" NUCL. SCI. ENG. 50(1973) p80

8. COX S.A. "Absolute yield and energy dependence of delayed neutron emission from $U^{235}+n$, $U^{238}+n$, $Pu^{239}+n$" BULL. AM. PHYS. SOC. 19(1974) p597

9. TUTTLE R.J. "Delayed neutron data for reactor physics analysis" NUCL. SCI. ENG. 56(1975)p37

10. KEEPIN G.R. "Physics of nuclear kinetics" ADDISON-WESLEY Publ. Co.(1965)

11. LITTLE W.W. Jr and HARDIE R.W. "Discrepancy between measured and calculated reactivity coefficients in dilute plutonium fueled fast assemblies" NUCL.SCI. ENG. 36(1969) p115

12. CLIFFORD D.A. "Absolute yields of delayed neutrons in the fast fission of U^{235} and U^{238}" Ph.D. Thesis(1972) London University

13. AZIMI D. "Fission rates in NISUS-A fast reactor neutron spectrum generator" Ph.D. Thesis (1975) London University

14. BESANT C.B., EMMETT J., CAPBELL C.G., KERRIDGE M., JONES T.C. "Design and construction of a fast reactor neutron spectrum generator NISUS" NUCL. ENG. INTER. 18(1973) p425

15. GRUNDL J.A., GILLIAM D.M., DUDEY N.D., POPEK R.J. "Measurement of absolute fission rates" NUCLEAR TECHNOLOGY 5(1975)p237

16. WILLIAMS J.G. Private communication

17. WEALE J.W., GOODFELLOW H., McTAGGART M.H., WARNKE E.G.
"The fast pulsed reactor VIPER"
J.B.N.E.S. 7 (1968)p313

18. WEALE J.W. Private communication
A.W.R.E.

19. BROOME N. Unpublished report, A.W.R.E., 1968

20. ALLEN W.D. "Flat response counters"
FAST NEUTRON PHYSICS, PART I, MARION J.B. and
FOWLER J.L.

21. PRICE W.J. "Nuclear radiation detection"
McGRAW-HILL Book Co. (1964)

22. KROONTZ P.G., KEEPIN G.R., ASHLEY J.E. "ZnS(Ag) phosphor mixture
for neutron scintillation counting"
THE REVIEW OF SCIENTIFIC INSTRUMENTS 26(1955)p352

23. WERLE H. "Spectrum measurements of radioactive neutron sources
in the 10Kev-10 Mev energy region with proton recoil
proportional counters"
INR-4170-25 (1970) KARLSRUHE NUCLEAR RESEARCH CENTER

24. BATCHELOR R. and HYDER H.R. "The energy of delayed neutrons from
fission"
J. NUCL. ENERGY 3(1956)p7

25. FIEG G. "Measurement of delayed fission neutron spectra of
U^{235}, U^{238} and Pu^{239} with proton recoil proportional
counters"
J. NUCL. ENERGY 26(1972)p585

26. FIELDHOUSE P., CULLIFORD E.R., MATHER D.S. "Calibration of the
Aldermaston Pu^{240} spontaneous fission neutron source"
J. NUCL. ENERGY 21(1967)p131

27. NUCLEAR DATA SHEETS, 12(1974) No.3

28. DEME SANDOR "Semiconductor detectors for nuclear radiation
measurement"
ADAM HILGER Ltd. (1971)

29. GIBBONS P.E., HOWES J.H., "Gamma ray spectrometer systems using
lithium drifted germanium detectors"
AERE-R5703

30. CANBERRA INDUSTRIES, CONNECTICUT, USA

31. DELANEY C.F.G. "Electronics for the physicist"
PENGUIN BOOKS Ltd, (1969)

32. HELMER R.G., HEATH R.L., PUTNAM M. and GIPSON D.H.
"Photopeak analysis program for photon energy and
intensity determination in Ge(Li) and NaI(Tl)
spectrometers"
NUCL. INSTR. METHODS 57(1967)p46

33. VARNELL L. and TRISCHUK J. "A peak fitting and calibration program for Ge(Li) detectors" NUCL. INSTR. METHODS 76(1969)p109

34. COVELL D.F. "Determination of gamma ray abundance directly from the total absorption peak" ANALYTICAL CHEMISTRY 31(1959)p1785

35. YULE H.P. "Computation of lithium-drifted germanuim detector peak areas for activation analysis and gamma ray spectrometry" ANALYTICAL CHEMISTRY 40(1968) p1480

36. QUITTNER P. "Peak area determination for Ge(Li) detector data" NUCL. INSTR. METHODS 76(1969)p115

37. LARSEN R.P., DUDEY N.D., HEINRICH R.R., OLDHAM R.D., ARMANI R.J., POPEK R.J., GOLD R. "The yield of short lived gamma ray emitting nuclides from fast and thermal fission" NUCL. SCI. ENG. 54(1974)p263

38. McELROY and KELOGG. "Fuels and materials for fast reactor dosimetry data development and testing" NUCLEAR TECHNOLOGY 25(1975)No.2

39. HUANG D.S. "Regression and economometric methods" JOHN WILEY and Sons (1970)

40. POWELL M.J.D. "Problems related to unconstrained optimisation" T.P. 439 REPORT, THEORETICAL PHYSICS DIVISION, UKAEA RESEARCH GROUP

41. MARQUARDT D.W. "An algorithm for least squares estimation of non linear parameters" S.I.A.M. J. APPL. MATHS. 11(1963)p431

42. NAG "Numerical Algorithm Group" Imperial College Computer Center

43. GARDNER D.G., GARDNER J.C., LAUSH J., MEINKEN "Method for the analysis of multicomponent exponential decay curves" J. CHEMICAL PHYSICS 31(1959)p978

44. SCHLESSINGER J. "Fit to exponential data with exponential functions using the fast fourier transform" NUCL. INSTR. METHODS 106(1973)p503

45. COOLEY J.W., LEWIS P.A.W., and WELCH P.D."Application of the Fast Fourier Transform to computation of Fourier Integrals, Fourier Series and Convolution Integrals" IEEE TRANSACTIONS ON AUDIO AND ELECTROACOUSTICS, June 1967, P79

46. KERLIN T.W. "Frequency response testing in nuclear reactors" ACADEMIC PRESS(1974)

47. ACTON F.S. "Numerical methods that work"
HARPER INTERNATIONAL (1970), page 253

48. SHALEV S. and CUTTLER J.M. "The energy distribution of delayed fission neutrons"
NUCL. SCI. ENG. 51(1973)p52

49. SLOAN W.R., and WOODRUFF G.L. "Delayed neutron spectra"
NUCL. SCI. ENG. 55(1974)p28

50. EVANS A.E. and KRICK M.S. "Spectra of equilibrium delayed neutrons from fast fission of U^{235}, U^{238} and Pu^{239}"
TRANS. AM. NUCL. SOC. 24(1976)p491

51. BENNETT E.F. "Fast neutron spectroscopy by proton recoil proportional counting"
NUCL. SCI. ENG. 27(1967)P16

52. KEMSHALL C.D. "The use of spherical proportional counters for neutron spectrum measurement"
AWRE 031/73 REPORT(1973)

53. BENJAMIN P.W., KEMSHALL C.D., and BRICKSTOCK A. "The analysis of recoil proton spectra"
AWRE 09/68 REPORT(1968)

54. BENJAMIN P.W., KEMSHALL C.D., REDFEARN J. "High resolution spherical proportional counter"
NUCL. INSTR. METHODS 59(1968)p77

55. SNIDOW N.L. and WARREN H.D. "Wall effect corrections in proportional counter spectrometers"
NUCL. INSTR. METHODS 51(1967)p109

APPENDIX A

THE SELF-MULTIPLICATION CORRECTION IN THE SAMPLES

The number of neutrons which will escape the sample is different from the number of delayed neutrons originally produced, because of the absorption of delayed neutrons by the sample and the production of prompt fission neutrons. Since the foils were very thin, the overall correction is very small and for this reason an approximate correction was applied.

A.1 The average escape length L - The Monte Carlo Method

We assume that we have a disk of radius R and height H, and that particles are produced uniformly over the volume of the disk and that they are emitted isotropically. We assume that the particles travel on a straight line, without suffering any type of collision. The average escape length L is defined as, the average distance between the point of origin of a particle and the point it escapes the disk.

The Monte-Carlo technique has been used for the calculation of L. The probability of each event and the calculation of L is given below. Figure (A.1) shows the geometry of the calculations.

The probability that a particle will be emitted in (x, x + dx) is

$$\frac{dx}{H} \qquad (A.1)$$

The probability that a particle will be emitted in (p, p + dp) assuming that it has been emitted in (x, x + dx) is

$$\frac{2pdp}{R^2} \qquad (A.2)$$

Because of the cylindrical geometry, the angle of the point of origin is indifferent. So, the equations (A.1) and (A.2) determine the point of origin of the particle M(x,p). The straight line going through the point M, and being parallel to the axis of the disk is called α.

The angle between the plane determined by α and the axis of the disk, and the plane determined by α and the direction of the particle, is called Φ. The angle between the direction of the particle and the line α, is called θ.

The probability that a particle will be emitted in $(\Phi,\Phi+d\Phi)$ is

$$\frac{d\Phi}{2\pi} \qquad \Phi\varepsilon(0,2\pi) \qquad (A.3)$$

and the probability that it will be emitted in $(\theta, \theta + d\theta)$, assuming that it has been emitted in $(\Phi, \Phi + d\Phi)$ is

$$\frac{1}{2}\sin\theta d\theta \qquad \theta\varepsilon(0,\pi) \qquad (A.4)$$

The equations (A.3) and (A.4) determine the direction the particle is being emitted. The distance L between the point of origin of the particle and the point it escapes the disk is given by the following equations

$$C = (MZ) = p\cos\Phi + \sqrt{R^2 - p^2\sin^2\Phi}$$

$$\theta_1 = \arctan\,(C/(H-x))$$

$$\theta_2 = -\arctan\,(C/x) + \pi$$

IF $\theta<\theta_1$ $\qquad L = (H-x)/\cos\theta$

IF $\theta_1<\theta<\theta_2$ $\qquad L = C/\sin\theta$

IF $\theta_2<\theta$ $\qquad L = -x/\cos\theta$

Ten thousand particles were traced and the average escape length was determined.

A.2 Approximate self-multiplication correction

The present approximate correction is based on a similar work of Keepin[10]. Let us assume that

Σ_f = macroscopic fission cross-section of sample

Σ_α = macroscopic absorption cross-section of sample

ν = number of prompt neutrons per fission

L = average escape length of sample

D_N = number of delayed neutrons emitted

D_{NC} = number of neutrons escaping the sample

F = true number of fissions (in VIPER pulse)

F_C = counted number of fissions

Σ_C = macroscopic capture cross-section of sample

$\Sigma_\alpha L \ll 1$

then

$$\frac{D_{NC}}{F_C} = \frac{D_N + D_N \nu \Sigma_f L - \Sigma_\alpha L D_N}{F + D_N \Sigma_f L}$$

or

$$\frac{D_{NC}}{F_C} = \frac{D_N}{F} \frac{1 + (\nu \Sigma_f - \Sigma_\alpha) L}{1 + \frac{D_N}{F} \Sigma_f L}$$

Since

$$\frac{D_N}{F} \ll 1$$

we conclude that

$$\frac{D_N}{F} = \frac{D_{NC}}{F_C} \frac{1}{1 + (\nu \Sigma_f - \Sigma_\alpha) L}$$

where D_N/F is the true yield per fission of the delayed neutrons and D_{NC}/F_C is the measured yield.

So, the self-multiplication correction is given by

$$M = \frac{1}{1 + (\nu \Sigma_f - \Sigma_\alpha) L} \qquad (A.4)$$

where the quantities $\nu, \Sigma_f, \Sigma_\alpha$ will be evaluated for the delayed neutron energy spectrum.

A.3 Calculation of the self-multiplication correction

Since the medium and large VIPER pulses have been normalised to the small VIPER pulse, the correction for self-multiplication will refer to the small VIPER pulse. The U^{235}, Pu^{239} small VIPER pulses have samples made of a single foil only. The necessary correction for these isotopes is given in Table - (A1).

The resulting modification in the yield, because of the self-multiplication of the samples, is .1% and .4% for the U^{235} and Pu^{239} respectively. Because of the crude assumptions and inaccurate data, we assume that the uncertainty in the yield is .1% and .4% for the U^{235} and Pu^{239} respectively.

The sample of the small VIPER pulse for the U^{238} study consisted of seven foils. The modification ofthe yield because of self-multiplication of the sample is negligibly small.

TABLE (A1) SELF-MULTIPLICATION CORRECTION[1]

ISOTOPE	DIMENSIONS OF FOIL		L (CM)	ν	$\sum_f (CM^{-1})$	$\sum_c (CM^{-1})$	M
	R (CM)	H (CM)					
U^{235}	.375	.005	.0136	2.5	.04	.01	.999
Pu^{239}	.300	.012	.0258	2.9	.09	.01	.996

(1) Data obtained from ANL-5800, for E=500Kev

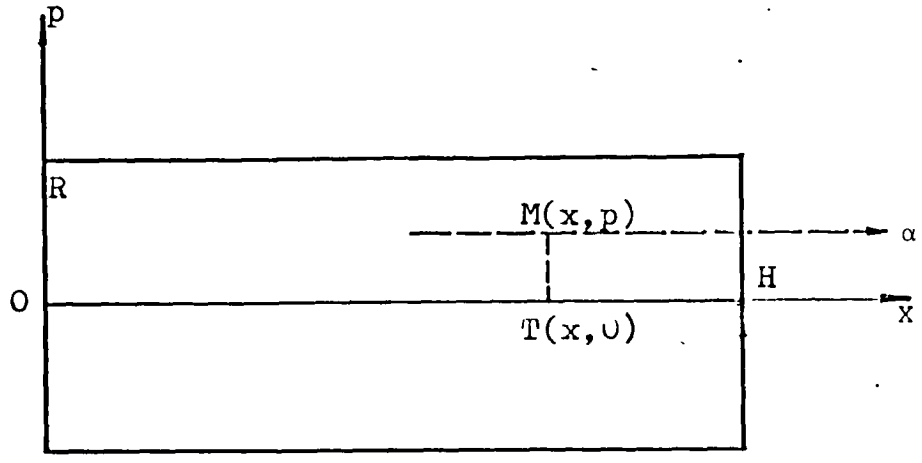

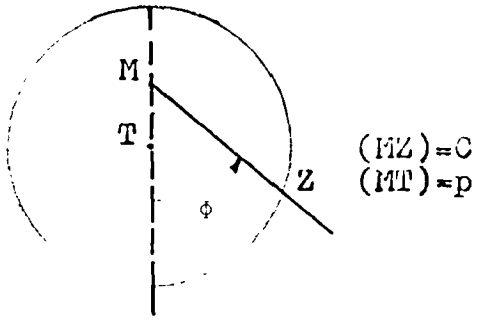

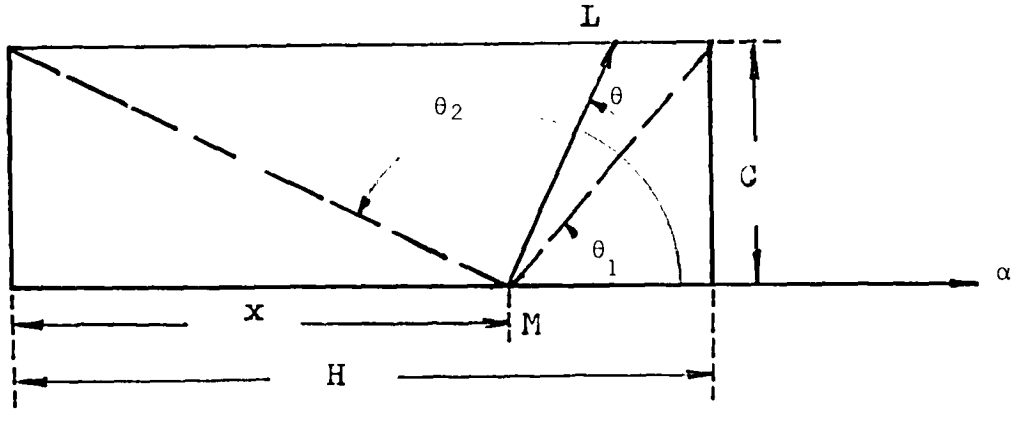

FIGURE A.1 MONTE CARLO CALCULATION.

APPENDIX B

THE GROUP CONSTANTS OF Pu^{239}

The group constants for the delayed neutrons emitted by Pu^{239} have already been given (Table 6.3.4). The statistical error of α_6 (relative abundance of the sixth group) is higher than α_6 thus, we can assume that $\alpha_6 = 0$. It is apparent that a five group structure is rather appropriate.

The first series of experiments consisted of the VIPER pulses 634, 617 and 615. The results obtained from these data are summarised below.

Table (B1) gives the four group constants obtained from the graphical analysis of the data. These values were used as the initial estimate required by the optimisation technique, the missing group constant estimates obtained from the data of Keepin et al[4].

A six group fit was attempted; the obtained values for the decay constants of the fifth and sixth groups were the same (within four digits). This implies that there are five groups.

A five group fit was attempted and the solution found was the same, as the previously described. Table (B2) gives the result of the five group fit.

A new experiment was done (pulse 668) identical to the pulse 634 so that, we could improve the statistical accuracy of the data over the time interval where the contribution of the sixth group is significant. Table (6.3.4) gives the group constants obtained by the pulses 634,668 (average), 617, 615.

Table (B.3) gives the period-reactivity curve, using all the available data; the period-reactivity curve based on the group constants

of Keepin et al[4] is given, too. It is apparent that,

a) The period-reactivity curve, calculated directly (Laplace transform technique) from the data obtained by the pulses 634,668,617,615 (statistical accuracy better than .5%) is in agreement with all the other curves, obtained by the present data, within .5% (excluding the point T = -100 sec).

b) The period-reactivity curves based on the present six group data and on the six group data suggested by Keepin et al[4] are in agreement, to within 2.5% (maximum discrepancy.)

Although it is probable that there are only five groups, we have suggested a six group structure so that a similar structure will exist for all the isotopes. These six group constants predict the period-reactivity curve to better than .5% (excluding the point T =-100 sec).

TABLE (B.1) ESTIMATE OF Pu^{239} GROUP CONSTANTS

GROUP	RELATIVE ABUNDANCE	DECAY CONSTANT (SEC^{-1})
1	.037	.0132
2	.306	.0318
3	.191	.129
4	.363	.354

TABLE (B2). Pu^{239} FIVE GROUP CONSTANTS

GROUP	RELATIVE ABUNDANCE	DECAY CONSTANT (sec^{-1})
1	.030 ± .002	.0127 ± .0002
2	.296 ± .006	.0302 ± .0002
3	.188 ± .035	.121 ± .009
4	.373 ± .032	.323 ± .014
5	.113 ± .009	1.91 ± .12

Number of points = 971

Minimum of function = 997.5

GRADIENT AT THE OPTIMUM					
VARIABLE	i = 1	i = 2	i = 3	i = 4	i = 5
$\alpha_i\lambda_i$	$-.37\ 10^{-3}$	$-.30\ 10^{-4}$	$-.78\ 10^{-6}$	$-.22\ 10^{-7}$	$.15\ 10^{-8}$
λ_i	$.35\ 10^{-4}$	$.64\ 10^{-4}$	$.38\ 10^{-4}$	$.85\ 10^{-5}$	$-.24\ 10^{-6}$

TABLE (B3) Pu^{239} REACTIVITY COMPARISON

PERIOD SEC	REACTIVITY ($)				
	Laplace Method Pulse 634	Laplace Method Pulses 634,668*	New Five Group Constants	New Six Group Constants	Keepin Six Group Constants
.2	.9397	.9394	.9398	.9394	.9377
.5	.8769	.8769	.8776	.8769	.8740
1	.8041	.8042	.8054	.8044	.7999
3	.6428	.6428	.6445	.6432	.6362
7	.4946	.4945	.4959	.4949	.4871
10	.4317	.4316	.4328	.4319	.4243
30	.2537	.2536	.2545	.2540	.2483
70	.1469	.1469	.1474	.1472	.1438
100	.1126	.1126	.1130	.1129	.1103
300	.04454	.04454	.04471	.04469	.04373
700	.02025	.02025	.02032	.02032	.01991
900	.01591	.01591	.01597	.01597	.01565
-900	-.01721	-.01721	-.01728	-.01728	-.01697
-500	-.03208	-.03208	-.03220	-.03222	-.03167
-200	-.09213	-.09217**	-.09248	-.09266	-.09156
-100	-.2866	-.2876**	-.2871	-.2913	-.2923

*Statistical error 0.5%. Contribution of missing data less than 1%.
**Contribution of missing data higher than 1%.

APPENDIX C

EFFECT OF THE DETECTOR RESPONSE ON THE GROUP CONSTANTS

The energy response of the detector, which was used to estimate the group constants of the delayed neutrons, is not flat, so that, systematic errors will be introduced in the group constants estimation. A correction can be applied provided that, we know the delayed neutron group spectra and the detector energy response function but, both these factors are poorly known. So, it was decided to estimate the effect of these factors on the group constants and especially on the reactivity (dollars)- period relationship.

If we assume that $n(t_j)$ and $\sigma(t_j)$ is the detected delayed neutron count rate per fission and its standard deviation at the moment t_j after the irradiation the least squares solution of the regression model, including the spectral effect, is

$$\text{Minimise } S = \sum_{j=1}^{J} \frac{1}{\sigma^2(t_j)} \left[n(t_j) - \sum_{i=1}^{M} \mu_i \lambda_i \varepsilon_i e^{-\lambda_i t_j} \right]^2 \qquad \text{C.1}$$

where

J = number of measurements

M = number of groups

μ_i, λ_i = the absolute group yield (d.n./fission) and decay constant of group i

ε_i = detector efficiency for the i^{th} group of delayed neutrons

If we assume that E is the efficiency of the detector for the Pu^{240} neutron source, the equation (C.1) is rewritten as

$$\text{Minimise } S = \sum_{j=1}^{J} \frac{E^2}{\sigma^2(t_j)} \left[\frac{n(t_j)}{E} - \sum_{i=1}^{M} \mu_i \frac{\varepsilon_i}{E} \lambda_i e^{-\lambda_i t_j} \right]^2$$

The new regression model, including the spectral effect, is equivalent to the one used in chapter 5 since $n(t_j)/E$ and $\sigma^2(t_j)/E^2$ is the delayed neutron emission rate per fission (based on Pu^{240} detector calibration) and its variance, respectively.

So, the non-flatness of the detector response will affect only the group yield but the same decay constants will be estimated for any response function of the detector.

We conclude that, a modified group absolute yield is calculated by the program, Z_i, given by the equation

$$Z_i = \mu_i \frac{\epsilon_i}{E} \qquad i=1,\ldots,M$$

So, the relative abundance of group i is given by

$$\frac{\mu_i}{\sum_{i=1}^{M} \mu_i} = \frac{Z_i/\epsilon_i}{\sum_{i=1}^{M} Z_i/\epsilon_i} \qquad \text{C.2}$$

The results presented in chapter-6, for the group structure of the delayed neutrons, assume that the detector efficiency is independent of the delayed neutron group spectrum (i.e. ϵ_i = constant, i=1, ..., M) and the relative group abundance has been calculated by

$$Z_i / \sum_{i=1}^{M} Z_i \qquad \text{C.3}$$

The calculation of the efficiency ϵ_i requires the detailed knowledge of the group spectra of the delayed neutrons and the response function of the detector. On the other hand, it depends on the definition of the group spectra. Usually, the group spectra have been determined using the group structure of Keepin et al[4] and they are not necessarily compatible with any (the present) group structure. Also, the available information on the group spectra is incomplete and the response function of the present detector is not known in detail.

So, instead of using equation (C.2) to predict the relative abundances of the group structure, we have used the simplified equation (C.3) - which is justified by the flatness of the response function of the detector-and we have attempted to estimate the systematic error introduced by this assumption.

Let us assume that the response function of the detector is a straight line determined by the two calibration points using the (γ,n) sources (chapter 3) and that the group spectra are monoenergetic with energies equal to their mean energies. Assuming that the mean energies of the groups are those given by Batchelor and Hyder[24] $(E_6=E_5=E_4)$ then, the group relative abundances of the delayed neutrons of U^{235} are:

GROUP	MEAN ENERGY (KEV)	EFFICIENCY ε_i	RELATIVE ABUNDANCE	
			EQUATION (C.3)	EQUATION (C.2)
1	250	$3.19\ 10^{-4}$	.035	.036
2	460	$3.25\ 10^{-4}$	.234	.234
3	405	$3.23\ 10^{-4}$	.216	.217
4	450	$3.25\ 10^{-4}$	.290	.289
5	450	$3.25\ 10^{-4}$	.178	.177
6	450	$3.25\ 10^{-4}$	.047	.047

We observe that the effect of the non-flatness of the response of the detector is only on the last rounding-off digit of the relative abundance.

Figure (C.1) gives the discrepancy of the reactivity (dollars), using the previously calculated group constants for different period values.

So, it is estimated that a systematic error of less than .6% is

FIGURE C.1 EFFECT OF SPECTRAL RESPONSE OF DETECTOR ON PERIOD-REACTIVITY RELATIONSHIP

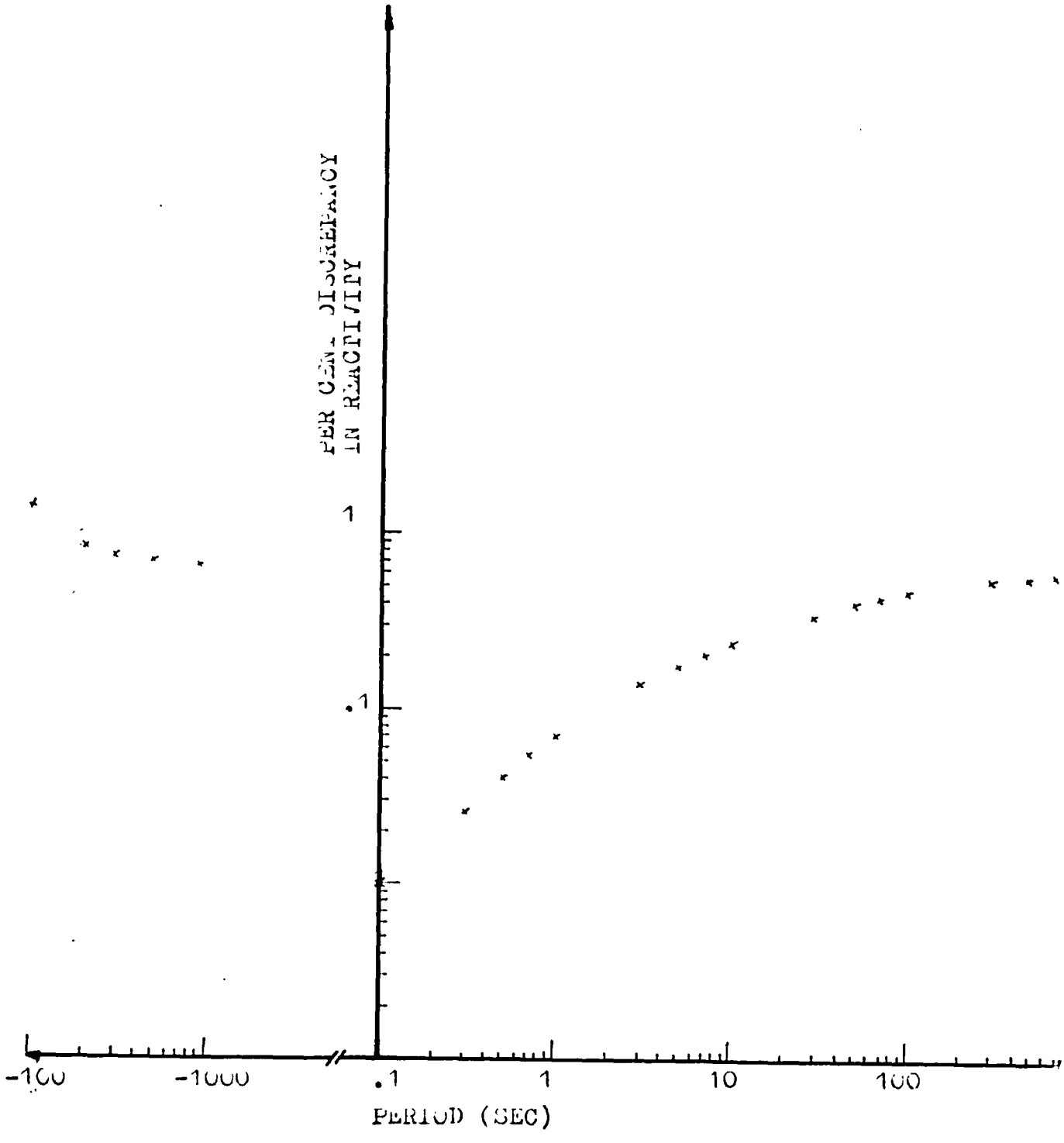

introduced into the reactivity (dollars)-period relationship because of the non-flat response of the detector, for any practical positive period. For large negative periods the discrepancy is slightly higher than .6% and it increases rapidly as the period approaches $-1/\lambda_1$.

This approximate treatment of the effect of the response function of the detector on the period-reactivity relationship indicates that we can safely assume that the detector response is flat.